

NON-INVASIVE CHARACTERIZATION OF IN SITU FORMING IMPLANTS

D i s s e r t a t i o n

zur Erlangung des akademischen Grades
doctor rerum naturalium (Dr. rer. nat.)

vorgelegt der
Naturwissenschaftlichen Fakultät I
Biowissenschaften
der Martin-Luther-Universität Halle-Wittenberg

von
Frau Apothekerin Sabine Kempe
geb. am: 02.02.1980 in: Frankenberg (Sachsen)

Gutachter /in

1. Prof. Dr. K. Mäder
2. Prof. Dr. J. Siepmann
3. Prof. Dr. J. Kreßler

Halle (Saale), 08.05.2012

Experience is what you get, when you didn't get what you wanted.

Randolph Frederick Pausch (1960-2008)

Table of contents

Table of contents.....	I
List of symbols and abbreviations	III
1 Introduction.....	1
1.1 In situ forming implants	1
1.2 In situ cross-linked systems	3
1.2.1 Photo-initiated polymerized systems	3
1.2.2 Physical cross-linked systems.....	4
1.2.3 Chemical cross-linked systems	5
1.3 In situ solidifying organogels	6
1.4 In situ phase separation systems	8
1.4.1 pH-induced gelling systems.....	8
1.4.2 Thermoplastic pastes.....	8
1.4.3 Thermally-induced gelling systems	9
1.4.4 Systems based on phase separation by solvent exchange.....	13
2 Objectives	17
3 Materials and Methods.....	18
3.1 Materials.....	18
3.1.1 Preparation of polymeric solutions for ISFI based on solvent exchange .	20
3.1.2 Preparation of thermally-induced gelling systems based on chitosan	21
3.2 Applied Methods – Basics and instrumentation.....	22
3.2.1 Electron Paramagnetic Resonance Spectroscopy	22
3.2.2 Magnetic Resonance Relaxometry and Imaging	31
3.2.3 Oscillating rheology of thermo-responsive hydrogels and emulsions.....	34
3.2.4 Sol-to-gel study of thermosensitive hydrogels by vial inversion method	35
3.2.5 Light microscopy	35
3.2.6 Statistical evaluation	35

4	Results and discussion	36
4.1	In situ forming implants based on phase separation by solvent exchange.....	36
4.1.1	Real-time monitoring of polymer precipitation and solvent exchange.....	38
4.1.2	<i>In vivo</i> monitoring of the phase inversion dynamics and the biological response to in situ forming depots by Benchtop Magnetic Resonance Imaging	58
4.1.3	In situ monitoring of microclimate pH	67
4.1.4	Conclusions and outlook.....	71
4.2	Thermally-induced chitosan-based gelling systems.....	74
4.2.1	Characterization of thermosensitive chitosan/ β -GP systems.....	76
4.2.2	Characterization of thermosensitive chitosan-based emulsions	95
4.2.3	Conclusions and outlook.....	103
5	Summary and further perspectives	106
5.1	English version.....	106
5.2	German version	109
6	Appendix.....	113
6.1.1	References.....	113
6.2	Acknowledgement.....	133
6.3	List of publications.....	134
6.3.1	Reviews.....	134
6.3.2	Research Papers	134
6.3.3	Oral Presentations	135
6.3.4	Abstracts	135
6.3.5	Posters.....	136
6.4	Curriculum vitae.....	140
6.5	Selbständigkeitserklärung	141

List of symbols and abbreviations

2PK	4-Dimethylamino-5,5-dimethyl-2-ethyl-2-pyridin-4-yl-2,5-dihydro-1H-imidazol-1-oxyl
API	active pharmaceutical ingredient
AT	4-Amino-2,2,5,5-tetramethyl-3-imidazoline-1-oxyl
BSA	bovine serum albumin
Bt-MRI	Benchtop Magnetic Resonance Imaging
Bt-MRT	Benchtop-Magnetresonanztomographie
CLSM	Confocal Laser Scanning Microscopy
DD	deacetylation degree
DMSO	dimethylsulfoxide
EPO	erythropoietin
EPR	Electron Paramagnetic Resonance
FDA	Food and Drug Administration, Agency of the United States Department of Health and Human Services
FITC-BSA	fluorescein isothiocyanate-labeled bovine serum albumin
G'	storage modulus
G''	loss modulus
GMO	glycerol monooleate
GRAS	generally recognized as safe
HA	hyaluronan
HD-PMI	2-Heptadecyl-2,3,4,5,5-pentamethyl-imidazoline-1-oxyl
hexPLA	hexyl-substituted polylactide
HM	2,2,3,4,5,5-Hexamethyl-imidazoline-1-oxyl
HPC	hydroxypropylcellulose
HPMC	hydroxypropylmethylcellulose
i.m.	intra muscular
i.v.	intra venous
IPC	interpolymeric complex
IR	infra red
ISFI	in situ forming implants
ISM	in situ forming microparticles
LCST	lower critical solution temperature
LD ₅₀	lethal dose at which 50 % of subjects will die
LHRH	luteinizing hormone-releasing hormone

logP	decadic logarithm of the octanol-water partition coefficient
MC	methylcellulose
MES	2-(4-morpholino)ethanesulfonic acid
MPEG	methoxy poly(ethylene glycol)
MRI	Magnetic Resonance Imaging
Mw	molecular weight
NaCl	sodium chloride
NMP	N-methyl-2-pyrrolidone
NMR	Nuclear Magnetic Resonance
o/w	oil in water
PCL	poly(ϵ -caprolactone)
PCM	3-Carbamoyl-2,2,5,5-tetramethyl-3-pyrrolidin-1-oxyl-1
PEC	polyelectrolyte complexes
PEG	poly(ethylene glycol)
PEO	poly(ethylene oxide)
pH _m	microclimate pH
PLA	poly(lactide)
PLGA	poly(lactide-co-glycolide)
PMA	poly(methacrylic acid)
PNIPAAM	poly(N-isopropyl acrylamide)
POE	poly(ortho esters)
PPO	poly(propylene oxide)
PVP	poly(vinyl pyrrolidone)
RF	radio frequency
s.c.	subcutaneous
SAIB	sucrose acetate isobutyrate
SAM	N-stearoyl-L-alanine methylester
SD	standard deviation
β -GP	glycerol-2-phosphate
TB	4-benzoyloxy-2,2,6,6-tetramethylpiperidine-1-oxyl
THF	tetrahydrofuran
UV	ultraviolet
VIM	vial inversion method
wt%	per cent per weight
η	dynamic viscosity

1 Introduction

1.1 In situ forming implants

Due to the steadily increasing number of biotechnology-based drugs and compounds which cannot be administered via the oral route, parenteral drug delivery systems received significant research interest in the last two decades. These systems can be designed to provide flexible delivery characteristics and offer many general advantages. Parenteral depot formulations enable to maintain effective drug concentrations over a period of weeks, months or even years [1]. Thereby parental depot systems enhance patient compliance by diminishing the frequency of applications. Further these depot formulations can minimize undesirable side effects caused by fluctuating drug blood levels e.g. affected by immediate release products [1]. In case of targeted parenteral delivery systems that allow for the drug to deposit directly at the site of action, the drug dosage and therefore the system toxicity can be reduced.

Various types of parenteral dosage forms are available, such as solutions, emulsions [2], liposomes [3], micelles [4], implants [5], microparticles [6], nanoparticles and nanocapsules [7]. A major development of the past decade has been the fabrication of implantable delivery systems based on biocompatible or biodegradable polymers. These implants were injected subcutaneously by minor surgery and in case of non-biodegradable polymers, the implants had to be removed after the release periods. To overcome these limitations an increasing number of injectable and biodegradable in situ forming systems have been developed as alternatives [8-10]. Prior to injection the in situ forming systems represent a low viscous and injectable system. Once administered these low viscous polymeric formulation solidify into a semi-solid or solid depots. Thus it turns into a 'solid' dosage form.

Biodegradable implants formed from injectable fluids have one general advantage compared to pre-shaped parenteral depot systems. From the patient's point of view, the application of in situ forming implants (ISFI) is less invasive and so less painful. An improved patient compliance and comfort can be achieved by the avoidance of invasive techniques in the implantation and removal of the implants. These characteristics

encouraged many researchers to investigate their use for various purposes. ISFI have been investigated for controlled drug delivery in systemic treatments as well as localized therapies. In addition ISFI have found applications in tissue engineering, three dimensional cell culturing, cell transplantation, orthopaedic or dental applications [9-12].

In situ forming systems can be classified according to their mechanisms of implant formation into (Figure 1):

- in situ cross-linked polymer systems
- in situ solidifying organogels and
- in situ phase separation systems.

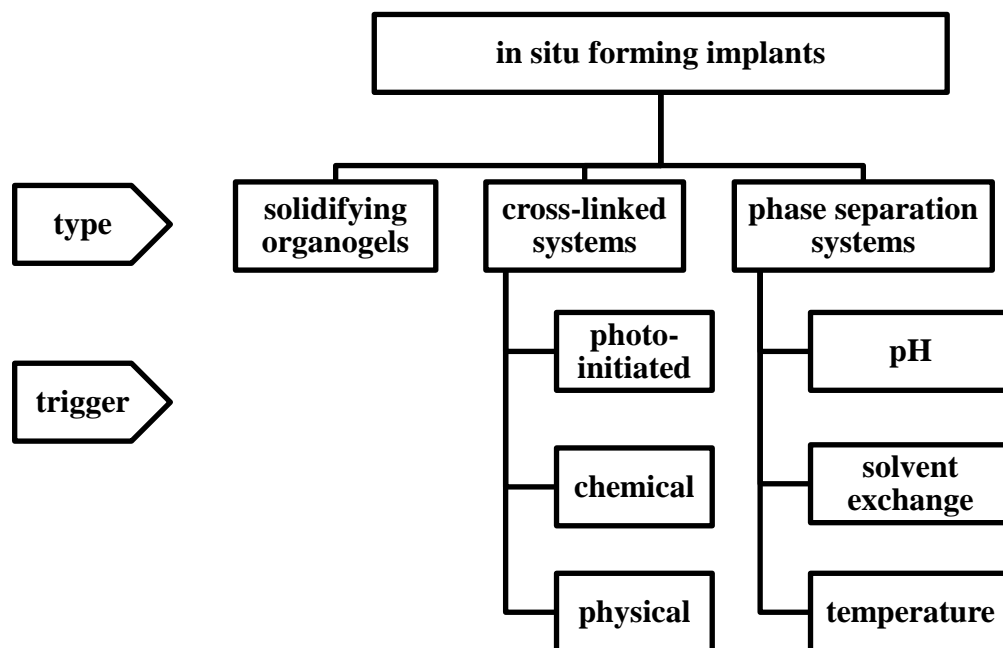


Figure 1 Overview of in situ forming implant technologies (modified from references [9;10])

1.2 In situ cross-linked systems

In situ forming cross-linked polymer networks can be achieved by photo-initiated polymerization [13;14], chemical cross-linking with cross-linking agents [15] or physical cross-linking [16] of specific monomers. There are several issues that must be considered. In particular the demands for *in vivo* reaction conditions are quite restricted, such as the need of non-toxic monomers, cross-linking agents and solvents, oxygen rich environments, narrow range of physiological acceptable temperatures and suitable rates of rapid polymerization [9].

1.2.1 Photo-initiated polymerized systems

Photo-initiated polymerization fulfils many of the requirements for *in vivo* polymerization. The initial materials are liquid solutions, which can be easily placed. Afterwards the rapid polymerization at physiological temperatures forms the polymer matrix of the required dimension. Photopolymerizable systems are used for various biomedical applications. Dentists polymerize dimethacrylate monomers in combination with silica particles for caries tooth restorations as alternatives to mercury amalgam fillings [17]. Other photo-initiated polymerized systems have been investigated for orthopaedic applications [18;19], tissue adhesion prevention [20;21], cell transplantation [22], tissue engineering [23] and drug delivery [22;24]. In general these systems need monomers with at least two free radical polymerizable regions, photosensitive initiators (e.g. eosin dyes) and ultraviolet (UV) or visible light. In the latter case the light sources are placed at the injection site by fiber optic cables.

To develop degradable polymers, meth(acrylate) groups were coupled to various water soluble polymers. For examples ABA triblock copolymers of poly(N-(2-hydroxypropyl) methacrylamide lactate) A blocks and poly(ethylene glycol) (PEG) B blocks have been used to encapsulate mesenchymal stem cells [23]. *Sawhney et al.* developed water-soluble macromers based on AB block copolymers of PEG and poly(α -hydroxy acids) with terminal acrylate groups. On treated wound site they were photo-polymerized from buffered saline solution. The resulting adherent hydrogel film formed a evenly coating on the tissue as a non-adhesive barrier to prevent postoperative adhesions [20]. Another approach used photo-crosslinkable polyanhydride polymers [13]. The resulting polyanhydrides degraded from surface inwards.

Photo-crosslinkable water soluble chitosan was obtained by introduction of lactose and photo-reactive azide groups in chitosan. When exposed to UV light the modified chitosan formed an insoluble, transparent and adhesive hydrogel within 60 seconds [25]. The resulted hydrogel degraded within one month *in vivo*. Toxicity tests for mutagenicity and cytotoxicity have shown the safety of the modified chitosan and its hydrogel. Paclitaxel was retained in this chitosan hydrogel and remained biological active for 21 days [26]. However an initial burst release was observed in the first 24 hours, followed by a slow release in the following 21 days due to the biodegradation of the gel.

In principle photo-initiated polymerization causes the creation of reactive free radical species. To minimize possible adverse side effects to the surrounding tissue and to protect bioactives from the free radical species, low photo-initiator concentrations and low-intensity UV light should be used.

1.2.2 Physical cross-linked systems

The physical cross-linking of polymers leads to the formation of a covalent network structure. They are formed by inter- and intra-molecular bonding via hydrogen bonds or various charge interactions, such as ionic interaction or polyelectrolyte complex (PEC) interactions [10;15].

Alginates are anionic linear polysaccharides derived from brown sea weed. The most important feature of alginate is the gelation in the presence of divalent cations, such as calcium [22]. This property has lead to a wide use as cell transplantation vehicles to grow tissues or as wound dressings. But high molecular weight alginates were reported to be non-biodegradable. Moreover high calcium concentrations(> 5 mmol/l) have inhibited the growth of cells in culture [22]. Under physiological conditions only the calcium concentration in the eye is sufficient to induce gelation. So far the use of in situ cross-linked alginate gels was limited to ophthalmic drug delivery [9;10].

Chitosan, a linear polycationic polymer, forms hydrogel networks through ionic bridges between the polymeric chains with negatively charged components. This cross-linker may either be metallic anions, as Molybdenum (VI) or anionic molecules, in particular tripolyphosphate, citrate or oxalate [15;27;28]. The nature of these interactions is the same as in PEC. Generally in ionic cross-linking the reacting entities are ions or ionic

molecules with a well-defined molecular weight. Whereas PECs are formed by polymers with a broad molecular weight distribution. Hydrogels formed by ionic cross-linked chitosan possess a pH-sensitive swelling behaviour and exhibit drug release by diffusion through their porous structure. They are generally thought to be well-tolerated and have been used for controlled release of various drugs [15;29]. However their main disadvantage is the risk of dissolution of the gel, due to the highly ion and pH-sensitive swelling and possibly low mechanical stability.

1.2.3 Chemical cross-linked systems

While physical cross-linking yields to reversible networks, chemical cross-linking is characterized by the formation of polymer networks via covalent links. However chemical modification of the polymers or the addition of cross-linking entities is needed. Cross-linking agents like benzoyl peroxide, dialdehydes (e.g. glyoxal and glutaraldehyde), oxalic acid or genipin were used to covalently link acrylic ester terminated pre-polymers of poly(lactide) (PLA), poly(ϵ -caprolactone) (PCL), chitosan and gelatin [9;15;28;30]. The toxicity of the cross-linking agents is the obstacle in the use of this ISFI. Because their dispersion into the body may be associated with severe side effects, even at low concentrations [15;31]. Among them benzoyl peroxide, in its function as a free radical producer, is described to induce tumour promotion [30]. The dialdehydes and oxalic acid are considered to be toxic [30]. The naturally occurring genipin has been investigated as a substitute [30]. It is an aglycone derivative from the iridoid glycoside geniposide. It can be found in fruits and is commonly used in herbal medicine and as a food dye. *In vitro* genipin has been tested to be non cytotoxic. After injection in rats it has been shown to be biocompatible [15]. However many of the described reagents yield to rather slow network forming reactions and possess a marked exothermic character, which limits their practical use.

Neither radiation nor radical-initiated polymerization is required for the cross-linking of thiol functional groups. Thiols are known to easily oxidize to disulfides in the presence of oxygen. So thiol groups were coupled to polyacrylates, chitosan and deacetylated gellan gum [32-34]. These thiolated polymers, designated thiomers, form inter- and intramolecular disulfide bonds within the polymer. The result are strong cohesive dosage forms (e.g. microparticles or gels) with high stability, prolonged disintegration times and controlled release of embedded peptides [34;35]. The formation of disulfide

bonds with mucus glycoproteins yielded to strong mucoadhesive properties. With this, the permeation of peptides through the mucus could be improved. By the inhibitory properties of some thiomers towards peptidases the pharmacological efficiency of peptides was enhanced. Nasally applied thiomers lead to a bioavailability of 2.75 % of human growth hormone, whereas the corresponding unmodified gels had only marginal or no effect [34]. But in situ gelation of thiomers requires often several hours and the formation of unwanted disulfide bond of the polymers with proteins can not be completely excluded. Based on the thiomers concept hydrogels with thioether-bonds in PEG-copolymers were used to entrap erythropoietin (EPO) [36]. These polymers consist of multiple thiol groups cross-linked by vinylsulfones. *In vivo* studies showed that the resulting hydrogel (DepoGel™) did not alter the EPO bioactivity. EPO plasma levels were sustained for two weeks. But the major drawback is the non-biodegradability of the polymer.

Covalent cross-linking without employing any extraneous cross-linking agents can further be obtained by condensation of natural proteins and polysaccharides. *Balakhrihnan et al.* developed an injectable biocompatible and biodegradable system of oxidized alginate and gelatin that is self-cross-linked within few seconds in the presence of small concentrations of borax [22;37]. Cross-linking is predominantly due to Schiff's base formation between the amino-groups of the lysine side groups of gelatin and the available aldehydes of oxidized alginate. The rapid gelation in the presence of borax could be attributed to the slightly alkaline pH of the medium. This pH facilitated the Schiff's reaction as well as the complexation ability of borax with alginate hydroxyl groups. The systems have been used multifarious as drug delivery vehicle, tissue engineering scaffold and as wound dressing [22;37].

1.3 In situ solidifying organogels

Organogels are semi-solid systems consisting of a three-dimensional network of self-assembled gelator fibers and a continuous liquid organic phase. The gels are prepared by dissolving the gelator, in concentrations up to 15 wt%, in the heated solvent. Upon cooling the solubility of the gelator decreased. The gelator self-assembled into aggregates, which formed the network by inter-molecular physical interactions [38]. As an example, L-alanine fatty acid derivatives form highly viscous gels in safflower oil by

Van der Waals interaction and hydrogen bonding [39;40]. To decrease their viscosity and to facilitate injection 10 wt% N-methyl-2-pyrrolidone (NMP) was added to the system. This N-stearoyl-L-alanine methylester (SAM) based gels were used for the long term delivery of leuprolide [40]. The system slowly degraded and released the luteinizing hormone-releasing hormone (LHRH) agonist within a period of 14 - 25 days. In rats chemical castration was induced up to 50 days [40]. The same system was further used to sustain the release of rivastigmine, a cholinesterase inhibitor used against Alzheimer's disease. After subcutaneous injection the drug was released up to 11 days in the therapeutic range. The initial burst within the first 24 hours was below 15 % and was fivefold lower compared to the control oil formulation [39]. In both studies these SAM based organogels possessed a good biocompatibility profile over the evaluation period.

Other extensively investigated organogels are formed from glycerol fatty acid esters, such as glycerol monooleate (GMO), glycerol monopalmitostearate (Precirol[®]) and glycerol monolinoleate [9]. These amphiphilic, water insoluble lipids swell in water and form various type of lyotropic liquid crystals. From a water content of 35 wt% onwards they build cubic phases with a gel-like character. These systems are highly viscous and the drug release depends on the water solubility of the incorporated drug. Insulin was released from GMO within 4 days, with an initial release of about 70 % during the first 24 hours. Somatostatine was released in only 6 hours. To ease injectability and to extend the release duration from the gels, vegetable oils were mixed to the glycerol fatty acid esters. *Gao et al.* incorporated glycolyzed apricot kernel oil in Precirol[®] to control the release of the lipophilic contraceptive steroids levonorgestrel and ethinyl estradiol. In *in vivo* studies the subcutaneous injected organogels completely blocked the oestrous cycle of rats up to 40 days [41]. The duration of the pharmacological effect, between 5 to 6 weeks, was the same time as needed for biodegradation of GMO by lipases. This fact suggests an erosion controlled release from the implant. An inflammatory reaction was histologically observed for one week and disappeared afterwards. Despite their low costs and biodegradation by lipases, the lack of toxicity data of the ingredients, as well as the purity and stability of oil and waxes currently limit the use of organogels in drug delivery. Another disadvantage is the need to apply heat for mixing and possible

differences between the melting points of waxes and oils which promotes phase separation.

1.4 In situ phase separation systems

Another strategy to form injectable drug depots is the phenomenon of phase separation from solution. Hereby polymers undergo abrupt changes in their solubility in response to changes in their environmental temperature, pH or by solvent removal.

1.4.1 pH-induced gelling systems

Sol-to-gel transitions induced by changes in environmental pH are related to polymers containing ionizable functional groups. Chitosan is a biocompatible and biodegradable pH-dependent cationic polymer [42]. The amino-polysaccharide is soluble in acidic solutions and phase separates at $\text{pH} > 6$ to form hydrogels, through deprotonation of primary amino groups. However without further chemical cross-linking the gels possess low mechanical stability and rapid release of low molecular weight drugs [15;29]. Poly(methacrylic acid) (PMA) and PEG form water-insoluble interpolymeric complexes (IPC) at $\text{pH} < 5.8$ [43]. The complexes result from hydrogen bonding between carboxylic acid groups from PMA and ether groups from PEG. These bonds are interrupted and IPC re-dissolve in water when at least 20 – 50 % of a non-aqueous co-solvent is added. This IPC solution transforms into a gel at physiological pH when water replaces the co-solvent. By time encapsulated drug is released as a result of dissociation of the IPC into the individual water soluble components, which were cleared via the renal pathway. Concentrations above 30 wt% and below 60 wt% IPC were required to form the gel and to facilitate injection. IPC dissolved in 1:1:2 NMP/ethanol/water was able to entrap and to control the release of macromolecules like fluorescein-labelled insulin and albumin for up to 6 days, *in vitro*.

1.4.2 Thermoplastic pastes

Thermoplastic pastes are based on polymers having a melting point or glass transition temperature in the range of 25 °C to 65 °C. Before injection these polymers are heated above their melting point and then injected as a liquid melt. In the body they form a semi-solid depot upon cooling down to body temperature. At injection temperature above 37 °C and below 65 °C these polymers behave like viscous fluids and flow easily

when pushed. Drugs are incorporated in the molten polymer by simple mixing without the use of organic solvents. Originally biodegradable thermoplastic pastes have been prepared from polymers such as polyanhydrides, PCL, PLA, and their blends with PEG as well as PLA-PEG-PLA triblock copolymers. But these polymers possess high melting points resulting in high injection temperatures partly above 60 °C. The injections were very painful and lead to necrosis at the injection site [44]. Further the encapsulation of the depot by scar tissue was observed, which inhibited the drug diffusion. Another disadvantage is the general slow drug release from these implants. As an approach to solve this problems *Heller et al.* developed biodegradable semi-solid poly(ortho ester) (POE) [45;46]. Low molecular weight POEs, with softening temperatures in the range of 35 °C to 45 °C, have shown to be highly biocompatible in animals as well as in humans [47]. Thus they are semi-solid at room temperature; therapeutic agents can be incorporated by simple mixing without heating or the use of solvents. To be injectable through a needle their intrinsic viscosity should not exceed 0.8 dl/g. POE possessing intrinsic viscosities below 0.5 dl/g failed to delay drug release [48]. The incorporation of lactic acid units in the backbone of the hydrophobic block polymers led to self-catalysed degradation behaviour. POEs underwent predominantly surface erosion. Depending on the polymer structure, drug release could be modulated from days to weeks [46]. Although POE showed good biocompatibility in pre-clinical studies full evaluation of their biodegradation and toxicity still have to be performed. Another point is to test the system stability and the stability of incorporated drugs. So far they are not approved for parental application.

1.4.3 Thermally-induced gelling systems

Thermally-induced gelling systems undergo sol-to-gel transition in water when the temperature increases. Thermosensitive polymers are especially attractive as they do not require organic solvents, co-polymerization agents or externally applied trigger for their gelation at physiological conditions. In spite of this, temperature induced phase transitions are controlled by the temperature dependence of certain molecular interactions, such as hydrogen bonds or hydrophobic effects. At the lower critical solution temperature (LCST) hydrogen bonding between water and polymer become unfavourable compared to interactions between the polymers itself. The solvated macromolecules loose there water of hydration and polymer-polymer interactions

increase. The polymers associate to a network structure, reflected by a sharp rise in system viscosity. Ideally the aqueous polymer solutions flow freely at room temperature and become a gel at body temperature. The shape of the gel depot and the drug release profile, e.g. initial burst of the incorporated drug is directly related to the kinetics of the sol-to-gel transitions and should therefore be fast [8;12]. Both synthetic and natural occurring materials may possess temperature controlled gelation behaviour.

The most studied synthetic polymers are copolymers of poly(ethylene oxide) (PEO) and poly(propylene oxide) (PPO) (PEO-PPO-PEO; known as Poloxamers) and copolymers of poly(N-isopropyl acrylamide) (PNIPAAm) [8;49-53]. However the use of these systems is limited because they are not biodegradable. Aqueous solutions PNIPAAm undergo reversible sol-to-gel transition at 32 °C. The LCST can be shifted to 37 °C by the addition of salts and surfactants [8]. The opaque PNIPAAm gels do not dissolve or swell in water. With increased temperature, the gels expel water and shrink in mass. PNIPAAm is not suitable for implantation purposes in human due its cytotoxicity, non-biodegradability and platelet activation upon contact with blood. Poloxamers are widely used as solubilizer and thickening agents. So far Poloxamer 188 is the only representative of these co-polymers approved for parenteral administration. Concentrations of Poloxamer 188 above 20 wt% are needed to achieve gel formation. The high polymer content often changes the osmolarity and consequently negatively influences the tolerability of the formulations. Although Poloxamers are usually regarded as non toxic, studies reported dose dependent systemic side effect. The chronic administration elevated the plasma levels of cholesterol and triglycerides [9]. Among the commercially available PEO-PPO-PEO co-polymers, Poloxamer 407 (Pluronic® F127) has been reported to be less toxic. Solutions of concentration range 16 - 30 wt% it forms a semisolid transparent gel and has been examined for various biomedical applications [54]. But the delivery periods rarely exceeded few days and the gels suffered from weak mechanical strength [8]. The physical cross-linking between the micelles was so weak that the gels rapidly eroded by dissolution from the surface. A 25 wt% Poloxamer 407 gel completely dissolved in PBS medium within 4 hours [55]. An increase in concentration to 35 wt% yielded to 50 % reduction in gel size within the same time period. After implantation in rats Poloxamer 407 gels could not be observed after two days [56]. In addition salt concentration in the media and additives, such as

PEG or poly(vinyl pyrrolidone) (PVP) strongly influenced the sol-to-gel transition behaviour [54]. These characteristics result in a low reproducibility and limit the use of Poloxamer gels to short-term therapies.

Block copolymers of PEG and poly(lactide-co-glycolide) (PLGA) were proposed as alternative and biodegradable materials. At temperatures below 15 °C both PEG-PLGA-PEG (BAB) and PLGA-PEG-PLGA (ABA) copolymers assemble to micellar structures in water, whereas the hydrophobic PLGA forms the inner core. Gelation at body temperature occurs via micellar aggregation mechanism. Polymer concentrations ranging from 10 to 30 wt% were needed to achieve reverse thermal gelation. The micellar properties and the LCST depend on several factors such as the length and composition of the blocks [54]. The hydrophobicity of incorporated drugs strongly affects their release profiles. *Jeong et al.* studied the release kinetics of ketoprofen and spironolacton from ABA hydrogels [54]. The hydrophilic ketoprofen was released continuously over 2 weeks and the release rate depended on the initial polymer concentration. The more hydrophobic spironolacton was released over 2 months. Macromed Inc. distributes low molecular weight ABA and BAB triblock copolymers under the trademark ReGel[®]. The block copolymers have been intensively investigated for solubilisation and stabilisation of water-insoluble (e.g. paclitaxel and cyclosporine A) drugs and proteins, including zink-insulin and porcine growth hormone [57]. The solubility of paclitaxel was increased by 400 fold in aqueous formulations containing 23 wt% PLGA-PEG-PLGA. The resulting gels released paclitaxel in a controlled fashion over 50 days *in vitro* [57]. *In vivo* ReGel[®] formulation was completely resorbed from injection site within 4 - 6 weeks. The efficiency of paclitaxel loaded ReGel[®] (OncoGel[®], 6 mg/ml paclitaxel) against human breast cancer was superior compared to maximum tolerated dose of commercial product (Taxol[®]). The direct intratumoral injection of OncoGel[®] and the slow drug clearance from the injection site resulted in minimal paclitaxel distribution to other organs and less drug-related adverse effects than in the Taxol[®] group. Currently OncoGel[®] is progressing in clinical studies Phase II for the treatment of oesophageal cancer, brain cancer and breast cancer [12]. Also diblock copolymers of PEG-PLGA form micelles in water that undergo sol-to-gel transitions at 30 °C [58;59]. To enable water solubility, the polymers compose of long PEG blocks combined with shorter PLGA blocks. *In vitro* the PEG-PLGA copolymers dissolved

within one week. Whereas more durable gel depots were formed *in vivo*. By modifying the copolymer composition the persistence of the gels could be varied from one week up to two months [58]. However PLA and PLGA degrade to their monomeric acids, that yield in an acidic environment [60;61]. To circumvent this limitation *Hyun et al.* developed methoxy poly(ethylene glycol) (MPEG) PCL diblock copolymers that underwent sol-to-gel phase transitions under physiological conditions [56]. Their degradation did not result in an acidic environment. *In vivo* the MPEG-PCL gels maintained their structural integrity longer than 30 days. The release of fluorescein isothiocyanate-labeled bovine serum albumin (FITC-BSA) was sustained within these 30 days.

As mentioned above thermo-sensitive gels can be prepared in almost the same manner with naturally occurring polymers. Cellulose itself is not soluble in water. By introducing hydrophilic groups, the cellulose derivatives become water soluble. When cellulose derivatives have an optimum balance of hydrophilic and hydrophobic moieties, they gel at elevated temperatures in aqueous solutions. Typical examples are methylcellulose (MC), hydroxypropylcellulose (HPC) and hydroxypropylmethylcellulose (HPMC). The LCST depends on the substitution at the hydroxyl group, e.g. MC shows phase transition between 40 °C and 50 °C, HPMC between 75 °C and 90 °C and HPC at about 55 °C [8;54;62]. The phase transition temperatures can be modulated by varying the molar substitution of cellulose or addition of salts. For example the addition of sodium chloride lowered the LCST of MC to 32 °C – 34 °C. However the thermal gelling properties of cellulose derivatives are not sufficiently fast for injectable drug delivery systems. *Gumpta et al.* blended MC with hyaluronan (HA) to achieve a fast-gelling injectable material for the localized delivery to the injured spinal cord [63]. The blend of HA with MC formed a shear thinning gel prior injection. The gel strength increased after injection due to phase transition of MC at body temperature. *In vivo* rat studies showed a biocompatibility in the intrathecal space for one month.

Chenite et al. developed thermally sensitive neutral solutions based on combinations of chitosan with polyol salts (e.g. β -glycerolphosphate, β -GP) [64]. Without additives chitosan is soluble in acidic solution and phase separates at $\text{pH} > 6$. The addition of β -GP to acidic chitosan solutions allows rising the pH to neutral without phase separation. These systems are thermosensitive and form hydrogels at temperatures around 37 °C

and above. Thermosensitive formulations are obtained at low polymer concentrations. Mainly the degree of deacetylation (DD) of chitosan, and minor its molecular weight, influences the stability of the sol as well as the gelation time and temperature. The chitosan/ β -GP systems could deliver macromolecular drugs from several hours to days [65;66]. However the high porosity of the gel yielded to a complete release of hydrophilic low molecular weight compounds within hours. To achieve a sustained release, independent from the drug molecular weight, hydrophilic compounds were first incorporated into liposomes. In the following the liposomes were mixed with the chitosan/ β -GP solution [67]. The release rate of the hydrophilic molecules could be controlled by the size and compositions of the liposomes. Besides pharmaceutical applications, the chitosan/ β -GP hydrogels were evaluated for tissue engineering purposes. The gel was capable to maintain the bioactivity and to release bone morphogenic protein [64]. Chitosan/ β -GP systems were also evaluated for cartilage repair. Entrapped chondrocytes in solidified Chitosan/ β -GP solutions initiated and proliferated the deposition of a functional matrix in an animal model [54]. BioSyntech Inc. developed a hybrid implant, named BST-Car-Gel[®] to improve cartilage healing. The mixture of chitosan/ β -GP and autologous blood solidifies within minutes via normal blood coagulation and the chitosan mediated mechanism [68]. The product is currently tested in Canadian pivotal clinical trials, which started 2006 and are still ongoing. Another BioSyntech Inc. product currently tested in human studies is BST-DermOn[®]. By using the haemostatic, bacteriostatic and mucoadhesive properties of chitosan, the chitosan/GP hydrogels were tested as adjective therapy in topical wound therapy. Creating a moist healing environment, the hydrogels promote the healing of long lasting chronic wounds [69].

1.4.4 Systems based on phase separation by solvent exchange

Only in situ polymer precipitation systems based on solvent removal have become commercial available so far. Examples include Atridox[®] which is used for the periodontal delivery of doxycycline [70] and Eligard[®], a subcutaneous depot of leuprolide for the treatment of prostate cancer [71]. This concept, conceived by *Dunn et al.*, employs biodegradable carriers dissolved in or diluted with water miscible, physiological compatible organic solvents [72]. Prior to injection the drug is added and forms an injectable solution or dispersion. After subcutaneous injection of the

formulation into the body the organic solvent dissipates into the surrounding tissue as aqueous body fluids penetrates in. This leads to phase separation and precipitation of the polymer, forming a depot at the injection site. The active pharmaceutical ingredient (API) gets entrapped within the matrix as it solidifies and is released by diffusion processes or as the implant biodegrades. The systems based on phase separation by solvent removal have been used in a large number of drug delivery applications ranging from small molecules, e.g. lidocaine [73], aspirin [74]), over peptides [75] to proteins [76;77]. Standard “hydrophobic” biodegradable polymers, such as polyhydroxyacids, polyanhydrides, polyorthoesters and others can be used as carriers. However PLA, PLGA and PCL are preferably used because of their approval by the American Food and Drug Administration (FDA).

The Atrigel[®] technology, introduced by *Dunn et al.*, dissolved the polymers in organic solvents with high water miscibility. Solvents include NMP, dimethylsulfoxide (DMSO), propylene glycol, acetone, tetrahydrofuran (THF), 2-pyrrolidone [72], ethyl acetate [76], glycofurol [78] or low molecular weight PEG [79]. NMP is most frequently used because of its solvating ability. Polymer concentrations in the prepared formulations range from 10 wt% to 80 wt%. Both, the concentration of the polymer in solution and its molecular weight affect the viscosity of the implant forming solutions [80]. The phase inversion dynamics are a complex phenomenon and are directly affected by the solvent properties. After contact with aqueous medium the high water miscibility of the solvents results in a fast phase inversion of the polymer solutions. Generally the solidification of these systems takes place in the order of seconds to minutes. Fast phase inversion of polymer solutions and high solvent affinity to the precipitant result in implants with large finger pores, directly related to high initial drug release [80]. The influence of several formulation parameters on the drug burst, like polymer type, type of solvent or co-solvent and additives, have been studied in detail *in vitro* [81;82]. Main factors of influence are the type of the polymer and its molecular weight. High polymer concentrations (40 wt% - 50 wt%) decreased the initial release. However these solutions were highly viscous, so that the injectability was impaired. The affinity of the API for the solvent-water versus the solvent-polymer phase has also a strong impact on the burst release. *McHugh et al.* discovered that protein release can be modified by varying the aqueous miscibility of injectable depots [83;84]. Reducing the

solvent/non-solvent affinity of PLGA solutions slowed the rate of phase inversion and yield to a more uniform release. Typical solvents include benzyl benzoate, ethyl benzoate, triacetin [77], triethyl citrate [85] or benzyl alcohol [86]. Polymer solidification in these slow phase inverting systems takes from hours to days. The morphology of the depot is more or less uniformly dense with a smaller pore size. However the solution viscosities of these systems are in a range that makes injection difficult without previous warm up to 37 °C.

Implants can also be formed from biodegradable non-polymeric carriers, e.g. sucrose acetate isobutyrate (SAIB). SAIB is a water insoluble high viscous (100000 mPa*s) compound, approved as a food additive to stabilize emulsions. Diluted with small amounts (15 % - 35 %) of pharmaceutically acceptable organic solvents, like ethanol, triacetin or NMP, it can be injected as low-viscosity formulations (50 mPa*s to 200 mPa*s). After injection the solvent diffuses away, leaving a viscous adhesive matrix of SAIB with incorporated active ingredients and additives. Various drugs have been tested for release by this delivery system including human growth hormone and risperidon [87;88]. The SAIB system is patented by Southern Biosystems and licensed to DURECT under the trade name SABER™. The SABER™ system has the advantage of low cost for raw material and ease of manufacturing. SABER™-Bupivacaine (POSIDUR™) has been developed for the local treatment of post surgical pain and is in clinical phase II. Injected during surgery it continuously releases bupivacaine and in this way provides up to three days of uninterrupted local anaesthesia.

The central issues of solvent removal in situ precipitation system are the potential of unwanted local irritations due to the use of high amounts of organic solvent, and the lag between the injection of the solutions and the formation of the solid implant. Biocompatibility studies of NMP/PLGA and DMSO/PLGA solutions in rhesus monkey showed no acute toxicity and tissue reaction similar to that for other biodegradable polymers [89]. The biocompatibility of PLA, dissolved in benzyl benzoate and benzyl alcohol, in rabbits showed normal inflammatory and foreign body reactions similar to blank and pure API solutions. Neither necrosis nor tissue damage was observed [86]. Contradictory myotoxicity studies showed a high acute myotoxic potential, comparable to the positive control for NMP, DMSO, benzyl alcohol, triethyl citrate and their polymeric solutions. 2-Pyrrolidone, triacetin and propylene carbonate caused less

muscle damage, whereas the myotoxicity of ethyl acetate was comparable to the negative control [90;91]. Another major concern is the stability of polymers, mainly PLGA, and the drug in the in situ forming systems. *Dong et al.* observed a faster degradation of PLGA with increased storage temperature and water content of the solvents [81]. For these reasons, polymeric solutions should be stored at 4 °C and the drugs added as dry powders to the solution prior injection. Additionally sensitive drugs like proteins may denature in the organic solvent. To overcome these limitations *the group of Prof. Bodmeier* dispersed the drug containing polymer solutions in a second external phase composed of oil for injection [90]. The polymer solution droplets solidified after contact with aqueous fluids to form microparticles in situ. The viscosity of in situ forming microparticle (ISM) systems is determined by the viscosity of the second phase. In comparison to ISFI, ISM can be prepared with higher polymer concentrations and the use of less organic solvent maintaining the injectability of the system. Further the ISM showed reduced initial release [92] and myotoxicity [90;91]. The main obstacle is the relatively low ISM emulsion stability [93]. *Voigt* reported that coalescence of polymer solution droplets have yielded to in situ formation of implant-like matrices and complicated injection.

To sum it up it can be said that an ideal in situ forming implant should:

- Possess a low viscosity of the implant solutions to allow a good injectability.
- Allow a simple drug load.
- Contain only biodegradable and biocompatible excipients.
- Possess good system stability.
- Yield a low variability of drug release with a low initial burst.

So far none of the presented systems fulfil all of mentioned requirements.

2 Objectives

As described in the previous section, ISFI have attracted increasing scientific attention during the last decade. Despite the intensive research in this field, the *in vivo* knowledge about the detailed mechanism of implant formation and disintegration is still very limited. A critical point in the design and optimization of these delivery systems is to understand this interplay between the biological system, the drug and the delivery device. The dynamics of the implant formation and the way the implants respond to its physiological surrounding directly determine their release characteristics and morphology. In particular quantitative characterization of the *in situ* implant formation is quite challenging because of the complex nature of the systems. When starting this work, there existed no systematic and continuous investigations about the mechanism of *in situ* implant formation *in vivo*. To extend the knowledge about ISFI this work focuses on the non-invasive and continuous characterization of their formation processes both *in vitro* and *in vivo*. The non-invasive analytical methods Electron Paramagnetic Resonance (EPR) spectroscopy, Benchtop Magnetic Resonance Imaging (Bt-MRI) and Nuclear Magnetic Resonance (NMR) Relaxometry will be combined to receive a more complete understanding of the formation and disintegration of ISFI. Moreover for the first time microclimate pH (pH_m) of disintegrating ISFI will be monitored by EPR spectroscopy. Due to their pharmaceutical relevance main focus will be set on ISFI prepared by phase separation in response to solvent exchange and temperature change, respectively. The first part of this work covers the characterization of *in situ* forming implants based on phase separation by solvent exchange. Thereby the quantification of polymer precipitation and solvent exchange, the influence of formulation parameters thereon, and on the release of model drugs will be regarded in detail. Further the localisation of and the response of the biological systems to the ISFI will be studied. The second part deals with the characterisation of thermally-induced chitosan-based gelling systems. The main focus will be set to the monitoring of phase transitions in chitosan solutions and newly developed chitosan-based O/W emulsions and the examination of the influence of formulation parameters on the phase transition behaviour and on the release pattern of model drugs.

3 Materials and Methods

3.1 Materials

The following materials were used as received from commercial suppliers:

Potato starch (ROQUETTE GmbH, Germany)

Polymers

Table 1 Abbreviation and properties of the investigated polymers

<i>Polymer</i>	<i>Properties</i>
PLGA Resomer RG503H (Boehringer Ingelheim, Germany)	D,L-lactide: glycolide, molar ratio 50:50 Mw 34 kDa Free carboxyl termini end groups
PEG10-PLGA Resomer RGPd 50105 (Boehringer Ingelheim, Germany)	AB di-blockpolymer of PLGA-PEG Mw 50 kDa A-block: D,L-lactide: glycolide, molar ratio 50:50 B-block: PEG (Mw 5 kDa) 10 wt%
PEG15-PLGA Resomer RGPd 50155 (Boehringer Ingelheim, Germany)	AB di-blockpolymer of PLGA-PEG Mw 33 kDa A-block: D,L-lactide: glycolide, molar ratio 50:50 B-block: PEG (Mw 5 kDa) 15 wt%
Chitosan Chitoclear [®] FG95 (Primex, Iceland)	deacetylation degree of 95 % viscosity 51 cP (1 % in 1 % acetic acid) Mw 1.3±0.2·MDa [94]

Solvents

NMP, ethanol, acetone, dimethyl sulfoxide (Merck, Germany), PEG 400 (Lutrol 400, BASF, Germany)

Oils

Olive oil (Oleum Olivarum EXTRA VIERGE), middle chain triglycerides (MCT, MIGLYOL[®]812) (Caesar & Loretz GmbH, Germany)

Buffering agents

Glycerol-2-phosphate disodium salt hydrate (β -GP, Sigma Aldrich, Germany)

Potassium dihydrogen phosphate, disodium hydrogen phosphate, sodium hydroxide, hydrochloric acid (Merck, Germany)

Animals

BALB/c mice (20 g – 25 g) (Charles River Wiga GmbH, Germany)

The animal experiments protocol was approved by Animal Ethics Committee of the state Saxony-Anhalt, Germany and the commissary of animal protection from Martin-Luther-University Halle. Animal housing feeding and treatment was performed according to the international standards and according to the European Community guidelines. Female BALB/c mice were housed under controlled conditions (12 h light/dark schedule, 24 °C) and received mice chow and tap water ad libitum.

Narcotics

Isoflurane (Forene[®], Abbott, Germany)

EPR spin probes

AT, HM, ¹⁵N-PCM, HD-PMI and 2PK were obtained by Prof. Vladimir Khramtsov (Institute of Chemical Kinetics and Combustion, Novosibirsk, Russia), (Figure 2)

Tempolbenzoate (TB) was obtained by Sigma, Germany (Figure 2)

Spin-labelled insulin was prepared from porcine insulin (a kind gift from Berlin Chemie, Germany) as described by *Besheer et al.* [95].

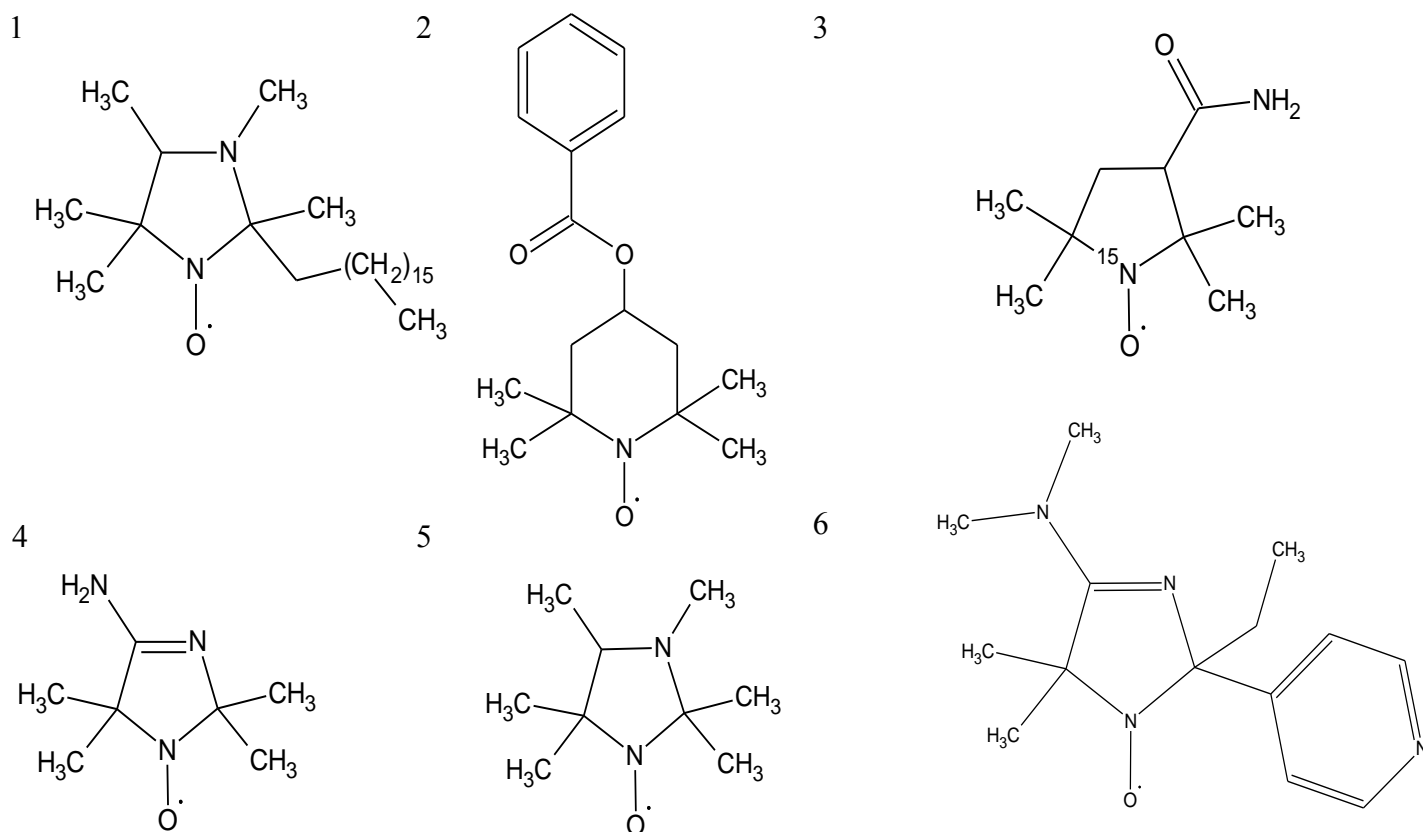


Figure 2 Used spin probes with different physicochemical properties:

(1; 2) lipophilic spin probes,

(3) hydrophilic spin probes,

(4-6) pH-sensitive spin probes

Nomenclature:

(1) HD-PMI – 2-Heptadecyl-2,3,4,5,5-pentamethyl-imidazoline-1-oxyl,

(2) TB (Tempolbenzoate) – 4-benzoyloxy-2,2,6,6-tetramethylpiperidine-1-oxyl,

(3) ¹⁵N-PCM – 3-Carbamoyl-2,2,5,5-tetramethyl-3-pyrrolidin-1-oxyl-¹⁵N,

(4) AT (ATI) – 4-Amino-2,2,5,5-tetramethyl-3-imidazoline-1-oxyl,

(5) HM – 2,2,3,4,5,5-Hexamethyl-imidazoline-1-oxyl,

(6) 2PK – 4-Dimethylamino-5,5-dimethyl-2-ethyl-2-pyridin-4-yl-2,5-dihydro-1H-imidazol-1-oxyl

3.1.1 Preparation of polymeric solutions for ISFI based on solvent exchange

PLGA; PEG10-PLGA or PEG15-PLGA was dissolved in NMP or PEG 400 upon stirring at room temperature, which lead to clear solutions with a final polymer concentration of 30 % (w/v). For EPR experiments the spin probes TB, AT, HM or 2PK were dissolved in the polymeric solutions with a final concentration of 5 mmol/kg polymer.

3.1.2 Preparation of thermally-induced gelling systems based on chitosan

3.1.2.1 Chitosan/ β -GP systems

Chitosan was dissolved in 8 ml of 0.1 M hydrochloric acid. To the cooled (4-6 °C) chitosan solution, 2 ml chilled (4-6 °C) aqueous β -GP was carefully added drop wise to obtain a clear and homogenous liquid solution in a final volume of 10 ml (Figure 3). The formulations contained 2.5 % (m/V) chitosan and 6; 8; 10; 12; 14 or 16 % (m/V) β -GP, respectively.

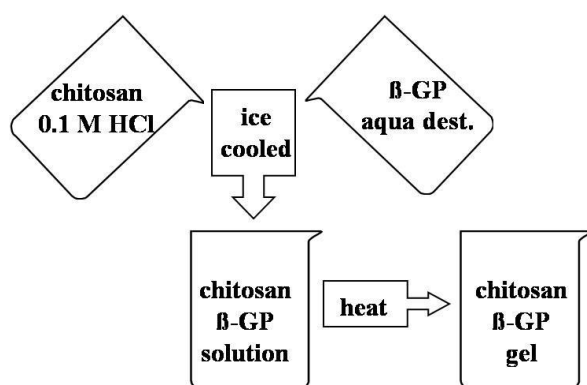


Figure 3 Schematic representation of the general procedure for chitosan/ β -GP gel preparation

3.1.2.2 Chitosan/olive oil/ β -GP emulsions

Figure 4 briefly describes the preparation of the chitosan/olive oil/ β -GP emulsions. Chitosan was dissolved in 16 ml of 0.1 M hydrochloric acid and. Olive oil was added and an emulsion was formed using a rotor-stator mixer (Ultra turrax®, IKA® T18 basic, IKA®-Works, NC) for 120 s at 22.000 rpm. To the cooled (4-6 °C) chitosan emulsion, 4 ml chilled (4-6 °C) aqueous β -GP was carefully added drop wise to obtain a clear and homogenous liquid emulsion in a final volume of 20 ml (Figure 4). The formulations contained 2.5% (m/V) chitosan, (1; 5; 10 or 20) % (m/V) olive oil and 16 % (m/V) β -GP, respectively. For EPR experiments the spin probes ^{15}N -PCM and HD-PMI were incorporated into the chitosan (2.5 % w/v)/olive oil (20 % w/v)/ β -GP (16 % w/v) emulsions with a final concentration of 2 mM.

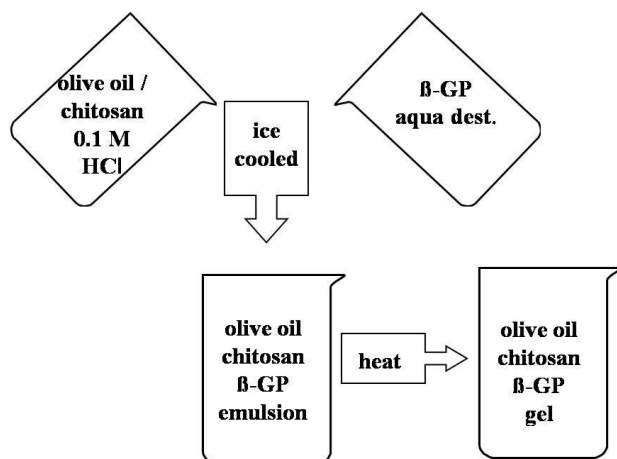


Figure 4 Schematic representation of the general procedure for chitosan/ β -GP/olive oil gel preparation

3.2 Applied Methods – Basics and instrumentation

3.2.1 Electron Paramagnetic Resonance Spectroscopy

Electron Paramagnetic Resonance, also known as Electron Spin Resonance (ESR), is a spectroscopy technique that allows the direct and non-invasive detection of paramagnetic species, consisting of one or more unpaired electrons. Paramagnetic species include short living or stable free radicals (e.g. spin probes, Figure 2) or transition metal ions, such as Mn^{2+} , Fe^{3+} and Cu^{2+} . The EPR method can be applied to complex and non-transparent samples. Since its discovery by *Zavoisky* in 1944 [96], EPR has been widely used in a number of research fields such as physics, chemistry, biology and material and food science [97]. Several textbooks have been published explaining the elementary theory and application of EPR in these fields [98-100].

The basic principles of EPR are very similar to the more familiar NMR. Both methods base on the interaction of electromagnetic radiation with magnetic moments, caused by electrons (EPR) or nuclei (NMR). The magnetic moment of an unpaired electron arises from its “spin”. When placed in an external magnetic field; the electron will align parallel ($m_s = +1/2$) or antiparallel ($m_s = -1/2$) to the direction of the magnetic field, which correspond to a lower or an upper energy state (Figure 5). The energy difference (ΔE) between these two states is proportional to the strength of the applied magnetic field (B_0) (Formula 1).

$$\Delta E = h\nu = g\mu_e B_0 \quad \text{Formula 1 Resonance condition in EPR experiment}$$

Where h is Planck's constant, ν is the frequency of the electromagnetic radiation, g is a constant termed g factor ($g = 2.0023$ for an unpaired electron), μ_B is the Bohr magneton. If electromagnetic radiation corresponding to the energy difference is applied to the sample, resonance transition is possible between the lower and upper energy state (Figure 5) [98;101].

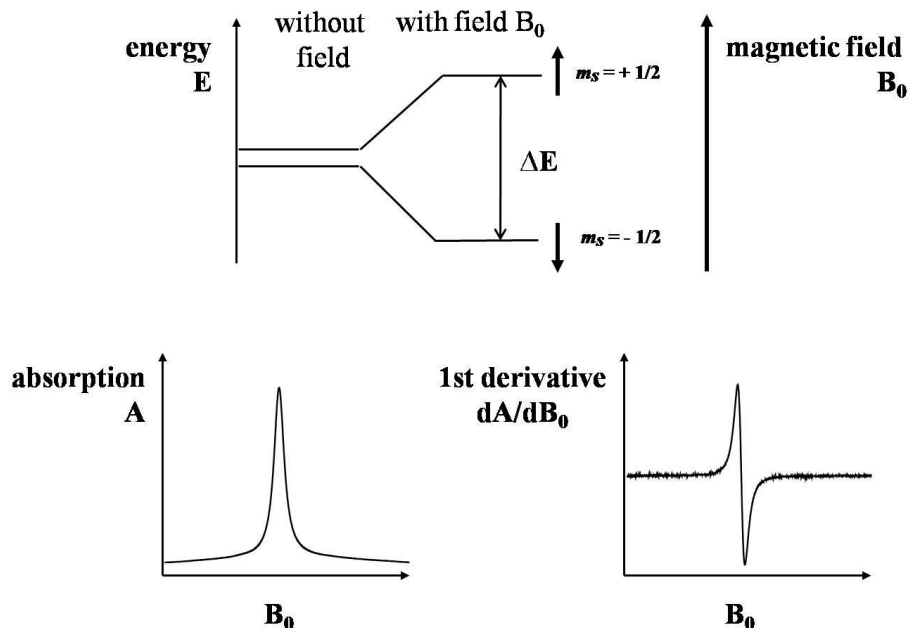


Figure 5 Basic principle of EPR: (top) Zeeman splitting of the energy levels for a single electron spin (spin quantum number $S = 1/2$, magnetic quantum number $m_s = \pm 1/2$) in the presence of an external magnetic field; (bottom) obtained absorption curve and its first derivative, which is the commonly detected EPR signal.

The unpaired electron may further interact with neighbouring magnetic nuclei to produce splittings in the EPR spectrum, called hyperfine splittings. The type and the number of the nuclei interacting with the electron determine the number of lines and their relative intensities. For example magnetic interaction in nitroxyl radicals between the free electron and the nuclear spin of nitrogen ($I = 1$, ^{14}N) results in a hyperfine splitting into three lines (Figure 6). In contrast the EPR spectrum of the ^{15}N spin probes shows only two lines because of the interaction of the unpaired electron with the different nuclear spin of the ^{15}N nuclei ($I = 1/2$). The unpaired electron is mainly localized in the p_z -orbital of the nitrogen atom. It can be also localized at the oxygen atom or delocalized over the ring structure of these nitroxyl radicals. Therefore nitroxyl radicals are very sensitive to small charge density variations caused by surrounding

molecules. The strength of the interaction between the electron and the nuclei and their magnetic moment determine the distance between the splitting of the lines.

This distance between the first and second peak describes the hyperfine splitting constant (Figure 6). It is labelled by the symbol a , followed by a subscript indicating the splitting nucleus.

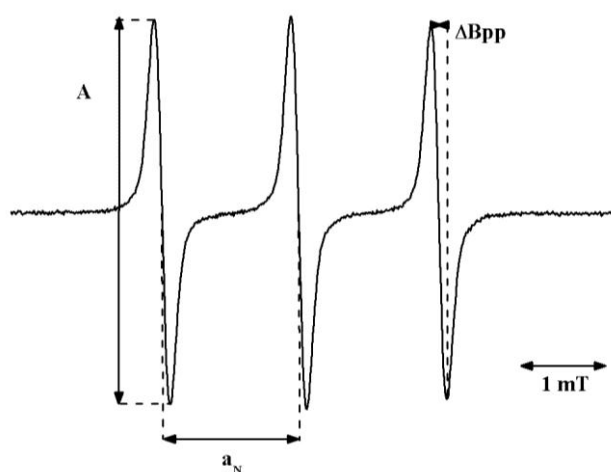


Figure 6 In vitro L-Band EPR spectrum of TB dissolved in NMP illustrating typical EPR parameter: A - signal amplitude, a_N - hyperfine splitting constant, ΔB_{pp} - peak-to-peak line width

Other parameters that can be easily obtained from the EPR spectra are the signal amplitude of the peaks (A) and the peak-to-peak line width (ΔB_{pp}) (Figure 6). By using these parameters, the rotational correlation time (τ_c) can be calculated from the EPR spectrum [102]. EPR spectra are usually recorded in the form of the first derivative (Figure 5, page 23). Therefore, the signal intensity can be calculated by the double integration of the EPR spectra. Molecular tumbling or molecular dynamics at a time scale from 10^{-10} s to 10^{-7} s induce relaxation processes, which influence the line width and the shape of the detected EPR lines and the spectral splitting. So the spectral splitting of the nitroxyl radicals is not only sensitive to the molecular motion and therefore the microviscosity of their surroundings, but also to the polarity of their direct environment. As mentioned earlier, the unpaired electron can be localized at the nitrogen atom, oxygen atom or ring structure of nitroxyl radicals (Figure 7).

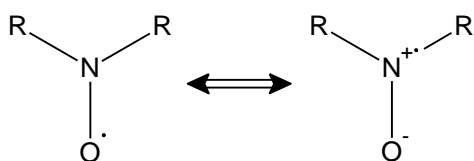


Figure 7 Mesomeric forms of the nitroxyl radical

Only the nuclear spin of the nitroxyl nitrogen contribute to the hyperfine splitting constant (a_N) of the EPR signal, because of the missing nuclear spin of the oxygen in the

other mesomeric form (Figure 7). Polar liquids (e.g. water) favour the existence of the mesomeric form at the nitrogen atom generating higher hyperfine splitting constants compared to apolar solvents (e.g. oil) [101].

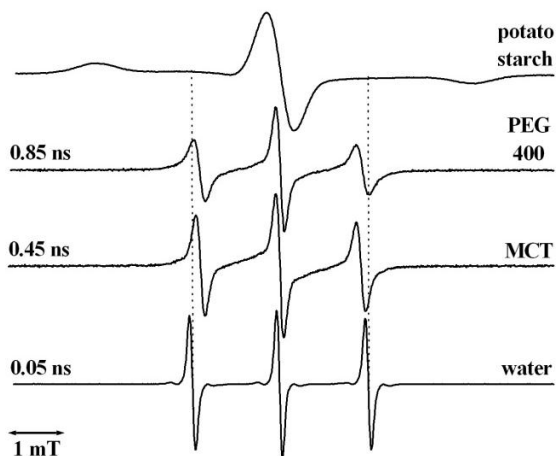


Figure 8 In vitro EPR spectra of AT in environments with different polarities and viscosities: potato starch, MCT, PEG 400 and water. The microviscosity of the spin probe environment is reflected by the corresponding rotational correlation times (τ_c in ns): higher correlation times indicate lower tumbling rates and therefore higher microviscosities.

In the EPR spectra of the nitroxyl radical AT in water the distance between the outer lines is increased, compared to the oil MCT (middle chain triglycerides) (Figure 8). The microviscosity, another parameter of the microenvironment strongly influences the tumbling behaviour of the nitroxyl radicals. In low viscous media they tumble free, resulting in highly symmetric spectra with three narrow lines and rotational correlation times τ_c in the order of 0.01 ns to 0.1 ns (EPR spectrum of the nitroxyl radical AT in water, Figure 8). Increasing the viscosity decreases the molecular tumbling rate of the nitroxyl radical. Due to their restricted motion the anisotropy of the hyperfine interaction is only partially or not averaged, which results in a line broadening, a decrease of the signal amplitude and an increase in τ_c [95;103]. The hyperfine interaction in nitroxyl radicals is anisotropic. In solution the anisotropic interactions are nearly completely averaged out and only the isotropic parts remain, resulting in a higher spectral resolution and signal amplitude. In solid material the anisotropy is no more averaged and typical “powder spectra” can be recorded (EPR spectrum of AT in potato starch in Figure 8). In the fast motional region τ_c can be calculated from the ratio of amplitudes [104]. However this method is limited to rotational correlation times shorter than 3 ns. The calculation of τ_c from slow motion EPR spectra requires more specific mathematical operations [105].

Normally the EPR spectrum is detected as the function of the magnetic field strength at a constant microwave frequency. Based on technical implementations the EPR spectrum is plotted as a first-derivative of the absorption spectrum (Figure 5, page 23). The first derivative figure is more sensitive to fast motional (“mobile”) spin probes with their narrow isotropic line spectra. Superimposed spectra are a combination of the “mobile” with the “immobile” anisotropic spectrum. Mobile species are detectable with a ratio below 1 %, whereas immobile species below 10 % can be easily missed [106].

Additionally special nitroxide radicals permit the measurement of microacidity [107]. These nitroxyl radicals consist of additional functional groups (mostly amino-groups) in their molecule (see structure 4 - 6 in Figure 9).

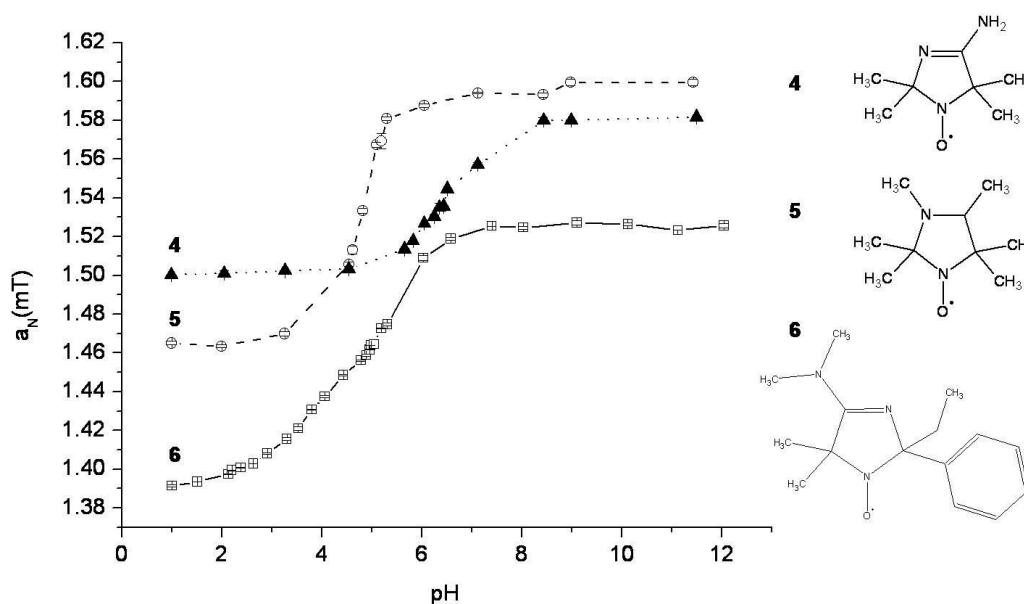


Figure 9 pH-sensitivity of the hyperfine splitting constant a_N of the nitroxides AT (4), HM (5) and 2PK (6)

Protonation of the amino-groups decreases the spin density at the nitroxyl nitrogen and result in a decrease in the hyperfine splitting. The calibration curve of the pH dependence gives the expected sigmoidal shape (Figure 9). As expected, the highest dependence occurs around the pKa (turning point of the curve). Increasing differences between pH and pKa decrease the response sensitivity. The curve shows that the pH range which can be assessed, reaches approximately from 1.5 units above and below the pKa. There exist a wide range of stable nitroxide radicals with different pKa values to cover the full pH range and therefore the measurement of more acidic and alkaline

environments is possible [108]. Recently developed nitroxides contain two protonable groups (structure 6 in Figure 9), presenting two different pKa values, so that a wider pH range can be covered by a single spin probe [109;110].

Furthermore there exist spin probes which reflect the influence of the oxygen concentration. Oxygen itself is paramagnetic. However, it possesses a very broad EPR line due to the fast relaxation and is therefore not directly measurable at room temperature. Yet it interacts with other paramagnetic species causing additional oxygen concentration dependent line broadenings. Recently *Swartz et al.* provided a detailed overview about the measurement of oxygen concentrations in tissues and *in vivo* clinical applications of EPR oximetry [111].

Commonly used EPR frequencies in drug delivery research are in the microwave range at 10 GHz (X-band) or 1 GHz (L-band). The L-band spectrometers are not as sensitive as X-band spectrometers, but they have the advantage of a higher penetration depth of the irradiation of about 5 mm - 10 mm into water containing samples, allowing the measurement of hydrated pellets and tablets or small animals such as mice. For X-band experiments the microwave penetration depth is limited to 0.5 mm - 1 mm in water rich samples due to the high dielectric constant and the microwave absorption of water or other high polar liquids. Therefore high frequency EPR is size limited on water containing biological and pharmaceutical samples. However, suspensions of micro- or nanoparticles, emulsions and also isolated skin can be measured at 10 GHz in capillaries or flat tissue cells. Recent reviews summarize the applications of EPR spectroscopy and imaging in drug delivery research [101;112].

3.2.1.1 *In vitro* EPR studies on ISFI based on phase separation by solvent exchange

200 µl of the TB-containing polymer solution (section 3.1.1, page 20) were injected through a 25 gauge needle into 50 ml of 0.1 M phosphate buffer (pH 7.4; 37 °C) placed in an incubation shaker (30 rpm). The polymer solutions were injected into perforated plastic cylinders placed in the buffer solutions, where the implants were formed immediately. The incubation medium was exchanged periodically to prevent the accumulation of degradation products. At determined time points the implants were taken out of the buffer, the plastic cylinders were dried with wipes and covered with plastic foil to prevent drying and subsequently transferred to the EPR spectrometer.

For the calibration measurement 0.5 mmol/l of TB was dissolved in different NMP or PEG 400 buffer mixtures. The values $2a_N$ were determined from the spectra and were plotted against the concentrations of the organic solvent in different organic solvent buffer mixtures.

The EPR measurements were performed using an L-band spectrometer (MagnetTech, Germany) with a re-entrant resonator, operating at a microwave frequency of about 1.1-1.3 GHz. Measurements parameter were set to: modulation amplitude 0.14 mT, scan width 6 mT or 10 mT, scan time 30 s or 60 s, respectively, centre field 49.1 mT, conversion time 0.2 ms, number of accumulations 3. All measurements were performed in triplicate; data are reported as mean \pm standard deviation (SD).

3.2.1.2 *In vivo* EPR studies on ISFI based on phase separation by solvent exchange

Prior to the EPR measurements the mice were fixed in special constructed polypropylene tubes, which facilitated repeated measurements without the use of anaesthesia. 100 μ l of the TB-containing polymer solution (section 3.1.1, page 20) were injected subcutaneously through a 25 gauge needle in the tight of the mice. Immediately after injection the mice were transferred to the EPR spectrometer and the first EPR spectra were recorded. After the measurement the mice were returned to the animal cage. At predetermined time intervals the femoral-implants were rescanned. The *in vivo* EPR measurements were performed by an L-band spectrometer (MagnetTech, Germany) equipped with a surface coil resonator, operating at a microwave frequency of about 1.1-1.3 GHz. Measurements parameter were set to: modulation amplitude 0.125 mT, scan width 10 mT, scan time 20 seconds, centre field 47.5 mT, conversion time 0.2 ms, number of accumulations 5-10. All measurements were performed in triplicate; data are reported as mean \pm SD.

3.2.1.3 pH-determination by EPR-spectroscopy

The pH-sensitive nitroxide spin probes AT, HM and 2PK (0.25 mM) were calibrated in citrate and phosphate buffer solutions in order to cover a pH range between 1.0 and 12.0. The pH was determined by means of a glass electrode. Aliquots of 1 ml were taken and measured at 1.3 GHz. The recorded EPR spectra (first derivative) were integrated, and the distances between the first and the third peaks were determined as the

measure of $2a_N$. The pH-calibration curves were obtained by a sigmoid Boltzman fit for AT and HM and by a double Boltzman fit for 2PK to the values of $2a_N$.

For the pH determination of the ISFI based on phase separation by solvent exchange AT, HM or 2PK, were incorporated in the polymeric solution to 5 mmol/kg polymer. Additionally 0.2 mmol/l of the corresponding spin probe was added to the incubation buffer (phosphate buffer pH 7.4) to achieve a sufficient signal-to-noise ratio of the EPR spectra even over the long time release process. 200 μ l of the spin probe containing polymer solution were injected through a 25 gauge needle into 50 ml of 0.1 M phosphate buffer (pH 7.4; 37 °C) placed in an incubation shaker (30 rpm). The polymer solutions were injected into perforated plastic cylinders placed in the buffer solutions, where the implants formed immediately. At determined time points the implants were taken out the buffer, the cylinders were dried with wipes and covered by plastic foil to prevent drying and subsequently transferred to the EPR spectrometer. The incubation media was exchanged every second day to prevent the accumulation of degradation products.

For the pH-determination of the chitosan/ β -GP gels, AT (0.25 mM) was dissolved in the chitosan/ β -GP solutions and EPR spectra were recorded from the solutions before and after incubation at 37°C for one hour. EPR spectra were recorded under the same conditions as described above (section 3.2.1.1, page 27). All measurements were performed triplicate, data are reported as mean \pm SD.

3.2.1.4 Spin-labelled insulin release studies

The spin-labelled insulin was dissolved in the chitosan/ β -GP solutions under stirring at room temperature, up to a final concentration of 2 mg/ml or 10 mg/ml, respectively. Samples of 0.50 g were placed in Eppendorf-cylinders and gelled at 37 °C for one hour. The incorporation of the insulin into gels was examined by EPR-spectroscopy at 1.3 GHz and 9.5 GHz.

For *in vitro* release experiments, the gels were incubated with 1.5 ml of phosphate buffer pH 7.4 at 37 °C. At several time intervals 0.5 ml of the buffer was taken as a sample and replaced by new buffer. The *in vitro* release was monitored by EPR-spectroscopy at 9.5 GHz. Therefore an X-Band (9.2 GHz) EPR spectrometer (Miniscope MS 200, Magnettech, Germany) was used. The measurements were conducted with the following parameters: field centre 335 mT, scan range 10 mT, scan time 30 sec, modulation

amplitude 0.1 mT. All measurements were performed triplicate, data are reported as mean \pm SD.

For the *in vivo* EPR measurements the mice were fixed in special constructed polypropylene tubes, as described in section 3.2.1.2 (page 28). 200 μ l of the insulin containing chitosan/ β -GP solution or phosphate buffer (insulin content 10 mg/ml in each case) were injected subcutaneously through a 25 gauge needle in the femoral of the mice. Immediately after injection the mice were transferred to the EPR spectrometer and the first EPR spectra were recorded. After the measurement the mice were returned to the animal cage. At predetermined time intervals the femoral-implants were rescanned. The *in vivo* EPR measurements were performed as described above (section 3.2.1.2, page 28). All measurements were performed in triplicate; data are reported as mean \pm SD.

3.2.1.5 EPR studies on thermally-induced gelling chitosan/olive oil/ β -GP emulsions

For the *in vitro* EPR measurements 200 μ l of the spin probes containing chitosan/olive oil/ β -GP emulsions were injected through a 25 gauge needle into perforated plastic cylinders placed in 50 ml of 0.1 M phosphate buffer (pH 7.4; 37 °C) tempered in an incubation shaker (30 rpm). Following measurements and sample treatment followed the same protocol as described in section 3.2.1.1 (page 27). The EPR spectra were recorded under the same conditions as described above (section 3.2.1.1, page 27). All measurements were performed triplicate, data are reported as mean \pm SD.

The *in vivo* EPR measurements followed the same protocol as described in section 3.2.1.4. Briefly 200 μ l of the spin probes containing chitosan/olive oil/ β -GP emulsions were injected subcutaneously through a 25 gauge needle in the femoral of the mice. Immediately after injection the mice, fixed only for the measurements in polypropylene tubes, were transferred to the EPR spectrometer and the first EPR spectra were recorded. At predetermined time intervals the femoral-gels were rescanned. EPR spectra were recorded at 1.1-1.3 GHz with an L-band spectrometer (MagnetTech, Germany) equipped with a surface coil resonator. The measurements parameter were set to: modulation amplitude 0.125 mT, scan width 6 mT, scan time 20 seconds, centre field 47.5 mT, conversion time 0.2 ms, number of accumulations 5-10. All measurements were performed in triplicate; data are reported as mean \pm SD.

3.2.1.6 Spectra evaluation

The “Cu3 v.6.1” program (MagnetTech, Germany) was used for data recording. The program “Analysis” (MagnetTech, Germany) served for calculation of polarity shifts inside the implants by determining $2a_N$ and double integration of the recorded and simulated spectra. Rotational correlation times τ_c and the proportion of immobilized TB inside the implants was calculated from EPR spectra fitted with “Nitroxide Spectra Simulation - Freeware Version. 4.99-2005” (Jozef Stefan Institute, Department of solid state physics, Ljubljana, Slovenia). For spin quantization the area under the curve of the doubled integrated EPR spectra was calculated with Microcal™ Origin® (Microcal Software Inc. USA) and normalized to AUC₁₀ as 100 %. In case of baseline drifts or low signal to noise ratios the recorded EPR spectra were simulated and the simulated spectra were used for double integration to improve the accuracy of the double integration and to eliminate noise and baseline distortion.

3.2.2 Magnetic Resonance Relaxometry and Imaging

Nuclear Magnetic Resonance is one of the most important spectroscopic techniques in biological and medical research, as well as in the fields of physics, chemistry and material sciences [113-116]. Certain nuclei (e.g. ^1H , ^{13}C , ^{31}P or ^{19}F) possess a magnetic moment. In the presence of a strong magnetic field these nuclear spins align either parallel or anti-parallel to the static magnetic field (B_0), analogous to the electron spins of unpaired electrons (section 3.2.122). The spins are distributed between the two different energy levels in a thermal equilibrium with the lattice, governed by the Boltzmann distribution (Formula 2).

$$\frac{N_{\downarrow}}{N_{\uparrow}} = \exp\left(-\frac{\Delta E}{kT_s}\right) = \exp\left(-\frac{\gamma\hbar B_0}{kT_s}\right)$$

Formula 2 Boltzman equation of the thermal equilibrium of nuclei distributed between the upper and lower energy level, where N_{\downarrow} and N_{\uparrow} are the number of spins in the upper and lower energy level, respectively, k is the Boltzman constant, T_s is the absolute temperature of the spin system and ΔE is the energy required for transition between the energy levels, characterized by the gyromagnetic ratio γ , the external static magnetic field B_0 and $\hbar = h/2\pi$, where h is Planck's constant

The very slight surplus of spins in the lower energy level results in a net magnetisation in one direction. The application of another magnetic field perpendicular to B_0 in the form of a short radio frequency (RF) pulse alters the spin distribution. The absorption of

energy under resonance conditions induces spin transfer from the lower to the upper energy level. In the absence of the RF-pulse spins in the higher energy level relax to the lower level to re-establish the initial spin population distribution. During this relaxation process the nuclei spins exchange energy with their surroundings (the lattice) or between the individual nuclear spins. The time of the relaxation process depends on the nuclear environment and is characterized by two major time constants: spin-lattice relaxation time (T_1) and spin-spin relaxation (T_2). The spin-lattice relaxation characterize the exponential recovery of the longitudinal magnetisation that is aligned with B_0 in the equilibrium [114]. T_1 describes the time required to regain the longitudinal magnetization. During spin-lattice relaxation the surplus resonance spin energy is transferred as motional energy to the lattice and so T_1 depends on the molecular motion and therefore macroscopic viscosity and density of the sample [117]. Further T_1 depend considerably on the NMR frequency and the magnetic field strength. The spin-spin relaxation is a marker of the precessing part of the magnetisation and describes the decay of the NMR signal [114]. T_2 is a measure of how long the resonating protons remain coherent (precess in phase) following a 90° RF pulse. The T_2 decay is caused by magnetic interactions between spinning protons, leading to a loss of coherence by local field non-uniformities. T_2 depends on the physical properties of the sample (density and viscosity) but also on the magnetic field strength. T_2 vary in different nuclear environments and may act as a marker for the molecular mobility of the spins [117;118]. Because the NMR signal is intrinsically weak, most applications detect ^1H nuclei due to it's naturally abundance of incidence in high concentration. Therefore bulk ^1H -NMR measurements of relaxation times and self-diffusion coefficients have been used to investigate the microscopic heterogeneity of samples and changes thereof [119]. Especially in food sciences NMR relaxometry has reached a wide public [117;119]. Examples include the detection of changes in water mobility during renneting and fermentation of casein solutions [120] and the detection of water content and mobility in cookies and cereals in milk [121]. In material sciences NMR Relaxometry was used to investigate lubricant oil decomposition [122] or the wetting and swelling kinetics in high-organic matter soils [123]. The application of NMR Relaxometry in drug delivery research has been recently reviewed by *Metz and Mäder [117]*. Water distribution in cellulose ether hydrogels was studied by analysing T_1 and

T_2 relaxation times and the diffusion properties of water in partly soluble pellets was investigated [119].

Lauterbur and Mansfield firstly introduced tomographic experiments by the concept of spatially resolved NMR signals. They were awarded together the Nobel Prize in 2003 for contributions to the development of the Magnetic Resonance Imaging (MRI). Spatial encoding of the NMR signal in up to three dimensions can be achieved by applying one or multiple magnetic field gradients in addition to the uniform static magnetic field during NMR acquisition. Further details on the backgrounds and the technique itself are published more detailed in textbooks and in literature [114;115;124;125]. The signal intensity of an MR image depends upon the spin density, which is related for ^1H -NMR to the water concentration, as well as T_1 and T_2 values of the sample, which are related to the water mobility. By application of appropriate pulse sequences the signal intensity of the image can be weighted to show variations of the relaxation times [114;119]. The majority of pharmaceutical applications of MRI focused on the hydration, swelling and dissolution of solid dosage forms, such as matrix tablets, film-coated tablets, pellets or polymeric implants [114;126-130]. Further it has been used to follow the fate of parenteral drug dosage forms *in vivo*, e.g. subcutaneously administered polymeric implants, lipid emulsions and hydrogels [130-132]. Pilot human studies investigated the food-dependent variability of the residence time of floating tablets in the stomach [133]. Compared to the widespread use for clinical diagnostic, MRI has found a limited application in drug delivery research, despite its high potential, especially for the *in vivo* analysis of the fate of drug dosage forms. The major reasons are the high installation and running costs of high-field NMR instruments with their superconducting magnet technology and the specific expertise to operate them. Low-field MRI instruments, that uses permanent magnets and no cryogenes, represent a low cost alternative, and have been used in food and petrochemical industries since many years. Recently the rather new technique of low-field MRI, also called Bt-MRI has been successfully applied to characterize tablets and scaffold *in vitro* [128;134], By the use of a prototype the fate of contrast agents [135] could be followed in mice. Despite the lower frequency the low-field NMR instruments yielded a sufficient image resolution to follow dissolution and distribution processes [117].

3.2.2.1 *In vivo* Bt-MRI studies

About 200 μl of the polymer solution and PEG 400, as control, were injected in the lower back of the mice. The mice were anesthetized prior to injection and each measurement by inhalation of isoflurane (Forene[®], Abbott, Germany) (initially 4 %; subsequently to maintain anaesthesia 2 % mixed with oxygen 4 l/min by a Vapor System, Dräger, Germany). MRI measurements were carried out at regular intervals after every 10 min within the first hour after injection and then after 2 h, 3 h, 6 h and 24 h. The subsequent measurements were performed once a week over a total period of 2 months. Two 50 μl glass capillaries filled with PEG 400 served as a standard. All measurements were performed in triplicate.

For the MRI measurements a 20 MHz NMR benchtop system (prototype based on Maran DRX2, Oxford Instruments Molecular Biotools, UK) was used. The system is capable of T_1 and T_2 relaxation time measurements, determination of diffusion coefficients and 3D imaging. The Bt-MRI machine is equipped with a 23 mm sample access, suitable for small animals and keeps a constant temperature of 37 °C inside the coil. So no additional heating device for the anesthetized mice was necessary. The mice were placed on glass slides with a fixed inhalation mask for anesthetization. A standard spin-echo sequence was used with a spin echo time (TE) of 9.8 ms and a repetition time (TR) of 178 ms. 16 averages were applied resulting in an acquisition time of about 352 s for each image. The field of view was 40 mm x 40 mm with a resolution of 128 x 128 points. 5 slices with a thickness of 3 mm and a separation of 3.5 mm were obtained.

3.2.2.2 NMR-Relaxometry on thermo-responsive hydrogels and emulsions

A 20 MHz NMR benchtop system (Maran DRX2, Oxford Instruments Molecular Bio Tools UK) was used. The instrument is equipped with 18 mm sample access, variable temperature control and imaging unit. NMR relaxometry was performed in the temperature range of 5 °C to 50 °C. The CPMG sequence was used for T_2 relaxation analysis. The transverse magnetization decays were fitted with the program WinDXP (Oxford Instruments, Abingdon, UK) and T_2 distributions were calculated.

3.2.3 **Oscillating rheology of thermo-responsive hydrogels and emulsions**

A strain controlled oscillating rheometer "Rheometrics Fluids Spectrometer RFSII" from Rheometrics Inc. (Piscataway, NJ, USA) was used at 25 °C. The rheometer was

equipped with a cone – plate geometry ($d = 50$ mm, taper angle $\alpha = 0.0412$ rad = 2.36° , cone – plate distance 0.051 mm. An amplitude test was carried out first at a radial frequency of $\omega = 6.28$ rad/s = 1s^{-1} with a strain range from 0.1% - 100% . The results indicated that a deformation of 1% is within the linear viscoelastic range. Therefore, the following parameters were used for the frequency sweep tests: strain (γ) 1% , frequency ranges 0.01 rad/s– 100 rad/s.

3.2.4 Sol-to-gel study of thermosensitive hydrogels by vial inversion method

The occurrence of the sol-to-gel transition was employed by vial inversion method [136], which has already been used to test the gelling time [137]. About 1 ml of the chitosan/ β -GP solutions were filled into glass vials, closed and stored for at least 12 h at 4°C to remove air bubbles. Then the vials were incubated in a temperature-controlled bath. The sol-to-gel transition was determined by inverting the test tube horizontally every minute, by increasing the temperature from 20°C to 70°C with a heating rate of $0.4^\circ\text{C}/\text{min}$. The sol phase was defined as a flowing liquid when the chitosan/ β -GP solution was inverted, the gel phase as a nonflowing gel [136]. The temperature at which the gel did not flow was recorded as transition temperature.

3.2.5 Light microscopy

An Axiolab light microscope (Carl Zeiss, Germany) with an optical zoom of 50×0.70 was used for sectional view of ISFI.

3.2.6 Statistical evaluation

Unless otherwise reported all data are presented as mean \pm SD. Statistical significance was proved by one-way ANOVA test followed by TURKEY'S test.

4 Results and discussion

4.1 In situ forming implants based on phase separation by solvent exchange

An increasing number of in situ forming depot systems based on solvent exchange induced phase separation that have been published in the recent years [73;74;76-78;85;87;92]. But only two products, Atridox[®] [70] and Eligard[®] [71], are currently on the market using this implant forming mechanism. Both pharmaceuticals base on the Atrigel[®] technology developed by *Dun et al.* [72]. They consist of PLGA dissolved in the water miscible, physiological compatible organic NMP. After injection the polymer precipitates during solvent (NMP)/non-solvent (body fluids) exchange. Initial drug release occurs simultaneously with the formation of the implant by non-solvent induced phase separation. In this connection the phase inversion dynamics of the polymer solutions have a direct effect on the drug release behaviour and the implant morphology. Typical release profiles consist of distinct regions of initial burst followed by diffusion and erosion controlled release and a final period of drug depletion [80;83;138]. To control the initial burst release is one of the greatest challenges to translate ISFI systems from bench to bed side. In order to influence the burst effect several formulation parameters have been examined to control the rate of polymer precipitation, e.g. the concentration and the type of polymer and the type of solvent or co-solvent [80;82]. But to really control the drug release characteristics it is important to quantify not only the release rates, but more important the dynamics of the phase separation process both *in vitro* and *in vivo* under physiological conditions. Only a few techniques are available to evaluate the dynamics of non-solvent-induced phase inversion. *McHugh et al.* developed a dark-ground video imaging technique to visualise and quantify the phase inversion dynamics of several PLGA solutions [83;84]. However this technique is limited to *in vitro* experiments and the evaluation of thin films over a short time scale (minutes to a few hours). So there is only very limited knowledge about the *in vivo* situation, due to the difficulty to study such complex systems. Unfortunately most frequently applied analytical methods for the characterization of implants, such as different kinds of chromatography, infrared spectroscopy, differential scanning calorimetry and optical microscopy with or without histological staining are either limited to *in vitro* experiments or require the surgical extraction of implants by killing

the animal. Additionally the required special sample preparation may lead to artefacts [83;139;140]. Another common imaging technique to study the implant's morphology is scanning electron microscopy [138]. One shortcoming of this technique is its destructive character, since the sample preparation involves freezing and sectioning of the implants. In addition, all these procedures exclude continuous studies with the same sample on a single animal. These conventional *in vivo* experiments require a large number of animals, which does not comply with the international efforts to reduce the number of animal experiments.

In 2010, parallel to presented studies below, *Solorio et al.* introduced diagnostic ultrasound to visualize and quantify non-invasively the process of implant formation by polymer precipitation *in vitro* and *in vivo* [141]. However ultrasound imaging is limited by the resolution of the images and therefore suited for the macro-scale analysis of the implants and cannot measure the solvent exchange process.

The aim of the present studies was to develop non-invasive methods to monitor the phase inversion dynamics and implant formation in real time *in vitro* and *in vivo*. Following the implant formation the implant localisation, disintegration and the response of the biological systems should be followed continuously. For this purpose the magnetic resonance techniques MRI and EPR spectroscopy were selected as suitable methods. Both techniques are well suited for serial and real time *in vivo* measurements because of their non-destructive and non-invasive nature [101;114]. The following section deals with investigation of the applicability of MRI and EPR spectroscopy for the real-time monitoring of ISFI formation and disintegration processes.

4.1.1 Real-time monitoring of polymer precipitation and solvent exchange

4.1.1.1 Feasibility study on PLGA-NMP in situ forming depots

As described in section 3.2.1 the EPR method allows the non-invasive detection of the interactions of paramagnetic compounds, consisting of one or more unpaired electrons, with their direct environment in complex and non-transparent samples. Using nitroxides as spin probes or spin labels unique information about the microviscosity, micropolarity and spatial distribution inside drug delivery systems can be obtained. Thus water penetration, drug release and polymer erosion of polymeric implants have been monitored *in vitro* and *in vivo* [60;130]. To test the applicability of EPR spectroscopy to monitor the phase inversion process, PLGA/NMP solutions derived from the Atrigel[®] technology were chosen. PLGA was selected because co-polyesters of lactic and glycolic acid belong to the most relevant polymers with respect to their clinical use [142]. The moderate lipophilic nitroxyl TB (structure Figure 2, page 20) was used as both a model drug and as marker molecule. TB is poorly water soluble ($\log P = 2.46$), comparable to Griseofulvin ($\log P = 2.18$) and Diazepam ($\log P = 2.92$) [143]. Due to the high sensitivity of the EPR method, only 415.5 $\mu\text{g/ml}$ polymeric solution of the spin probe were used. Therefore any effects of the incorporated marker molecule on the phase inversion kinetics can be neglected.

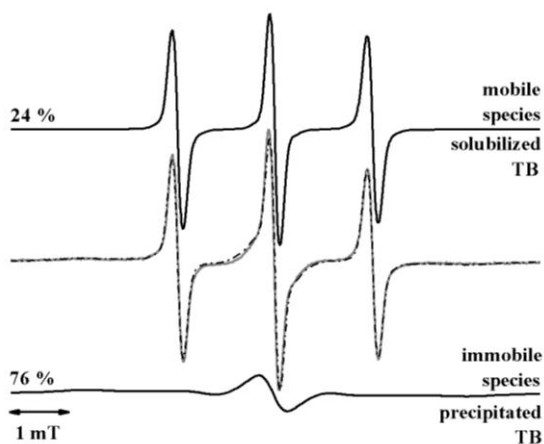


Figure 10 *In vitro* EPR spectra of TB loaded implant exposed to phosphate buffer (center) (after 30 min) and simulation (dashed line) of mobile (solubilized TB, top) and immobile (precipitated TB, bottom) spectral pattern

Typical parameters that could be obtained from EPR spectra are the hyperfine coupling parameter ($2a_N$) and the rotational correlation time (t_c). Magnetic interaction between the free electron and the nuclear spin ($N = 1$) of the nitrogen results in a hyperfine splitting of three lines (Figure 10). The distance between the low and high field lines of the EPR spectrum ($2a_N$) depends on the polarity of the nitroxide environment (Figure

11). In regions with high polarity (e.g. water) the distance between the outer lines of the EPR spectra is increased, compared to region with low polarity (e.g. oil) [101].

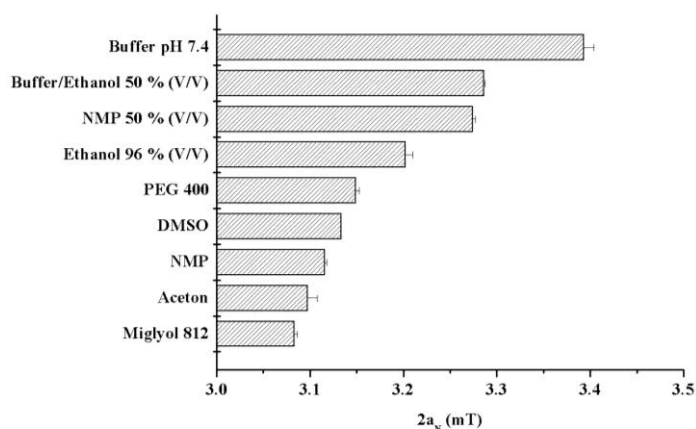


Figure 11 Influence of environments with different polarities on the hyperfine splitting $2a_N$ of TB

The microviscosity, another parameter of the microenvironment, strongly influences the tumbling behaviour of the nitroxyl radicals. In low viscous media they tumble freely, resulting in highly symmetric spectra with three narrow lines and rotational correlation times in the order of 0.01 ns to 0.1 ns (Figure 12). An increase of the viscosity decreases the molecular tumbling rate of the nitroxide.

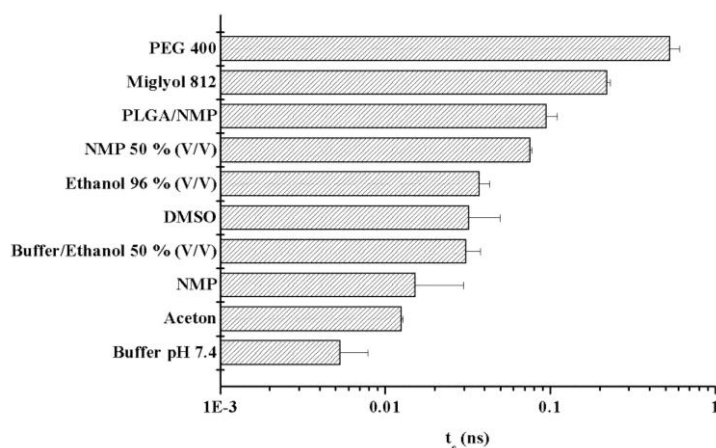


Figure 12 Influence of environments with different viscosities on the rotational correlation time t_c of TB

Due to their restricted motion the anisotropy of the hyperfine interaction is only partially or not averaged, which results in a line broadening and a decrease of the signal amplitude (Figure 14) and an increase in t_c (Figure 12) [95;103].

To follow ISFI formation, PLGA/NMP implant solutions were injected into buffer or mice and the changes in the EPR signals were monitored. The EPR spectra of the PLGA-NMP solutions indicated a highly mobile environment with the typical three sharp lines (Figure 14) and rotational correlation times of $0.095 \text{ ns} \pm 0.015 \text{ ns}$. The

dissolved polymer led to a fourfold increase of the rotational correlation time of TB dissolved in the PLGA/NMP solution ($0.022 \text{ ns} \pm 0.003 \text{ ns}$).

After injection, the NMP diffused into the surrounding aqueous environment, while water diffused into the PLGA matrix. The PLGA precipitated and formed a solid implant with an NMP containing core inside (Figure 13).

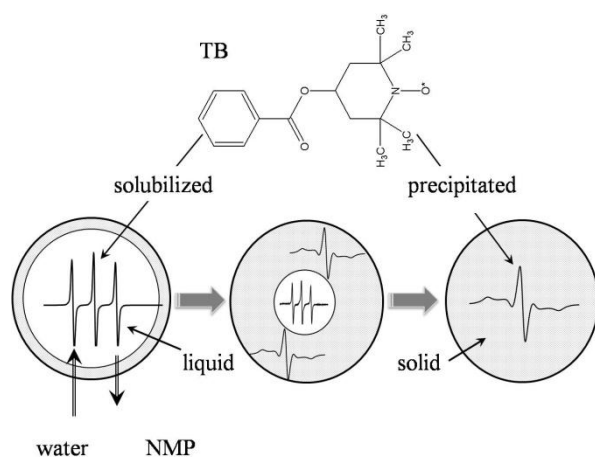


Figure 13 Schematic illustration of the formation-mechanism of an injectable in situ forming system and its characterization by EPR

Thus implant formation could be followed by EPR. Figure 10 shows EPR spectra from the PLGA-implant *in vitro* after 30 minutes of incubation with phosphate buffer. A superposition of two species within the spectra was detectable. TB precipitated within the PLGA and its mobility was restricted. The immobilization of TB resulted in so-called powder-like spectra (Figure 10) with an increase by one order of magnitude in t_c $0.816 \text{ ns} \pm 0.060 \text{ ns}$. About 24 % of the entrapped TB molecules were still mobile and located in the NMP containing core at this time point, showing the same mobility as in the PLGA/NMP solution ($0.096 \text{ ns} \pm 0.033 \text{ ns}$). Similar spectra were obtained from *in vivo* EPR measurements. The EPR spectrum, detected as the first derivative, is very sensitive to mobile nitroxides with their narrow lines. In superimposed spectra they are detectable below one per cent [106]. Due to their broad lines and low signal amplitude, the immobilized TB is much more difficult to detect. It can be easily overlooked if only the first derivative (the most common form) of EPR spectra is considered. To increase the visibility of the immobilized (precipitated) species the EPR spectra were integrated. Figure 14 shows TB spectra from the implants after different times of incubation in buffer or living mice in the recorded (first derivative) and integrated form.

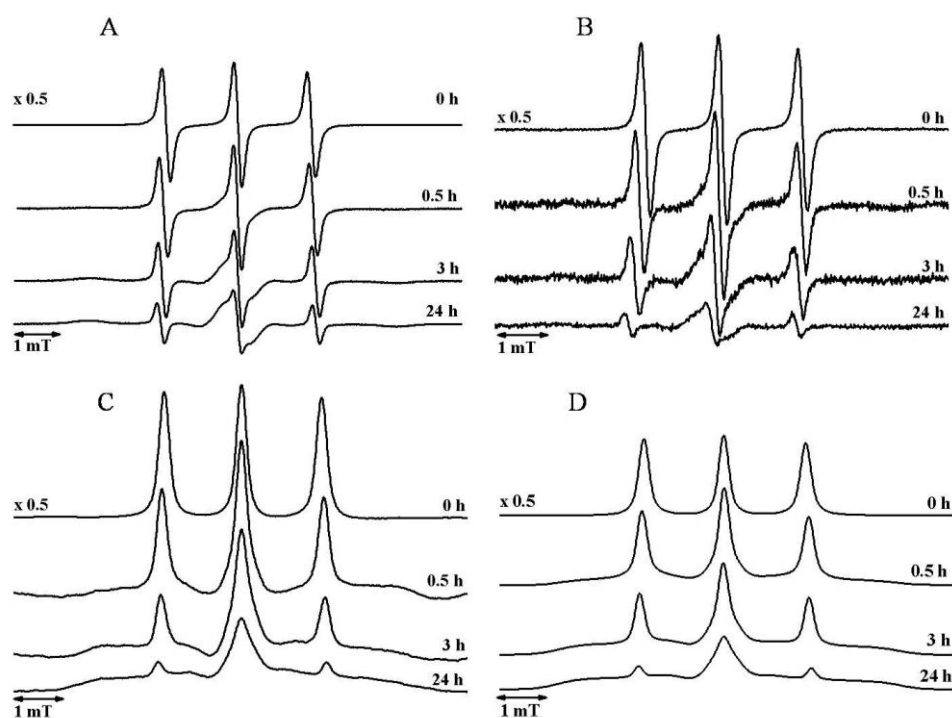


Figure 14 EPR spectra of TB loaded implants exposed to buffer (A - recorded, C - integrated) or in mice (B - recorded, D - integrated).

With increasing incubation time a decrease in the signal amplitude of the outer lines and line broadening was detectable both *in vitro* and *in vivo*. The progress of implant solidification was quantified by simulation of the mobile and immobile species and determination of the proportion of the immobile spin probe (Figure 15).

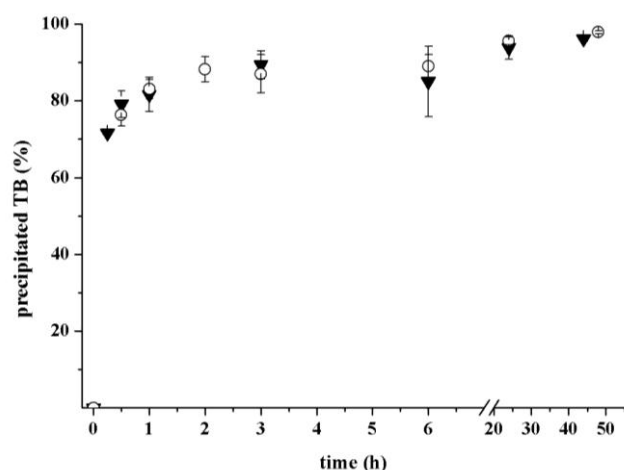


Figure 15 In vitro (○) and in vivo (▼) distribution of precipitated TB in the implant during implant formation

To assure that no spin probe containing buffer interferes with the determination of the TB distribution inside the implant, adsorbed buffer was carefully removed prior to the

in vitro measurements. The EPR signals observed *in vivo* are only caused by TB entrapped inside the implant. The released TB molecules diffused rapidly into the surrounding tissue or blood stream where a fast reduction to the EPR silent hydroxylamine occurred.

The phase inversion dynamics and precipitation of PLGA took place by variable velocity. Immediately after injection a thin PLGA shell was formed. The solvent NMP and dissolved TB diffused through the polymer shell into aqueous environment. At the same time water diffused inside the implant and induced PLGA and TB to precipitate. After 30 minutes $76 \% \pm 3 \%$ and $72 \% \pm 0.1 \%$ of the TB was immobilized within the polymer matrix, *in vitro* and *in vivo* respectively. Furthermore TB was located in an aqueous environment which was created via water penetration inside the implant. Thereafter the phase inversion and polymer precipitation decelerated. Due to the increasing hardening of the PLGA and further precipitation of the polymer the diffusion distances increased. With progressing polymer precipitation the shell thickness grew (Figure 13). The extended diffusion distances inside the implant and resulted in prolonged diffusion times for NMP outside and water inside the implant. According to the Einstein-Smoluchowski equation (Formula 3) [144], where D is the diffusion coefficient, d the distance and t the time, the diffusion time increased with the square of the diffusion distance.

$$D = \frac{d^2}{2t} \rightarrow t = \frac{d^2}{2D} \text{ Formula 3 Einstein-Smoluchowski equation}$$

As a result polymer precipitation decelerated. After a period of fast TB precipitation in the first 60 minutes ($83.1 \% \pm 2.1 \%$ *in vitro* and $81.7 \% \pm 4.5 \%$ *in vivo*), the proportion of immobilized TB increased to a minor rate within the subsequent five hours ($89.1 \% \pm 3.0 \%$ *in vitro* and $85.0 \% \pm 9.2 \%$ *in vivo*). The implant formation was almost completed ($95.6 \% \pm 1.0 \%$ *in vitro* and $94.0 \% \pm 3.0 \%$ *in vivo*) after about 24 hours (Figure 15). The remaining TB located in a mobile environment is supposed to be located in inner pores.

The obtained results are supported by experiments from *McHugh et al.*, who described the formation of a rigid, interconnecting porous structure framed by a polymer skeleton [77]. The authors observed an initial burst effect of human growth hormone followed by

prolonged period of little protein release. The initial burst was correlated with the rapid diffusion of the protein in or near these interconnecting pores. While the little long time release rate was related to protein being entrapped in the hardening polymer.

The phase inversion dynamics of PLGA solutions are complex processes, which are directly affected by the solvent properties [83], solvent/non-solvent affinity [84] as well as the molecular weight [138], end-group functionality [82] and concentration of the polymer [78;84]. The release rate of drugs is interdependent to the rate of implant formation [80]. In the recent years the main focus of the research on ISFI based on PLGA in organic solvents was to characterize the drug release behaviour and the implant morphology. So there is scarce data available to compare the results of the dynamics of PLGA precipitation and solvent exchange. *Solorio et al.* used diagnostic ultrasound to quantify the process of implant formation *in vitro* and *in vivo* of a 40 wt% PLGA (50:50, MW 29 kDa) solution in NMP [141]. *In vitro* the fluorescein release within the first 48 h showed a high degree of correlation with the precipitation of the polymer. The direct relation between polymer precipitation and drug release diminished as the way of drug release proceeds from burst to a form of diffusion mediated type. Although *Solorio et al.* used higher concentrated polymeric solution (40 wt% versus 30 wt%) the phase inversion dynamics were similar *in vivo*. Within 8 hours about $86 \% \pm 5.0 \%$ of the polymer precipitated of the total cross sectional area and reached a plateau after 24 h with a maximum value of $90 \% \pm 6.4 \%$. By comparison the presented data obtained by EPR spectroscopy exhibited a higher initial quantity of precipitated TB within the polymer of $85.0 \% \pm 9.2 \%$ after six hours. But comparable value of $94.0 \% \pm 3.0 \%$ of precipitated PLGA was achieved after 24 hours. *Graham et al.* found that higher polymer concentrations entailed a higher viscosity of the injected solution and decreased the system diffusivities. The increase in polymer concentration resulted in lower water influx and phase separation rate and the morphology of the implants changed to less porous sponge type-structures [83]. The different analysis techniques gave different insights from the implants, reflected by different results for the precipitation rates within the first hours. By EPR information about the whole implants microviscosity and micropolarity were obtained. Whereas only the cross sections of the middle of the implant were analysed by diagnostic ultrasound. As mentioned before the polymer precipitation proceeds from the shell to the core of the implant (Figure 13). In

the early steps of implant formation the centre is still liquid consisting of PLGA/NMP solution. Despite similar results for *in vivo* precipitation rate of PLGA, they differ *in vitro*. In *Solorio*'s experiments the implant formation was delayed compared to *in vivo*. The polymer reached about 90 % precipitation after 96 h [141]. To facilitate ultrasound imaging and imitate *in vivo* conditions implant solutions were injected into agarose phantoms instead of water. But solvent/water exchange is limited in the agarose phantoms hindering phase inversion [141]. The direct implants environment plays a crucial role during implant formation process [84]. *Kranz et al.* compared the *in vitro* bupivacaine release from in situ forming implants and in situ forming microparticles obtained by different *in vitro* methods [145]. The initial drug release decreased along with increased contact of implant surface to the medium in the following order: direct injection method > dialysis bag > vial method (water contact restricted to one site). So far no regulatory guidelines have been established for experimental conditions to assess the performance of parenteral controlled drug delivery systems and ISFI in special. Various experimental setups have been reported in literature, e.g. agitated or non-agitated vials, dialysis membranes or agarose gels [84;145]. Further the composition of the release medium and the device to bulk fluid ratio directly affect the performance of the systems [80;146-148]. Therefore special cautions to the experimental conditions have to be paid when comparing results. An optimal *in vitro* method that assure sink conditions, reproducibility of sampling, prediction of *in vivo* release has not been developed yet.

The replacement of NMP by water is a critical step during implant formation and strongly influences the drug release. Alterations in the surrounding micropolarity of TB can be detected via the hyperfine splitting parameter $2a_N$. The higher the water content, the more polar the environment of TB, the larger is the distance between the first and the third peak. Therefore the values $2a_N$ were determined from the spectra and were plotted against the concentrations of NMP in different NMP-buffer mixtures (Figure 16). The micropolarities of the implants were determined from the obtained calibration curve.

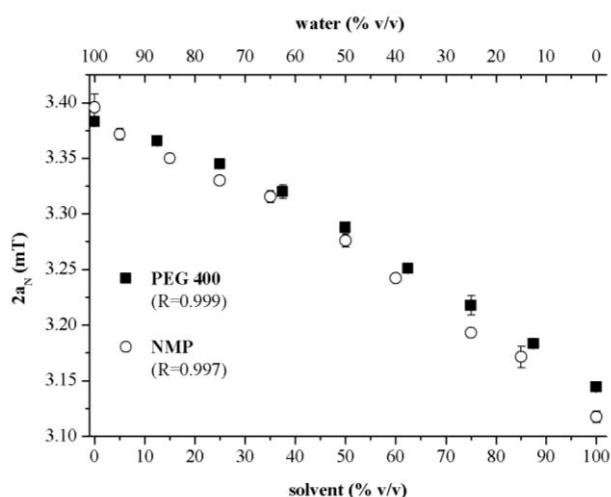


Figure 16 Dependence of the isotropic hyper-fine splitting $2a_N$ in different NMP-buffer and PEG 400-buffer mixtures. The hyperfine splitting parameter correspond to the NMP and PEG 400 concentrations and can therefore be used to determine phase inversion induced changes in micropolarity inside the implants

Within one hour water penetrated into the implant and replaced approximately 50 % of the NMP *in vitro* inside the PLGA-implant (Figure 17). *In vivo*, the velocity of the NMP-water exchange was slightly slower; where approximately 40 % of the NMP was displaced by water. Further solvent release decelerated with increasing thickness of the polymer shell. The initial faster *in vitro* water influx rate could be associated with a higher volume of the aqueous environment. Remarkably over 25 % of the NMP was still incorporated inside the implants after 24 hours *in vitro*, compared to about 10 % *in vivo*. This fact may be attributed to different surface to volume ratios, formed depending on the subcutaneous cavity into which they were injected and the different surface tension and available volume of the body fluids.

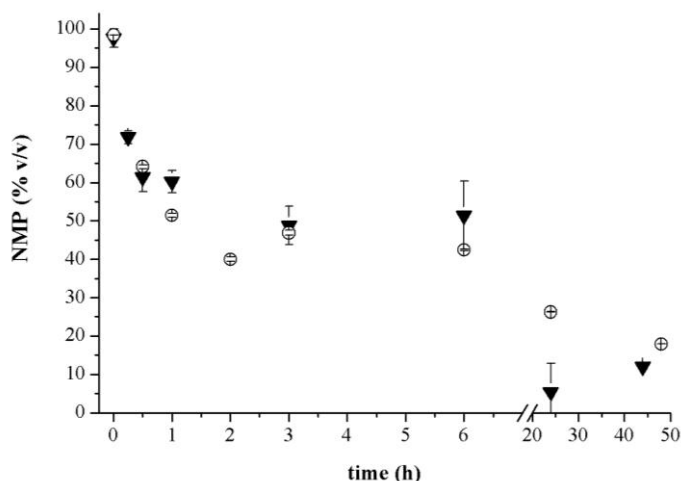


Figure 17 *In vitro* (○) and *in vivo* (▼) kinetics of NMP-water exchange in the implant core (determined by EPR)

Both the kinetics of solvent exchange (Figure 17) and polymer precipitation (Figure 15) showed similar behaviour and good *in vitro* - *in vivo* correlation (Figure 18).

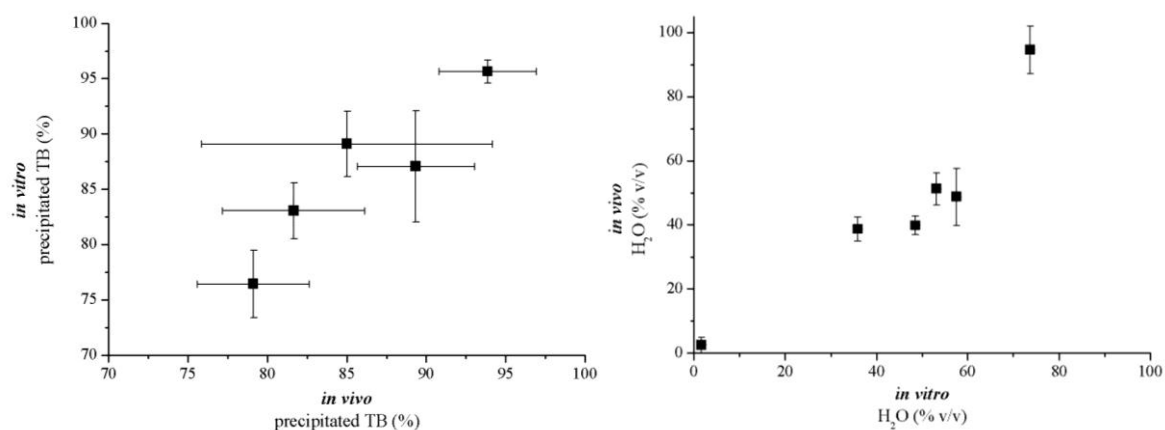


Figure 18 *In vitro* - *in vivo* correlation of (left) the kinetics of polymer precipitation and (right) NMP-water exchange

It is widely known that the device geometry, size and shape, strongly impacts the release rates and degradation kinetics of PLGA based microparticles, films and scaffolds [139;146]. However the influence of the implant geometry on the performance of ISFI received little attention so far. The geometry of ISFI depends on several factors, such as injection speed, size and volume of the cavity to inject and resistance of the surrounding tissue. To evaluate the impact of the implant shape on the phase inversion kinetics, the solvent exchange of worm-like implants (string) was compared to bubble like implants (Figure 19). Different implant shapes were obtained by varying the degree of syringe movement during injection. The shape determined the distance for NMP diffusion outside the implant and therefore the exchange rates. Due to increasing polymer precipitation, diffusion distances extended inside the implant. This effect is more pronounced in later steps (6 hours to 24 hours after injection) of implant formation. Since NMP is a good solvent for TB, the differences in the solvent exchange were also reflected with the total amount of spin probe incorporated inside the implants (Figure 19). To quantify the amount of incorporated spin probe the area under the curve (AUC) of the double integral of the EPR spectra were determined. Quantitative EPR is a challenging task, since spectra with baseline drifts and low signal to noise ratios decrease the accuracy and reproducibility of double integration and afterwards calculating of the AUC [149]. Therefore the simulation of the spectra was used to improve the accuracy of the double integration and to eliminate noise and baseline distortion.

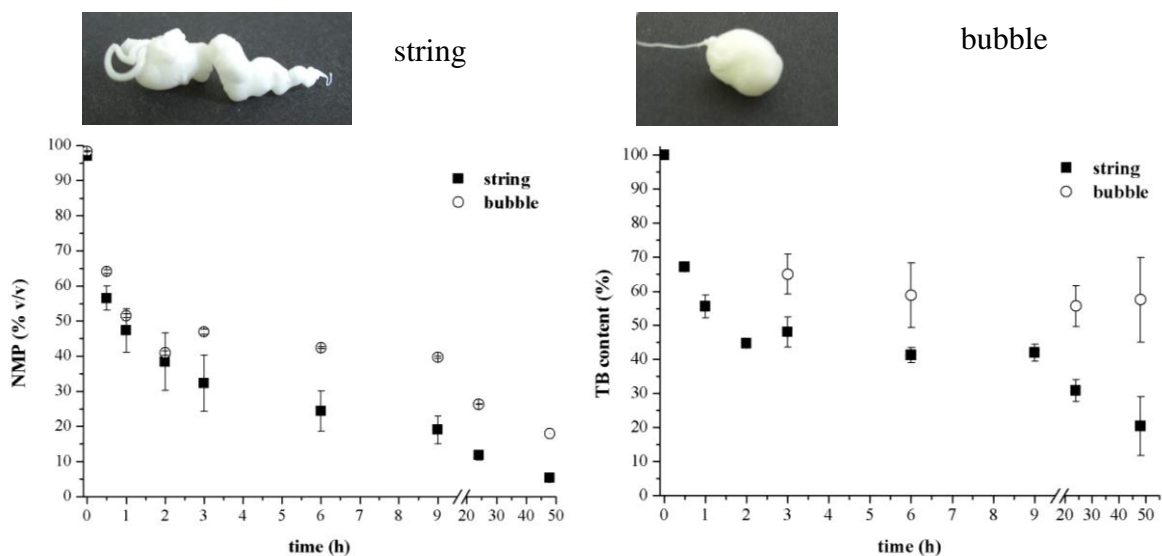


Figure 19 (top) photograph of implants with different shapes: (left) string and (right) bubble and (bottom) the impact of the implant shape on kinetics of NMP-water exchange (left) and content of incorporated TB (right), (■) string (○) bubble (determined by EPR *in vitro*)

The release of TB is characterized by a burst followed by only moderate release. Within the first three hours the TB content in the bubble-shaped implants decreased to $65.0\% \pm 5.8\%$ compared to $48.1\% \pm 4.5\%$ in the string-shaped implants. Meanwhile water replaced about 60% of the NMP in the bubble-shaped implants versus about 68% in the string-shaped implants. After 24 hours still $55.6\% \pm 6.0\%$ versus $30.8\% \pm 3.2\%$ of the spin probe and $26.3\% \pm 0.1\%$ versus $11.7\% \pm 1.3\%$ of NMP were detectable inside the bubble-shape and string-shaped implants, respectively. In summary the geometry of the formed implant strongly affected the amount of the entrapped and release rates of as well the organic solvents as the model drug. To minimize the form-dependent variations in the *in vitro* experiments implant solution were injected to obtain bubble-shaped implants.

The determination of the remaining NMP is important for the development and characterization of ISFI for protein delivery. For example leuprolide acetate tends to aggregation when dissolved in NMP [81]. The few solvent removal studies published in literature all measured the amount of migrated solvent from the polymeric implant into the buffer [150;151]. *Bakhshi et al.* found that the drug release profile of naltrexone hydrochloride of PLGA/NMP ISFI were in good agreement with the solvent removal profiles. The formulation composed of 33 wt% PLGA (50:50, Mw 13 kDa) exhibited a

high initial solvent exchange (about 50 %) within the first day continued by a prolonged period of slow continuous removal of NMP. The higher NMP content in the depots after one day may be explained by the experimental setting in a vial, which permitted diffusion to take place only in one direction. More comparable results were reported by *Schoenhammer et al.* [150]. They investigated solvent diffusion kinetics in dependence of the implant surface area, PLGA content and the affinity of the solvent to water. The release kinetics of the solvents were in accordance to the initial release of the dissolved hydrophilic compound methylene blue. The removal rates for NMP from 40 wt% PLGA solutions were in good agreement with the presented EPR results. After three hours small surface area implants remained about 65 % of NMP, constantly decreasing to about 36 % after 24 hours. Whereas from implants with nearly threefold increased surface areas a complete NMP release was observed within 48 hours.

4.1.1.2 The influence of the polymer type on phase inversion dynamics

Over the past decades PLGA polymers have been investigated extensively for a wide variety of pharmaceutical and biological applications [152]. The advantage of PLGA includes their biodegradability by simple hydrolysis of the ester backbone in aqueous environment. The degradation products can be further metabolized to carbon dioxide and water. However the strong hydrophobic character of these polymers has caused some limitations, especially for delivery of hydrophilic molecules like proteins [103;153;154]. The hydrophilic proteins may lose their activity by deamidation, misfolding or acylation [153]. Another contributing factor for activity loss is the degradation of PLGA. PLGA degradation is characterized by autocatalysis. The carboxylic end groups of degraded products are able to accelerate the degradation and decrease the local pH inside matrices to values as low as pH 2. The acidic microclimate is further responsible for protein degradation [60;155]. One strategy to minimize hydrophobic interactions is the incorporation of the hydrophilic PEG into biodegradable polyesters. PEG is a non-toxic water soluble polymer. Low molecular PEGs can be easily excreted by humans. Various kinds of block copolymers with different block structure and composition have been developed. According to their block structure they can be classified as AB diblock, ABA, or BAB triblock, multi-block, and star-shaped block copolymers, in which A is a hydrophobic block made up of biodegradable

polyesters and B is a hydrophilic PEG block [156]. The degradation kinetics and water-solubility of block copolymers can be tailored by varying the chemical composition and molecular weight. In general low molecular weight polymers composed of shorter hydrophobic blocks are soluble in water. Whereas polymers with high molecular weight and longer hydrophobic blocks are not water soluble but swell in water. Degradation times are shorter for low molecular weight polymers and more hydrophilic polymers [157]. Di- and triblock copolymers of PLGA have been investigated for a variety of drug formulations, such as micelles [55], hydrogels [158], implants [159], thermoresponsive gels [57;160] or as nano- and microparticles [156].

Recently diblock copolymers of PEG and PLGA have become commercial available, what foster their use for nano- and microparticles [161;162]. But the use of these polymers for in situ forming depots based on phase inversion has not been investigated yet. Therefore the influence of polymer hydrophilicity and molecular weight on the phase inversion dynamics was examined by comparing PLGA with PLG-PEG of different PEG-content. The composition and molecular weight of the studied polymers are listed in Table 2. All polymers were dissolved in equal concentration of 30 wt% in NMP. The kinetics of polymer precipitation and solvent exchange were determined by EPR spectroscopy as described in section 4.1.1.1.

Table 2 Composition and molecular weight of investigated polymers

<i>Polymer</i>		<i>Lactic/ glycolic acid ratio</i>	<i>PEG content [wt%]</i>	<i>PEG Mw [kDa]</i>	<i>Total Mw [kDa]</i>
<i>Brand name</i>	<i>Abbreviation</i>				
Resomer [®] RG 503H	PLGA	1:1	--	--	34
Resomer [®] RGP d50105	PEG10-PLGA	1:1	10	5	50
Resomer [®] RGP d 50155	PEG15-PLGA	1:1	15	5	33

Independent from the polymer composition all polymeric solutions showed a fast polymer precipitation (Figure 20). Implant formation was almost completed after 24 hours. There was no statistic significant difference in the phase inversion kinetics of the polymers.

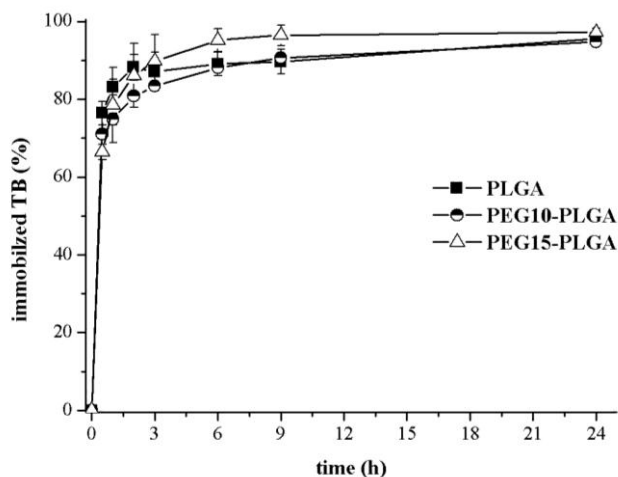


Figure 20 Effect of polymer type on the degree of TB precipitation from NMP solutions (determined by EPR in vitro)

In contrary the hydrophilic character had a strong impact on the solvent removal (Figure 21). PEG15-PLGA possesses nearly the same molecular weight as PLGA (Table 2). But due to its more hydrophilic character, a significant faster solvent exchange was observed after three hours ($p < 0.01$). After 6 hours the water replaced $87.4 \% \pm 4.4 \%$ of NMP inside the implant (versus $57.6 \% \pm 0.3 \%$). In PEG15-PLGA implants the complete solvent exchange was achieved after two days, whereas it took 7 days to remove the solvent from the PLGA implants. As expected the incorporation of PEG blocks favored the water influx into the polymer and therefore accelerated solvent exchange. *Witt et al.* found that the water uptake and swelling degree of pre-shaped implants of PEG-PLGA-PEG triblock copolymers is directly related to the PEG content of the polymers [159].

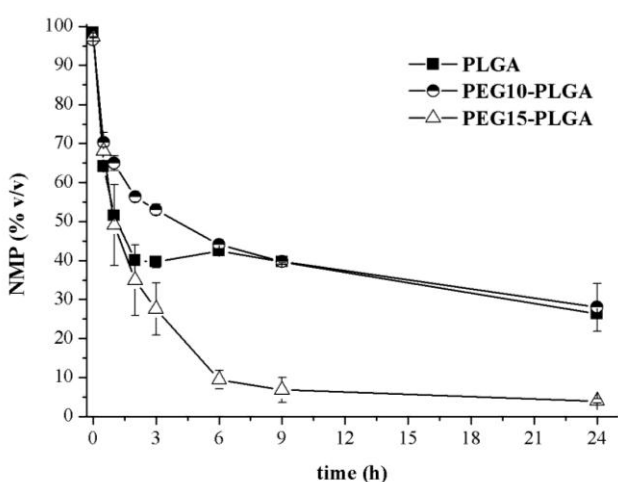


Figure 21 Effect of the polymer type on NMP removal from in situ formed implants (determined by EPR in vitro)

Initially PEG10-PLGA implants showed slower solvent removal compared to the other polymers. The rate of solvent exchange realign with that of PLGA after 6 hours, but is

still less than PEG15-PLGA. PEG10-PLGA possesses a higher molecular weight compared to PEG15-PLGA resulting in a higher intrinsic viscosity of the polymeric solutions expressed by higher rotational correlation times of the EPR spectra ($0.080 \text{ ns} \pm 0.005 \text{ ns}$ versus $0.053 \text{ ns} \pm 0.004 \text{ ns}$). It is usually assumed that in solutions of higher molecular weight polymers, the longer polymer chain lengths get more entangled and therefore the system diffusivities increased. The hydrophilic character of PEG10-PLGA had an effect in the later steps of solvent removal. The PEG blocks of the precipitated polymer eased water diffusion inside the polymer and yielded to complete solvent exchange after 5 days in comparison to 7 days for PLGA.

The relationship between polymer molecular weight and release of ISFI has been reported contradictory in literature. *Eliaz et al.* investigated the effect of PLGA molecular weight on the release of tumor necrosis factor receptor and found that the higher molecular weight caused a faster solidification of the slow phase inversion systems and thereby decreased the diffusion and release rates of proteins [78]. Whereas *Astaneh et al.* observed an increased precipitation rate in fast phase inversion systems of lower molecular weight systems, resulted a more porous matrix. But also ISFI of low molecular PLGA possessed a more pronounced initial burst. In the higher molecular weight polymers the diffusion rate during the burst phase was decreased by higher solution viscosity. As a result a stronger matrix with a lower porosity was formed [163]. Another study described a parabolic relationship between the polymers molecular weight and the amount of naltrexone released [164].

Initial drug release from phase inversion based depots strongly depends on the diffusion rate of the organic solvent from the polymer solution into the aqueous environment. *McHugh* distinguishes two general classes of PLGA solution depots depending on the solvent strength and water miscibility [80]. Fast phase inversion occurs in the case of hydrophilic solvents with a strong water affinity. Rapid solvent diffusion causes fast polymer precipitation into a porous polymer matrix with solvent water filled pores. In most cases three different phases of drug delivery can be observed for ISFI based on phase separation by solvent exchange. These systems favor a high initial release as the drug diffuses parallel with the solvent out of the systems during polymer solidification. In the second phase of drug release, the drug associated with the surface is primarily released followed by drug diffusion through the formed matrix. At the end of the second

phase the drug release often cover a steady state. Later in the third phase the drug release is accelerated and controlled by erosion of the matrix. Drug release is mainly controlled by erosion. Slow phase inverting systems base on solvent with a weaker water affinity and possess reduced initial and prolonged sustained release. Solidification takes place up to days resulting in dense structures with few or no pores.

PLGA/NMP solutions belong to the fast inverting systems with a typical burst in drug release. The initial release of the model drug substance TB is clearly affected by the hydrophilic character of the implant matrix (Figure 22, left). Increasing the PEG content of the polymer resulted in higher release rate within the first 24 hours, 44.3 % \pm 6.0 % for PLGA compared to 88.9 % \pm 5.9 % for PEG15-PLGA. After the burst phase the AB diblock copolymers showed a continuous release pattern. The PLGA with higher PEG content with showed a faster TB release (Figure 22, right). Because of the greater extent of water hydration in PEG-PLGA, hydrolysable ester linkages were more accessible a to water and so polymer degradation and erosion started immediately upon incubation [159].

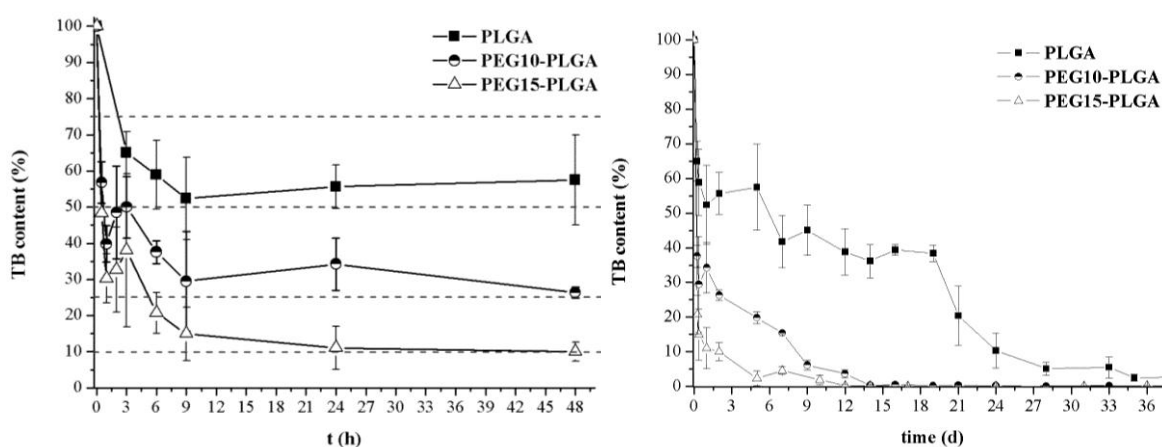


Figure 22 Effect of the polymer type on the initial (left) and the total (right) release of TB indicated by the decrease in the content of incorporated TB inside polymer/NMP depots (determined by EPR in vitro)

The PLGA implants showed a typical steady state in their TB content within the first week that corresponded with the observed lag time in polymer degradation of pre-formed implants [130]. As preformed implants, in situ formed PLGA implant typically showed a biphasic degradation pattern. The initial lag phase was characterized by slow water penetration from the surface into the matrix [60]. After soluble degradation

products have been formed by hydrolysis of the polymer chains, polymer erosion started after about one week, along with slow decrease in TB content (Figure 22, right).

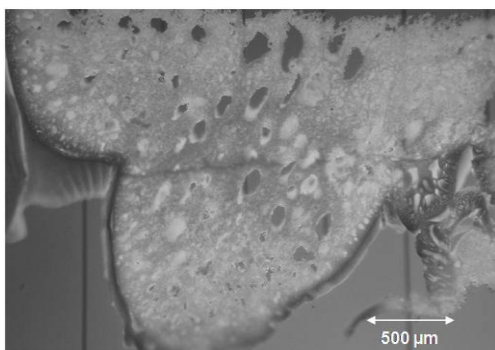


Figure 23 Optical micrograph of the cross section of PLGA/NMP implant after 24 h incubation in buffer

Figure 23 shows the cross section of a PLGA/NMP implant after one day incubation on phosphate buffer. In the core of the PLGA/NMP implant spongy and closed pores with no continuous path to the surface can be detected. Because PLGA undergoes bulk erosion, accumulation of degradation products in the pores accelerated degradation in the central regions. As a result the polymer degraded faster in the central region than at the surface layer. After 21 days *Eliaz et al.* observed small pores all over the implants surface and a further increase in pore size with time till a highly porous implant surface by day 36 [78]. These results correlated with the progressive loss in the TB content as seen in the PLGA implants after 20 days. *Luan et al.* reported similar release profile for leuprolide acetate from equivalent PLGA/NMP systems. An initial release of 48.1 % was followed by a slow release to about 60 % at day 20 and a rapid release to nearly 100 % at day 35 [82].

4.1.1.3 The influence of type of solvent on the phase inversion dynamics

Although NMP is used in commercially products, its application is controversially discussed. NMP is described as a mild irritant to the eyes, the mucous membranes and the skin, and to be harmful to muscles [165;166]. Furthermore NMP caused hyperglycaemia after intravenous use in rabbits [165]. Beyond that the solvent NMP facilitated the degradation of proteins and polymers based on lactic and glycolic acid [81;167]. Therefore PEG 400 was tested as well tolerated non-toxic solvent for PLGA [79] and compared to NMP. PEG 400 is considered to be among the safest organic solvents and has been used for injectable formulations of lorazepam (Antivan[®]) [168].

Low molecular weight PEGs have already been used as a solvent or co-solvent for ISFI [74;79]. The addition of PEG 400 into PLGA/NMP based formulation suppressed the initial burst release of aspirin, but did not prolong the total release period [74].

All investigated polymers could be dissolved in PEG 400 up to concentration of 50 % (w/v); even it took up to five times longer to dissolve compared to NMP. After injection into buffer, all solutions immediately formed implants. As described in the previous section, dissolution induced changes in micropolarity could be determined by EPR. As for the solvent NMP the values of the isotropic hyperfine splitting $2a_N$ could be correlated to the PEG 400 concentrations in different PEG 400-buffer mixtures (Figure 16). The regression coefficients for both calibration curves were $R = 0.99$. The EPR data also show that PEG 400 is slightly more polar compared to NMP (Figure 16, page 45). For all systems, PEG 400 showed a faster solvent/non solvent exchange than NMP. After three hours the PEG 400 content decreased to $9.6 \% \pm 0.2 \%$; $3.6 \% \pm 0.4 \%$ and $12.1 \pm 0.02 \%$ inside the PLGA, PEG10-PLGA and PEG15-PLGA implants, respectively (Figure 24).

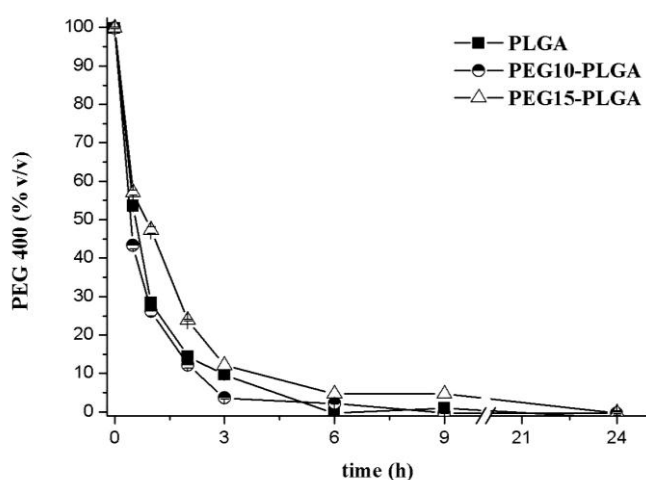


Figure 24 Effect of the polymer type on PEG 400 removal from in situ formed implants (determined by EPR in vitro)

After 6 hours the PEG 400 was completely replaced by water within the PLGA implant. This fast and complete exchange was not observed for PLGA/NMP implants, where $42.4 \% \pm 0.3 \%$ NMP was still present in the implant after 6 hours, although the initial exchange was also very fast. For the PEGylated polymers complete solvent removal was obtained after 24 hours. In a recent study similar results were obtained for PLGA/PEG 600 systems [150]. Within three hours about 90 % of the PEG 600 diffused into the release medium and complete solvent exchange was achieved after 24 hours.

The faster PEG exchange was not unexpected, because PLGA is better soluble in NMP compared to PEG 400. At high polymer concentrations, as in the present study, the viscosity is lower in good solvents than in poor solvents [169]. The spin probe TB tumbled more slowly in PLGA/PEG 400 solutions (t_c 1.222 ns \pm 0.001 ns) compared to the PLGA/NMP solutions (t_c 0.095 ns \pm 0.015 ns), which reflected a much higher viscosity. An increase in one order in magnitude in the systems microviscosity was also observed for both PEG-containing PLGAs. Comparable viscosity shifts have been observed for PLGA dissolved in NMP and PEG 600 [150]. Further PEG 400, as polar protic solvent, has a strong hydrogen bond capacity and therefore a higher water affinity than the polar aprotic solvent NMP [81].

In addition a faster polymer precipitation was observed for the polymer/PEG 400 systems compared to NMP (Figure 25). The maximum of proportion of immobilized spin probe in the precipitated polymer was already achieved after three hours independent of the type of polymer.

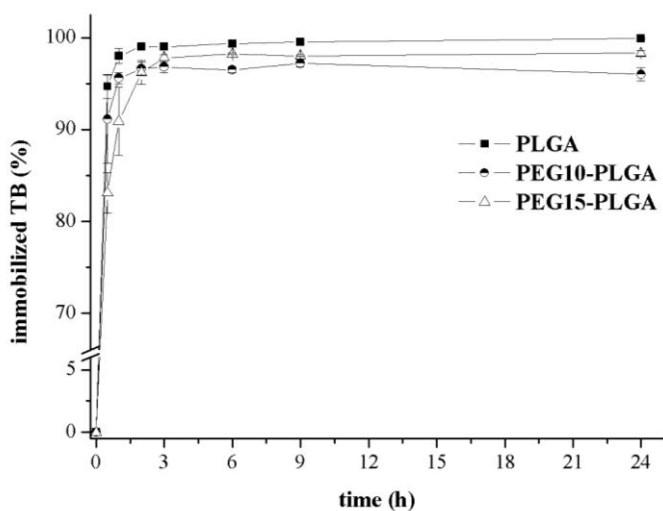


Figure 25 Effect of polymer type on the distribution of precipitated TB during implant formation in with PEG 400 as solvent (determined by EPR in vitro)

This effect can also be explained by the high water affinity and lower polymer solubilising capacity of PEG 400. *Schoenhammer et al.* compared the phase separation of PLGA dissolved in NMP and PEG 600 by ternary phase diagrams [150]. A lower amount of water was necessary to precipitate the PLGA from PEG 600 compared to NMP.

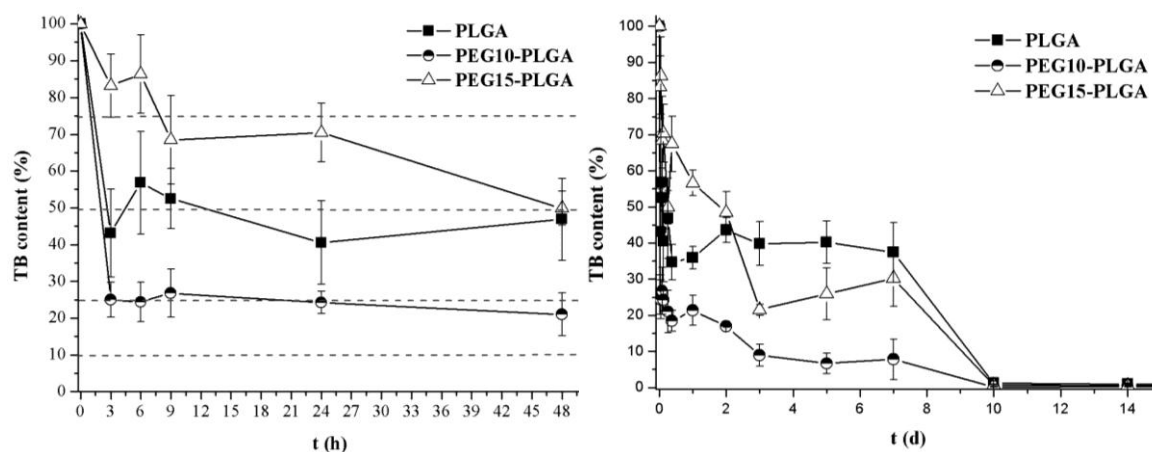


Figure 26 Effect of the type of the polymer on the initial (left) and the total (right) release of TB indicated by the decrease in the content of incorporated TB inside polymer/PEG 400 depots (determined by EPR *in vitro*)

As a consequence to the more rapid solvent exchange and faster polymer precipitation a higher initial release was observed for PLGA/PEG 400 (Figure 26 left). The TB content inside the implants decreased within 24 hours to $35.9\% \pm 3.0\%$ versus $55.6\% \pm 6.0\%$ for NMP containing systems. The first week of incubation was characterized by the typical steady state and a drastic decrease in TB content with the onset of polymer degradation in the second week. Figure 27 shows the morphology of the implant after one day immersion in phosphate buffer. During polymer precipitation macrovoids and little channels with direct contact to the surface have formed.

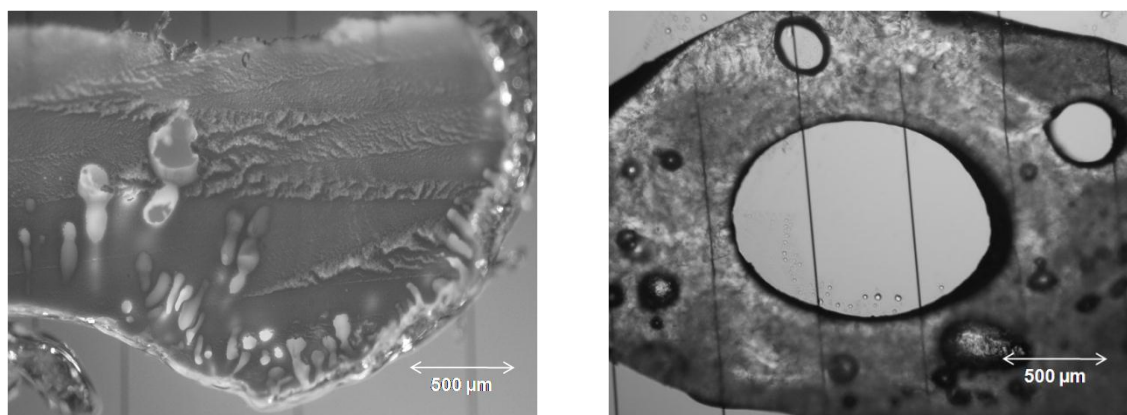


Figure 27 Optical micrographs of the cross section of situ forming depot after 24 h storage in buffer: (left) PLGA/PEG 400; (right) PEG15-PLGA/PEG 400

Degradation products accumulated inside these channels promoted autocatalysis and cracks in the surface formed. It can be assumed that small molecules like TB diffuse out

through the formed pathways, explaining the fast TB release in the second week of incubation. Low molecular PEGs are widely used as pore forming agents. Pores on the implants surface facilitated water diffusion inside the implants. A steadily increase of the mobile part in the EPR spectra was detected that reach a maximum at about 4 weeks (Figure 28). The mobile part of the spectra corresponded to a compartment with a viscosity comparable to aqueous solutions of TB, reflecting water penetration into the implant through pores on the surface accompanied by TB solubilisation and polymer degradation.

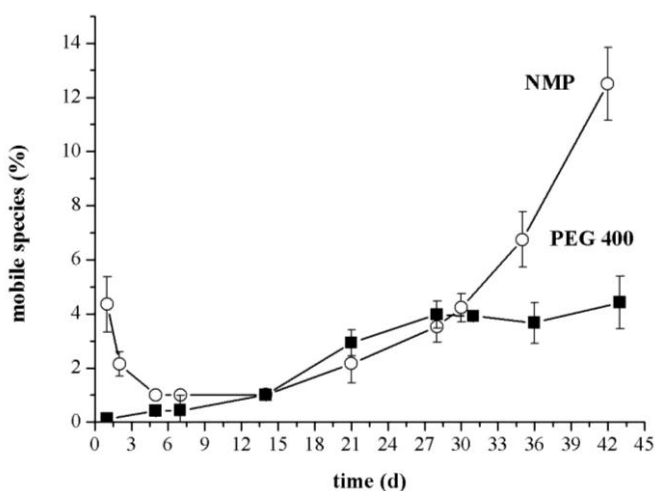


Figure 28 In vitro distribution of mobile TB inside the implants. The slight increase of the mobile compartment indicates water diffusion inside the implant. (determined by EPR in vitro)

In contrast the proportions of mobile spin probe in PLGA/NMP systems did not increase within the first two weeks. The rise of the mobile part after 21 days correlated well with the observed decrease of the incorporated spin probe (Figure 26). Similar results were obtained from pre-shaped PLGA implants. After a lag time the contribution of the mobile part to the EPR spectrum increased steadily with time [130].

As expected the more hydrophilic PEG10-PLGA yield a higher initial release during the first 24 hours $78.7\% \pm 4.1\%$ compared to both PLGA/PEG 400 ($64.1\% \pm 3.0\%$) and PEG10-PLGA/NMP systems ($65.7\% \pm 7.2\%$). After the initial burst TB was released in a continuous manner (Figure 26). Surprisingly PEG15-PLGA possessed the lowest initial release of all polymeric solutions in PEG 400. Even the PEG15-PLGA solution in NMP released more spin probe during the first 24 hours $88.9\% \pm 5.9\%$ versus $43.3\% \pm 3.5\%$. Afterwards the TB content of the implants decreased continuously within the next three days. Beyond all expectation it reached a steady state till day 7 in order to decrease again. Normally one would assume the highest initial burst followed by a continuous release as detected with the solvent NMP. The optical image of the

implants cross section after one day immersion in phosphate buffer might explain the discrepancies between the expected and obtained results (Figure 27, right). The morphology totally differs from PLGA. Neither there is spongy network nor macrovoids with contact to the surface. Instead big pores have formed in the centre of the matrix that enabled higher entrapment efficacy. With increasing water diffusion into the implant part of the TB is released. Another part can accumulate inside the pores. With progressive degradation of the polymer and pore opening to the surface the micro reservoirs will be washed out.

4.1.2 *In vivo* monitoring of the phase inversion dynamics and the biological response to in situ forming depots by Benchtop Magnetic Resonance Imaging

Although the kinetics of solvent/non-solvent exchange and polymer precipitation could be followed by EPR, no direct information about the response of the biological system to the implant (e.g. edema, inflammation or encapsulation) was obtained. Furthermore EPR spectroscopy provides no spatial information about the shape and size of the formulation after injection and its disappearance from the injection site. To circumvent these limitations MRI was applied as a complementary non-invasive method.

In general ^1H -MRI is a non-invasive imaging method that detects the local concentration and physical state of protons. It has been used to monitor hydration, swelling and erosion of non-coated and coated tablets or implants [114;130;170]. Recently MRI has been applied to follow carbon dioxide formation in floating tablets [171] and the fate of several parental formulations such as oils, lipid emulsion and water solutions of block co-polymers after subcutaneous injection [132]. Although MRI has proven to be useful in a number of biomedical applications and as diagnostic tool in clinics, there are only a few reports dedicated to drug delivery research [114;117]. The main reasons for its rare application are the high installation and running costs of common superconducting MRI machines. An alternative present commercial low cost benchtop NMR systems using permanent magnets [121;123]. Bt-MRI has been successfully implemented for the *in vitro* characterization of tablets [127;129;171] and scaffolds [134]. So the next step was to explore the possibility of Bt-MRI for preclinical *in vivo* studies [135].

Contrast agents and markers are used for most biomedical and clinical applications of MRI. But in drug delivery research their use has to be critically revised [132]. The addition of contrast agents may influence the general properties of the formulation, affecting stability, release rates or its biocompatibility. It was therefore the aim of the present study to evaluate the use of benchtop MRI for studying ISFI without the use of marker substances and contrast enhancing agents.

MRI signal intensities depend on the total amount of protons in the sample, the relaxation times and the MRI measuring parameter. To follow a dynamic process, the repetition time (TR), which describes the time span between the pulse echoes, was set to 178 ms resulting in an acquisition time of about 6 minutes (16 averages). Under the present conditions all MR images were acquired in a T_1 weighted mode.

NMP and water possess nearly equal T_1 times and therefore give similar contrast in MRI (Table 3).

Table 3 T_1 relaxation times in different tissues and samples measured at 20 MHz

<i>component</i>	<i>T_1 (s)</i>
Buffer	2.95 ± 0.03
NMP	2.19 ± 0.03
PEG 400 (50 %)	0.60 ± 0.12
Muscle	0.58 ± 0.42
Subcutaneous fat	0.21 ± 0.42
PEG 400	0.13 ± 0.03

Under the present conditions ($TR \ll T_1$) the imaging sequence is finished before the magnetization of the free water proton is able to return to equilibrium and therefore water appears dark. In contrast to NMP, PEG 400 possesses a much lower T_1 relaxation time (Table 3) and is therefore quite distinguishable from water up to concentrations of 25 % (Figure 29). PEG 400 with its lower relaxation time ($TR \approx T_1$) appears brighter in the images than water. Thus and for toxicological safety aspects the MRI experiments were only performed with PEG 400 as solvent.

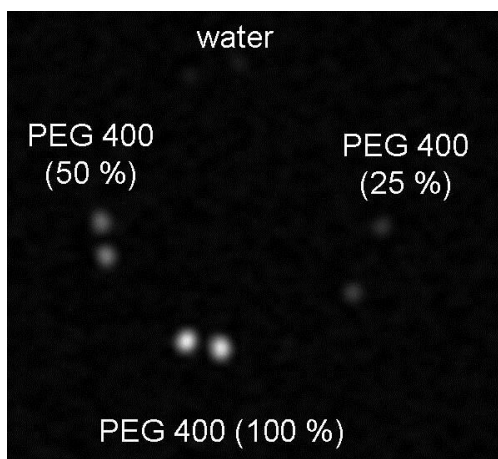


Figure 29 In vitro MRI image of capillaries (diameter 0.5 mm) filled with different PEG 400-water mixtures showing the dependency of the MRI signal intensity on the PEG 400 content.

Also in mice the PLGA/PEG 400 implant solution could be easily distinguished from the surrounding tissue, since the contrast and signal intensities were sufficient enough (Figure 30). The polymer solution, with nearly the same relaxation times as subcutaneous fat appeared bright. It could easily be detected under the skin and distinguished from subjacent muscle tissue, which appeared darker in the MR image. In addition to the location of the implant anatomical details were able to be visualized. One can differentiate skin from back and leg muscles, subcutaneous fat and the urine filled bladder (Figure 30).

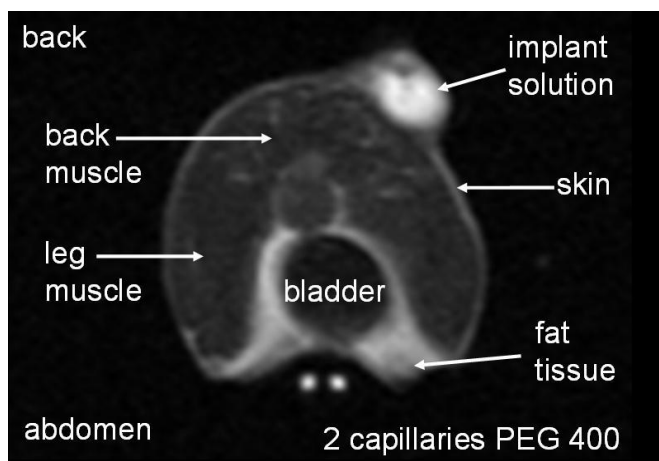


Figure 30 In vivo MRI image 5 minutes after s.c. injection of PLGA/PEG 400 implant solution, showing the location of the implant and anatomical details of the mice. 2 Capillaries filled with PEG 400 placed under the abdomen of the mice served as internal standard.

All formulations were injected in the lower back of the mice in position of the bladder to easily relocate the implants during the repeated measurements.

In initial trials pure PEG 400 was injected to get more information about the solvent dispersion and disappearance from the injection site. MR images were taken repeatedly every 10 minutes within the first hour after injection and then after 2, 3, 6 and 24 hours (Figure 31). PEG 400 spread rapidly after injection under the skin and dissipated over

the whole lower back. PEG 400 attracted water and caused a subcutaneous edema. This edema was already detectable after 30 minutes and had a maximum in size after one hour. Between one and three hours it could be easily localized macroscopically and was palpable under the skin. The water/PEG 400 mixture was eliminated within few hours. After 6 hours the edema consisting of water and PEG 400 was solely detectable by MRI. After 24 hours it disappeared completely. The edema formation can be attributed to local conditions and the physical properties of the low molecular weight PEGs.

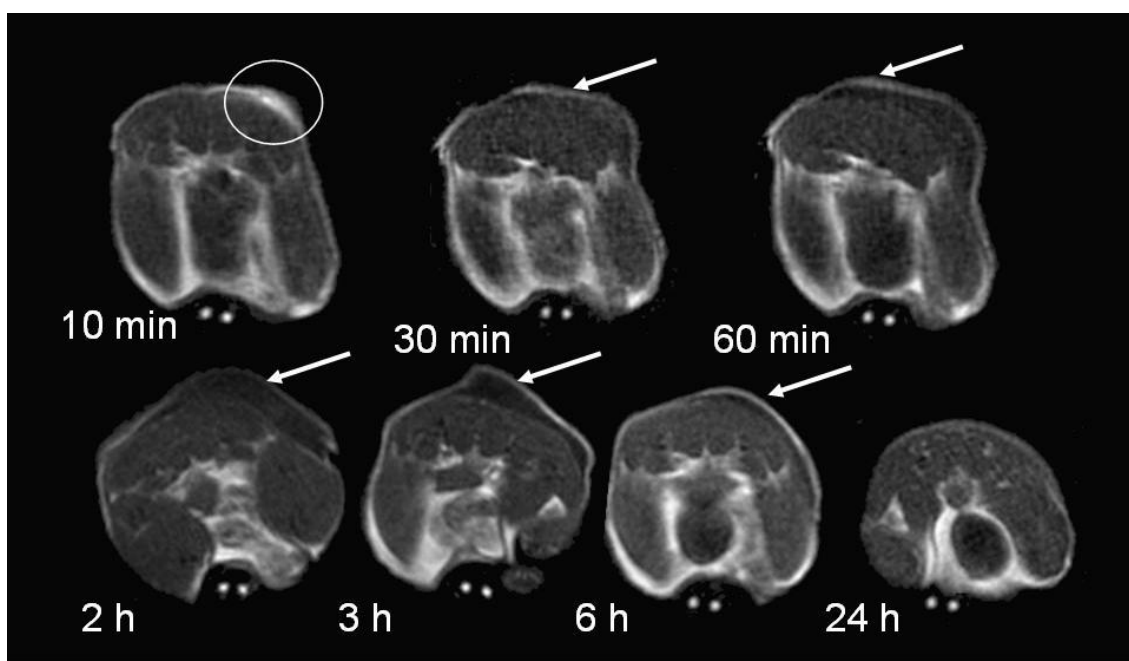


Figure 31 In vivo MR images of the distribution and disappearance of PEG 400 after s.c. injection. The white circle marks the point of injection, white arrows indicate subcutaneous edema. Two capillaries filled with PEG 400 placed under the abdomen of the mice served as internal standard.

The subcutaneous space offered a reduced volume flow away from the injection site compared to i.v. or i.m. injection [168]. PEGs are known to be osmotically active. This effect is widely used in medicine to stimulate the gastrointestinal mobility [172]. All the mice gained weight steadily during the study. Macroscopic evaluations at the injection sites showed no untoward local reaction. Edema formation is not supposed for NMP, as NMP poses skin permeation enhancement properties [173] and rapidly diffuses from the injection site. In the EPR experiment no edema formation with the PLGA/NMP solutions have been observed. Studies on rats and dogs showed also no vasodilatation, erythema or edema formation [174].

In contrast to the PLGA free PEG 400 solution the polymer solution did not disperse rapidly after injection. The PLGA/PEG 400 concentrated locally at the point of injection (Figure 32).

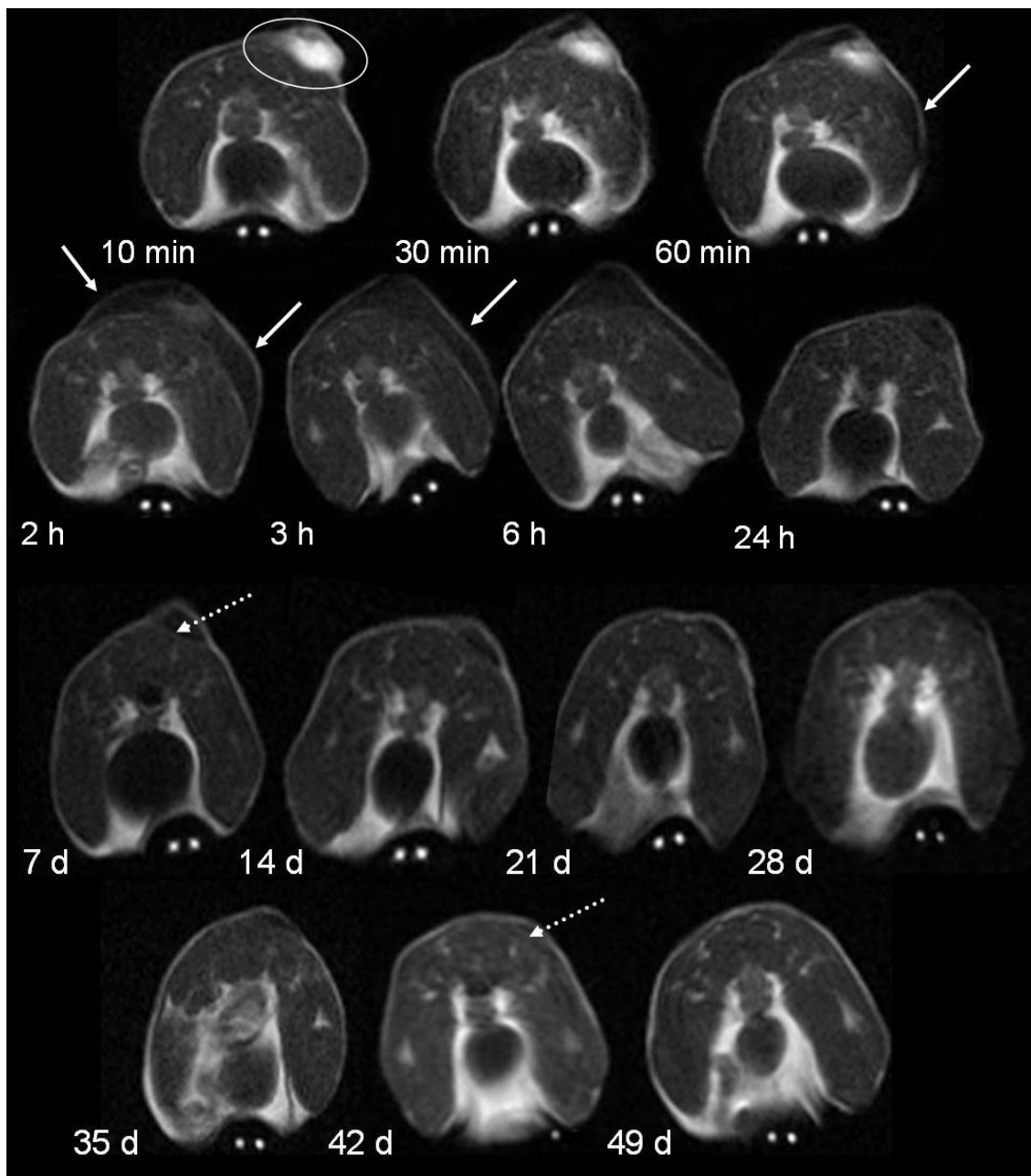


Figure 32 In vivo MR images of the distribution and disappearance of PLGA/PEG 400 implant solution after s.c. injection. The white circle mark the point of injection, the solid white arrows indicate subcutaneous edema and the dashed white arrows point to connective tissue adhesion on implant surface. Two capillaries filled with PEG 400 placed under the abdomen of the mice served as internal standard.

The precipitated PLGA appeared dark in the image due to the shorter relaxation times of the solid polymer [130]. A part of the solvent was entrapped in the core of the

forming implant. The bright intensity of the implants core faded with time. Water penetrated inside the implant and replaced the PEG 400. The PEG 400 dispersed in the surrounding subcutaneous space and caused the same edema as observed for the pure solvent. The largest extend was also detectable after one and two hours by MRI and visible and palpable externally. After three hours the edema diminished and was no more detectable after 24 hours. Like in the *in vitro* EPR measurements PEG 400 was eliminated after 6 hours. Within the first week the size and the shape of the PLGA implant did not change remarkably (Figure 32). Similar results were obtained from subcutaneous implanted PLGA tablets [130]. The onset of the decrease of the implant size after two weeks corresponded to the increase of the mobile compartments detected by EPR. The erosion occurred faster *in vivo* than *in vitro*. The implant was no more detectable after 7 weeks by MRI and after 8 weeks by visual histological examination. The faster *in vivo* erosion may have several reasons. On the one hand the development of a more acidic microenvironment *in vivo*, due to the autocatalytic degradation mechanism of PLGA and different buffer capacities *in vitro* and *in vivo*, have been reported to cause faster erosion of PLGA scaffolds *in vivo* [139]. On the other hand additional factors, like enzymatic degradation *in vivo* or different implant shapes and therefore different surface areas might also contribute. *Tschakaloff et al.* examined the erosion kinetics of PLA implants depending on the site of implantation [175]. In all cases PLA was eroded faster *in vivo* than *in vitro*. The effect was explained by differences in perfusion. *Pamula and Menaszek* compared the *in vitro* and *in vivo* erosion of PLGA films and scaffolds [139]. Under both conditions the thinner films eroded much faster than the scaffold.

Furthermore the development of a bright ring around the implant, with a good contrast to the subjacent darker muscle tissue, was observed (Figure 32). The bright ring can be attributed to encapsulation of the implant which was verified by visual examination after sacrificing of the mice at the end of the experiment. The formation of connective tissue capsules as biological response to polymers based on lactic acid is a common observed phenomenon. Fibrous capsule formation or the association of connective tissue bands have already been reported as well as with common pre-shaped implants of PLA and PLGA [130;139], microparticles of PLGA-PEG-PLGA [156] and ISFI of PLGA/NMP [174] and PCL/NMP [89]. The implantation of biomaterials either by

injection or surgical insertions in living organism generally injures the tissue. As a response to injury a series of complex mechanisms that involve inflammation, wound healing and foreign body response are activated. Their intensity and duration depend upon the extent of injury and the geometrical, chemical and physical properties of the biomaterial [176]. Acute inflammation occurs directly after injury, lasting from a few minutes to days subject to the grade of injury. The main characteristics are the emigration of leukocytes and edema formation by the exudation of fluid and plasma proteins. Subjacent chronic inflammation is characterized by proliferation of blood vessels and connective tissues and the migration of macrophages, monocytes and lymphocytes. In the next step of the healing process, the foreign body reaction, granulation tissue is formed. The end stage is generally fibrosis or fibrous encapsulation that yields to the isolation of the biomaterial from the surrounding tissue.

The MRI investigations confirmed the results of the fast solvent exchange from the EPR measurements. Also with the pegylated polymers, PEG10-PLGA and PEG15-PLGA, PEG 400 was removed from the implant and dissipated in the subcutaneous space within the first 6 hours. Likewise edema formation was observed. The edema developed in the first hours and dissipated within one day (Figure 33 and Figure 34 top).

It is worth to note that the applied injection volumes of 200 μ l in a 25 g mouse would correspond to 0.6 l in a 75 kg patient and represent an unrealistic injection volume per body weight. In a recent study transient local edema at the injection site have been reported after the injection of 0.25 ml of DMSO in mice and was linked to the local toxicity of the solvent [177]. Despite edema development the animals remained healthy and active throughout the experiments. No changes in food and water consumption, weight loss or abnormal behaviour were observed. The tissue response was limited to tissue adjacent to the implants. The mild fibrosis was similar to other PLA or PLGA-based delivery systems [89;178]. Therefore polymeric formulations can be considered as acceptable safe for the use of injectable in situ forming depot systems.

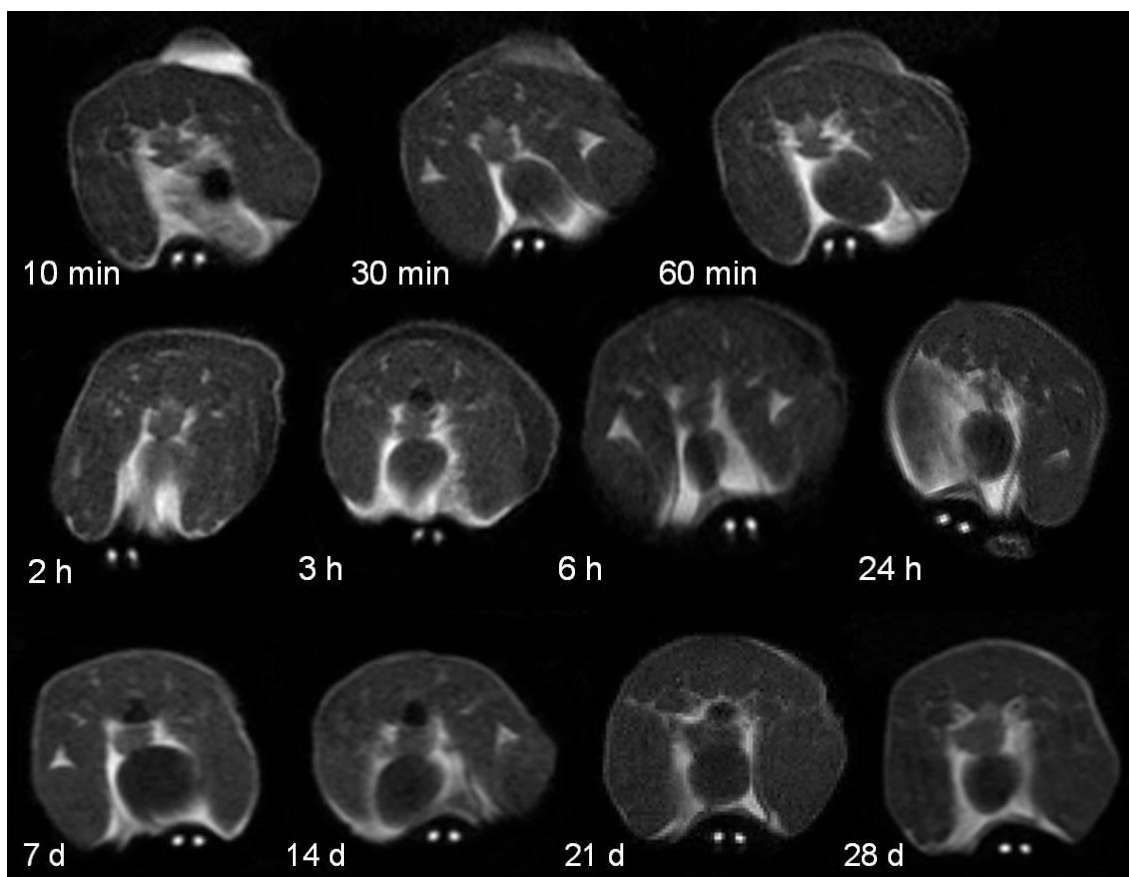


Figure 33 *In vivo* MR images of the distribution and disappearance of PEG10-PLGA/PEG 400 implant solution after *s.c.* injection. Two Capillaries filled with PEG 400 placed under the abdomen of the mice served as internal standard

The PEG10-PLGA implant formed a disk and not a nodule structure under the skin as observed for PLGA (Figure 33). The ability of the implant to expand is limited *in vivo* because of tissue compressive forces exerted on the implant. So the mechanical strength of the formed implant determines their shape [179]. Due to their more hydrophilic character, associated with higher water uptake, the PEG10-PLGA eroded more rapidly. The geometry of the implant, especially the higher surface to volume ratio, further accelerated polymer degradation [139]. No implants were detected after 4-5 weeks *in vivo* (Figure 33 bottom) compared to total signal loss after 7 weeks *in vitro*.

In situ forming depots of PEG15-PLGA precipitated in a similar form as PLGA depots (Figure 34). The nodule shaped implants started to erode after about two weeks, which was in good agreement with a sharp increase of the mobile proportion of the EPR spectra. The incorporation of the PEG moieties in the PLGA backbone facilitated the water penetration in the implants. Therefore PEG15-PLGA implants appeared brighter

in the MRI images compared to PLGA implants. Similarly twice the mobile compartment was detected in the EPR spectra after two weeks. As expected the PEG-containing PLG eroded faster than PLGA. *In vivo* the implant disintegration was completed within 6-7 weeks (Figure 34).

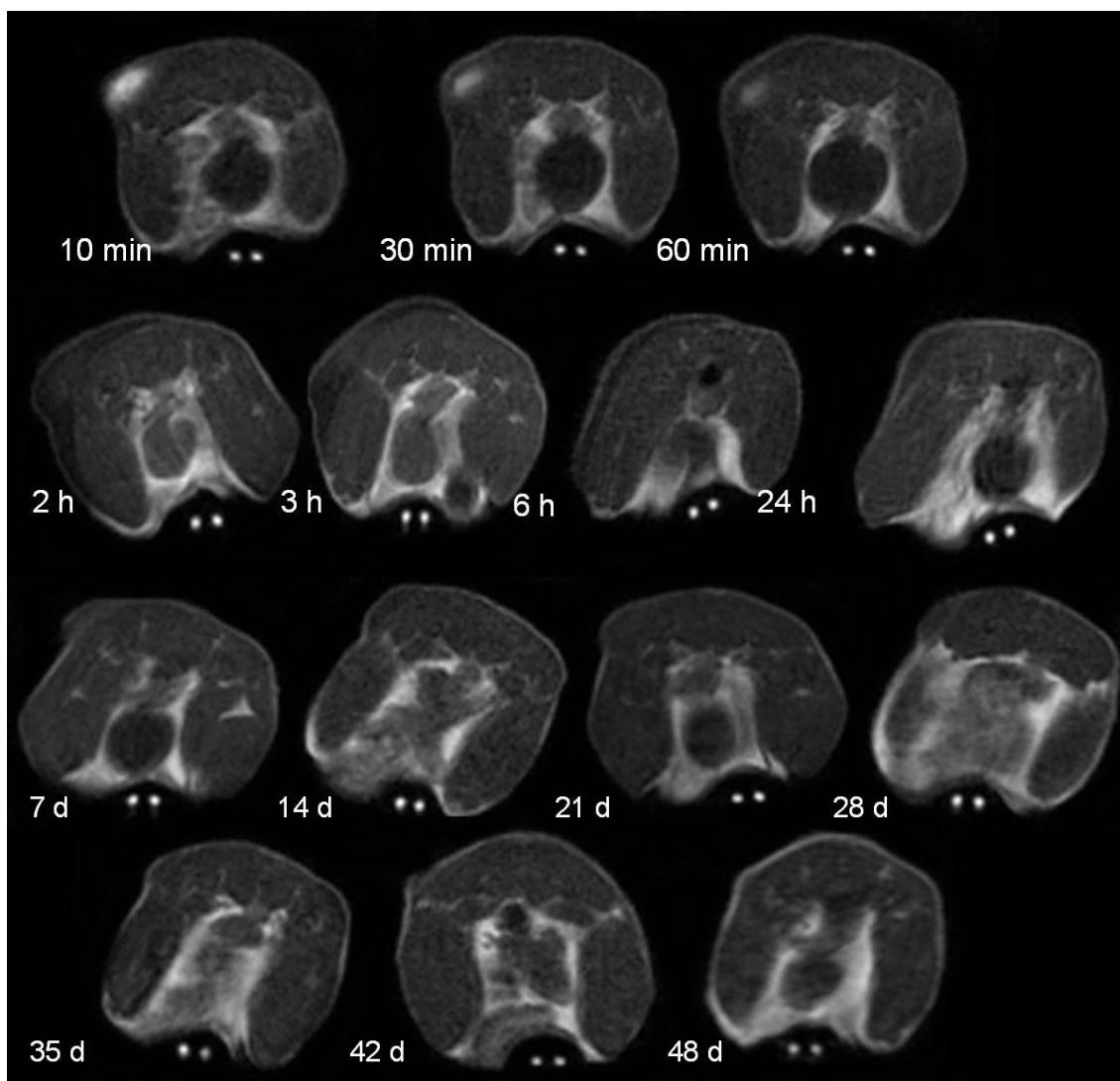


Figure 34 *In vivo* MRI images of the distribution and disappearance of PEG15-PLGA/PEG 400 implant solution after s.c. injection. Two Capillaries filled with PEG 400 placed under the abdomen of the mice served as internal standard.

Normally one would expect a faster rate of disintegration for the more hydrophilic polymer with the higher PEG content [159]. The slower erosion of PEG15-PLGA compared to PEG10-PLGA is mainly attributed to the different geometry of the implants. A faster erosion of rod shape implants versus tablet shape implants was already reported for ABA triblock copolymers [159]. Another observation was that the impact of surface to volume ratio on the degradation kinetics was more pronounced than

the PEG content of the polymers. Fibrous encapsulation as the typical wound healing response also occurred with PEG15-PLGA (Figure 34).

4.1.3 In situ monitoring of microclimate pH

The determination of microclimate pH inside drug delivery systems is of great interest since it directly influences the physical and the chemical stability of the ingredients, especially their solubility and consequently the release performance of the systems. For example the microclimate pH inside the aqueous pores of PLGA devices can become very acidic as a result of acidic polymer impurities and ester hydrolysis to acidic oligomers and monomers. It has been reported that the internal pH of PLGA matrices dropped to pH ranges of 2-3.5 [60;180], leading to acid catalyzed PLGA hydrolysis and the deactivation of ingredients. The acidic microclimate in PLGA microspheres was found to be responsible for acid-induced deformylation of vincristine, acid-induced aggregation of bovine serum albumin (BSA) and acylation of peptides by the formations lactoyl lactyl-drug conjugates [180-183]. The pH_m quantification and determination of affecting factors is critical for a better understanding of PLGA delivery systems and for formulation design. But there are only a few techniques available to measure the pH_m continuously and non-invasively. Many researchers focused on the determination of alterations in the pH of the incubation media by standard glass pH electrodes [163]. Decline in the bulk fluid pH has been attributed to acid liberation from the polymer. But this approach can give only indirect reflections of the internal pH of the systems. The conditional accumulations of degradation products in the unchanged media may further accelerate ester hydrolysis and thus do not reflect *in vivo* conditions. Non-invasive methods to assess the internal pH in degrading PLGA devices include the direct visualization by confocal laser scanning microscopy (CLSM) with pH sensitive dyes [155], potentiometric detection [180], the use of ^{31}P - NMR probes [184] or analysis of pH sensitive spin probes by EPR [60;103;185].

By potentiometric measurements pH_m values in thin polymer films have been examined. Hereby standard glass pH electrodes were coated with PLGA [180]. With this approach the pH_m varied with the thickness of the coating. Highly acidic pH_m values (pH 2-3.5) were measured after one day of incubation in neutral buffer solution. After one week neutral values (pH_m 6.5) were detected in the case of 7 μm thick coatings. Whereas pH_m

remained acidic up to 4 weeks when investigating 30-250 μm thick films. The pH of the thin water film between the electrode and the polymer was proposed to mimic pH_m of aqueous pores inside polymer matrices. But this experimental setup is not suited for small scale systems like nano- or microspheres. Acidic pH_m within PLGA microspheres was detected by direct visualization using confocal microscopy with pH sensitive dyes. The group of *Prof. Schwendeman* related the fluorescence intensity with pH_m [155;186]. Since changes in fluorescence intensity could arise from both altered pH values and concentrations of the dye [186], pH quantification was expected to be semi-quantitative. In order to eliminate the effects of dye concentration and pore distribution two different dextran conjugated fluorescent dyes were co-encapsulated inside microspheres and images at two emission wavelengths were taken [186]. Recently developed ratiometric measurements of dextran conjugated dyes provides pH_m mapping of microparticles with better signal-to-noise ratios [155;186]. For CLSM, the size of the delivery device is the limiting factor since light transmission through the object is a prerequisite. As described in section 3.2.1 (page 22) the use of pH-sensitive nitroxides permit average pH-measurements by EPR spectroscopy. EPR has been used to show that pH drop down to pH 2 inside PLGA implants subcutaneously administered to mice [60]. Other studies used EPR spectroscopy to assess the microacidity in degrading PLGA and PEG-PLGA-PEG implants [159] and microparticles [103]. Also pH gradients have been detected inside eroding polyanhydrides [187] and HPMC matrix tablets by spectra spatial imaging [188]. As for CLSM the pH probes are only sensitive in a narrow pH range. Therefore a combination of several sensitive reporter molecules is necessary in both techniques to cover a wider pH range.

Although the internal pH of PLGA implants and microparticles has been studied extensively, no direct and continuous investigations about the pH_m in ISFI have been published yet. Regarding their release pattern ISFI take an interim position between pre-shaped implants and microparticles. One can suppose a similar performance regarding the pH_m during implant disintegration.

Due to their non-destructive nature, EPR spectroscopy was chosen for serial pH_m measurements of the previous described in situ forming depots (section 4.1.1.2 and 4.1.1.3). To achieve sufficient signal-to-noise ratio of the EPR spectra even over the long time release process, the pH sensitive spin probes were incorporated in both, the

polymeric solutions and incubation buffer. To assure that the spin probe containing buffer does not interfere with the pH_m determination in the implants, the absorbed buffer was carefully removed prior EPR measurements. The investigated nitroxides AT, HM and 2PK were sensitive as well to changes of the microclimate pH (Figure 9, page 26) as to changes of the micropolarity and microviscosity (Figure 8, page 25). To avoid possible superposition of the middle peak with spectral components derived from immobilized species the distance between the first and the third peak ($2a_N$) was measured. Due to the fact that the solvent replacement dominated in the first day of incubation at all investigated implant, no reliable data about the pH_m within the first 24 hours could be obtained.

In the first week of incubation the pH_m inside PLGA/NMP implants decreased slowly, followed by a pH drop to pH_m 2.5 to 3 in the second week (Figure 35). Such acid pH_m value due to accumulated acidic polymer degradation products were already reported for PLGA implants [60] and microparticles [155;186].

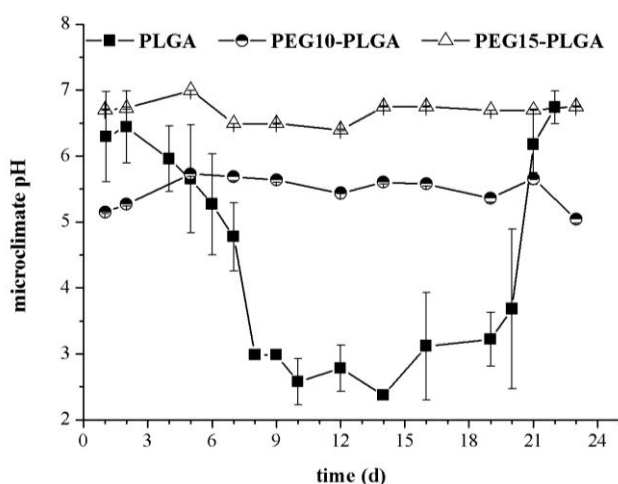


Figure 35 Effect of the type of the polymer on the average microclimate pH inside polymer/NMP depots (determined by EPR in vitro)

Recent erosion studies with PLGA/NMP in situ forming implants reported a lag phase of about 3 - 4 days in lactic acid release [163]. The amount of lactic acid released from the implants slowly increased from day 5 till 8 and afterwards steadily increased to a steady state after three weeks. After 14 days of incubation the pH_m began to rise and reached nearly neutral ranges after 21 days [163]. During polymer degradation the mechanical strength of the thin polymer membranes on the surface decreased. Furthermore the dissolved polymer degradation products accumulated inside the pores and therewith increased the osmotic pressure inside the implants. Both, the decreased

mechanical strength and the increased osmotic pressure yielded to polymer rupture on the surface. Pores and channels were formed that allowed the replacement of the monomeric and oligomeric acid by neutral incubation media inside the implants. The acidic steady state in the second week of incubation and the increase in the pH_m in the third week correlated well with the observed release pattern for the model drug TB in section 4.1.1.2 (Figure 22, page 52). Similar processes have been reported for PLGA microparticles before [155].

Two distinct differences can be observed for the AB diblock copolymers compared to PLGA. The pH_m inside PEG-PLGA/NMP implants remained almost constant during incubation and did not drop below pH 5 (Figure 35). EPR investigation on pre-shaped PEG-PLGA-PEG implants also yielded a pH of about 6 during incubation [159]. After 8 weeks of incubation the pH_m reached the pH of the medium. *Witt et al.* concluded that acid degradation products did not accumulate inside the implants and degradation started immediately after incubation. As for PLGA-based ISFI, the pH_m of the ISFI from pegylated PLGA can be correlated with the release pattern (Figure 26, page 56). The higher PEG content resulted in a more hydrophilic character of the polymers, and thus facilitated both the diffusion of the model drug and the acidic degradation products out of the implants.

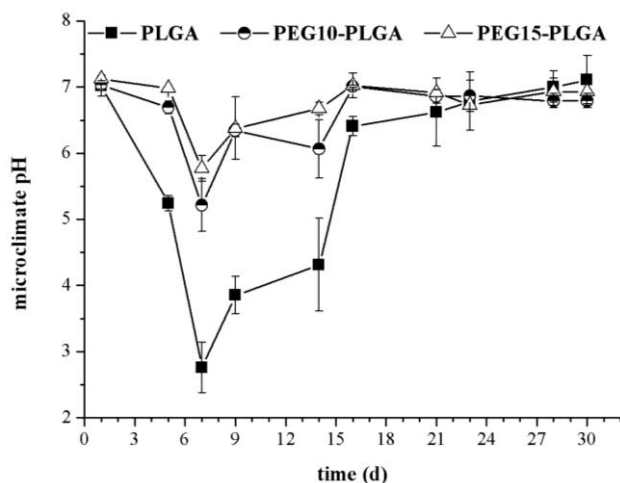


Figure 36 Effect of the type of the polymer on the average microclimate pH inside polymer/PEG 400 depots (determined by EPR in vitro)

As mentioned in section 4.1.1.3 (page 53) the substitution of NMP by PEG 400 as the polymer solvent yielded to more rapid polymer precipitation, solvent exchange and consequently total release of the model drug compound TB. This effect is also reflected

by the pH_m during incubation in neutral phosphate buffer. Figure 36 shows in the first week of incubation an initial decrease in pH_m for all polymers.

The most intense pH drop was observed for PLGA. Compared to implants prepared with NMP as solvent, no steady state acid pH_m was observed during the second week of incubation. Instead the pH inside the implants rose again to the neutral range after 21 days. This pH rise is related to the replacement of the entrapped acidified water by neutral buffer solution through the formed pores after 8 to 10 days and corresponded to the drastic increase in the release of the incorporated spin probe TB (Figure 26, page 2). The microenvironment in the PEG10-PLGA and PEG15-PLGA implants was less acidic than in PLGA implants, as shown in Figure 36. The pH_m of the implants exhibited above pH 5 during the whole time of incubation. Two factors contributed to the increased rate of acid release from the pegylated polymers: First the increased water uptake of the AB diblock copolymers was able to dilute acid concentration inside the implants pores. Second, according to *Witt et al.* PEG was preferentially lost from PEG-PLGA-PEG triblock bulk polymers during degradation. The dissolution and diffusion of PEG further created more water channels and pores and increases the permeability of the implant matrices. In conformity with these results *Ding et al.* reported that blending PLGA with 20 % PEG during microparticle preparation increased significantly the microclimate pH ($\text{pH} > 5$) during incubation [186].

4.1.4 Conclusions and outlook

Solutions of PLGA in organic solvents have been extensively investigated as novel drug depots in the recent years. Many researchers concluded that the phase inversion dynamics of the polymer solutions directly affect the drug release of the implants. But when starting this work, there existed no analytical methods to quantify directly and continuously the polymer precipitation and solvent exchange *in vitro and vivo*. Also systemic investigations about the internal pH of the formed implants were missing.

EPR was applied to shed more light into these in situ forming drug delivery systems. For the first time it was possible to detect implant formation of PLGA/NMP solution online, non-invasively and continuously both *in vitro* and *in vivo* in living mice. Also the distribution of a model drug substance within the polymer was monitored. Furthermore the replacement of the organic solvent NMP by water was measured and

could be quantified by detected polarity shifts within the implant. Both, the kinetics of NMP/water exchange and polymer precipitation showed good *in vitro* - *in vivo* correlation. The EPR method was further successfully applied to other solvent (PEG 400) and polymers. Novel AB diblock copolymer of PEG and PLGA were firstly explored as polymeric matrices for ISFI. The phase separation kinetics were highly dependent on the polarity and the polymer affinity of the solvents, as much as the hydrophilic character of the used polymers. The ability to quantify the amount of the remaining organic solvent inside the implants gives unique opportunities to assess the stability of sensitive drug molecules, like proteins, in these formulations. Another parameter that affects the stability of incorporated ingredients is the microclimate pH. It could be shown that the pH inside PLGA-based in situ forming depots acidifies during incubation down to pH_m 2.5-3. Whereas implants made from pegylated PLGA exhibited $pH_m > 5$ during whole time of incubation. Therefore the novel AB diblock copolymers represent a promising alternative biomaterial for in situ forming depots intended for the parenteral delivery of pH-sensitive drugs. The EPR data further suggest that drug release from in situ forming implants is a complex mechanism including water penetration and drug diffusion and can be varied by the choice of solvent and polymer.

The presented non-destructive EPR method gives unique information about the micropolarity, microviscosity and pH inside in situ delivery systems and can be used as a valuable tool of their development and optimization both *in vitro* and *in vivo*.

To get more direct information about the biological response to the in situ forming depot, Bt-MRI was firstly applied to monitor the formation and disappearance of ISFI. The images were conducted with a newly developed *in vivo* benchtop MR Imager without the use of contrast agents in a non-invasive and continuous manner. PEG 400 provided an excellent MRI signal and contrasts to the biological tissue and allowed to follow the processes of solvent/non-solvent exchange and polymer precipitation. The results were in good agreement with previous EPR measurements. The high water affinity of PEG 400 caused the formation of subcutaneous edema. Even though it is regarded as a well tolerable and biocompatible solvent; the local injection of high amounts has to be critically revised. Beside the formation of the transient edema, encapsulation of the implant as a response of the biological system was detected with all investigated polymers, followed by disintegration over a period of two months.

MRI has the potential to enable new insights into the *in vivo* fate of in situ forming implants as well as other parenteral formulations then studied. This information may help to understand mechanisms of implant formation and to optimize drug release. The obtained results with the prototype of the benchtop apparatus proof that Bt-MRI is a new alternative for superconducting MRI machines for *in vivo* MRI on small mammals. Due to its low installation and running costs, Bt-MRI will be used more frequently in pre-clinical formulation research.

Recently *Schoenhammer et al.* reported that low molecular PEGs accelerate the degradation of PLGA in solution as a result of trans-esterification [167]. So the stability of PLGA in PLGA/PEG 400 solutions may be beside edema formation another obstacle in its use as an alternative solvent. The long-term stability of PLGA or PLGA-based polymers is a general issue that has not been resolved yet. Two different approaches have been followed to overcome this limitation. One attempt is to search for new solvents, e.g. PEG-dialkylether [167], which do not or minor cause polymer alteration [167]. The alternative approach is to develop new degradable biomaterials that need less or no organic solvents. *Trimaille et al.* synthesized alkyl substituted polylactides. The created hexyl-substituted polylactides (hexPLA) possessed unique physicochemical properties [189]. They are semi-solid and injectable without or with only small (< 5 %) amounts of NMP. The hexPLA systems can be sterilized by dry heat and degrade in a continuous manner without the formation of acidic microenvironments.

4.2 Thermally-induced chitosan-based gelling systems

As illustrated in the previous section, the need of organic solvents is one of the major reasons for the fact that in situ forming implants based on phase separation by solvent exchange have not reached the wide public so far. Aware of those problems many researchers oriented towards environmentally responsive hydrogels. Of special interest are hydrogels that respond to temperature changes in their environment as the sole stimulus for their gelation. Ideally the aqueous solutions are liquid at ambient temperature and gel under physiological conditions [67;190]. Many new formulations based on this principle have been proposed for drug delivery [66;191-193], tissue engineering [11;194] and cell encapsulation [68;195;196] purposes. Among the natural polymers that exhibit gelation upon temperature change, particularly chitosan-based systems have been studied in detail in the past decade [65;137;197-200]. Chitosan is an amino-polysaccharide obtained by alkaline deacetylation of chitin, obtained from the exoskeleton of crustaceans such as shrimps or crabs. It is one of the most abundant natural polymers on earth [198]. The chitosan production is of low cost due to the biological renewable sources and thus ecological and economical interesting. Applications include wastewater treatment, agriculture, food and cosmetics [42]. Additionally chitosan possess unique properties that have yield in many biomedical applications [42;198;201]. Chitosan is biocompatible [42;201] and biodegradable, as it can be metabolized by certain human enzymes, e.g. lysozyme [202]. The biopolymer lacks irritant or allergic effects and has a very low toxicity. The oral LD₅₀ for mice is 16 g/kg body weight, which is in the range of sugar [201]. Further it is bioadhesive [203], promotes wound healing [204] and has shown antibacterial activity [201] and permeation enhancing effect for peptides [203]. Chitosan is soluble in acidic solution because of the protonation of the free amino groups in its molecular structure and at pH > 6 it shows phase separation. The addition of polyol salts, e.g. β -GP to acidic chitosan solutions allows rising the pH to neutral without phase separation. These chitosan/ β -GP systems are thermosensitive and form hydrogels at temperatures of 37 °C (Figure 37) and below [3]. Three types of interaction are discussed to be involved in the gelation process: (1) electrostatic attraction between the ammonium groups of chitosan and the phosphate groups (2) hydrogen bonding mainly between the hydroxy groups and (3) hydrophobic interactions between the chitosan chains.

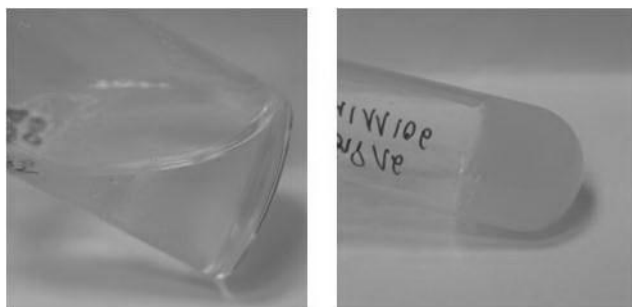


Figure 37 Chitosan/ β -GP system at room temperature (left) and after treatment at 37 °C (right)

In general the drug release rate from gels is determined by several parameters, including the size of the drug, the microviscosity and the mesh size of the polymer network [205]. Up to date, chitosan/ β -GP systems have been characterized mainly by measurements of macroviscosity. No data concerning the molecular properties inside the gel are known so far. It was the aim of the studies below to shed more light onto the microviscosity and microacidity inside the thermogelling chitosan/ β -GP systems and the release pattern of a model protein by EPR spectroscopy. These molecular parameters are important especially for an understanding and optimisation of these promising drug delivery systems. In previous studies the sol-gel transition of chitosan/ β -GP systems has been mainly examined by rheology [200;206]. But rheology methods, which are widely used to characterize hydrogels, are often time consuming, risking dehydration of the gels and report only on systems macroviscosity. $^1\text{H-NMR}$ Relaxometry was tested as an alternative non-invasive method to resolve in real time the phase transition behaviour of chitosan/ β -GP hydrogels in dependence of formulation parameters. To make chitosan/ β -GP hydrogels accessible for lipophilic drugs, an oil loaded chitosan hydrogel system was developed. It is described below how the composition of these thermoresponsive chitosan-based emulsions was optimized to high oil contents and sol-gel transition near body temperature. Further the release pattern and the microenvironment of incorporated model drug compound was examined by EPR spectroscopy.

4.2.1 Characterization of thermosensitive chitosan/ β -GP systems

4.2.1.1 Influence of formulation parameters on the macro- and microviscosity

When heated above room temperature, the initially clear chitosan/ β -GP solutions transformed into opaque gels (Figure 37). With the investigated chitosan concentration (2.5 % (w/v)) no temperature induced gelation of chitosan/ β -GP preparations was observable for β -GP concentrations below 6 % (w/v). This result was in agreement with the findings by Wang [207]. The systems described by Wang did contain acetate and they presented thermo-reversible gels within a pH range from 6.6-6.9 and were partially thermo-reversible above pH values of 6.9 at concentrations ranging from 0.5-2 % for chitosan and 2-8 % for β -GP [207]. The acetate free preparations, presented within these studies, did not show any thermo-reversibility of gelation. Once the gelation did occur, the systems did not reliquefy.

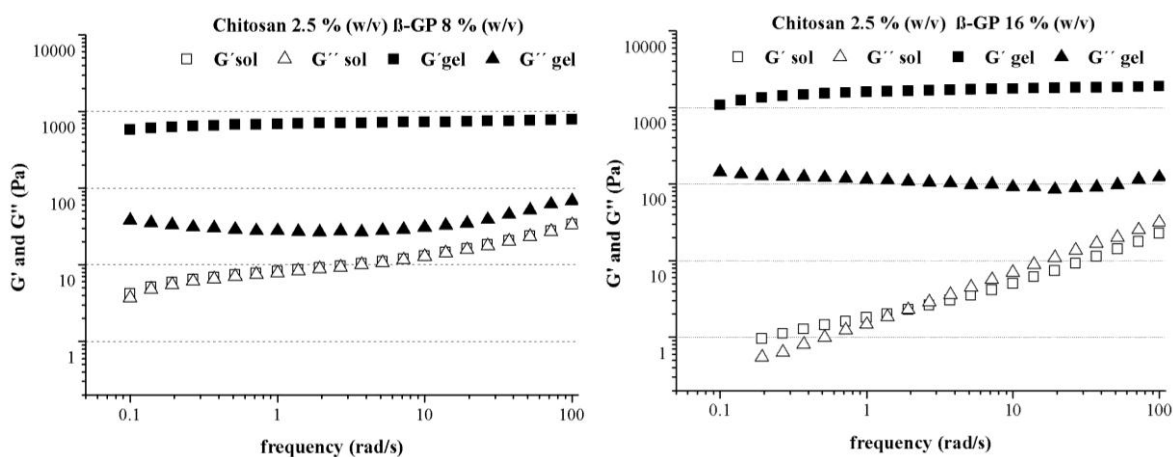


Figure 38 Frequency dependence of storage (G') and loss (G'') moduli of chitosan/ β -GP mixtures with different GP content before(sol) and after(gel) thermally-induced gelation

The rheological characterisation showed significant differences between the sol and gel state of chitosan/ β -GP systems. For the sol systems low values (0.5 Pa up to 35 Pa) of the storage (G') and the loss (G'') modulus (Figure 38) were found. The loss and the storage moduli were comparable, leading to a phase angle of about 45° (tan delta around 1, see Figure 39). The values of the storage and the loss moduli and the phase angle were typical for low viscous systems with a low degree of elasticity. Higher β -GP content resulted in a decrease in both G' and G'' . Chenite *et al.* reported a similar rheological behaviour when they compared chitosan/ β -GP solutions with chitosan solutions [200]. The effect can be explained by charge neutralisation of the chitosan and therefore

increased flexibility of the polymer chains and hampered chain interactions of the polymer in the presence of β -GP. The increased G' with increasing frequency is characteristic for unlinked polymers. The gelled systems showed a much higher viscosity compared to the sol systems of the same composition (Figure 38). A considerable increase of the loss modulus was noticed, which is higher for the gel system with 16 % β -GP. However, the increase in the storage modulus was much higher compared to the increase of the loss modulus for both systems, indicating the formation of a strong gel network with high elasticity (Figure 38). The frequency independent behaviour of G' was typical for highly cross-linked polymers or rigid gels. The storage modulus of the 16 % β -GP gel exceeded 1000 Pa, the storage modulus of the 8 % β -GP system remains slightly below this value, indicating that a higher β -GP amount leads to stronger gels. The high elasticity was also reflected in very low values of tan delta, which are around 0.1 and below (Figure 39).

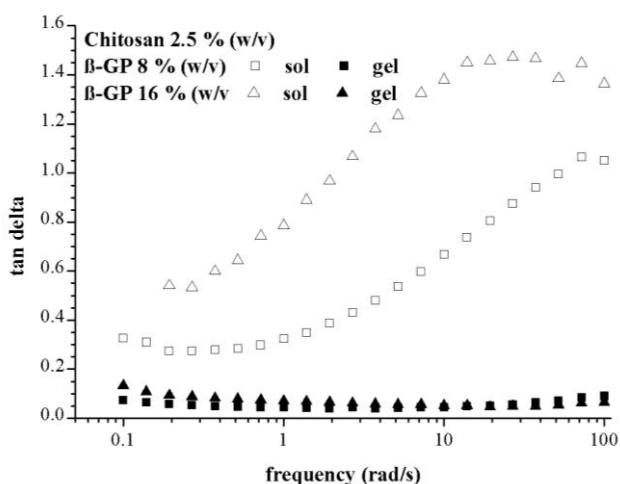


Figure 39 Tangents of the phase delta of chitosan/ β -GP mixtures before (sol) and after (gel) thermally-induced gelation

In conclusion, oscillating rheology proved the formation of strong elastic gels by the thermogelling of the chitosan/ β -GP systems. The gel formation was visible in a strong increase, more than two orders of magnitude, of the storage modulus G' and a decrease of the phase angle, as it has been reported for similar chitosan/ β -GP systems before [200;207]. Differences between systems containing 8 % and 16 % β -GP were detectable, but small compared to the temperature induced gelling effect.

The viscosity at the molecular level (microviscosity) was explored by EPR spectroscopy. The EPR spectra of the hydrophilic, low molecular weight nitroxide AT had very similar shapes before and after gelation (Figure 40). The spectral shape

[208]. They also investigated the microenvironment of chemically cross-linked chitosan gels by EPR spectroscopy using the nitroxide tempol and spin-labelled lidocaine. The correlation times of both spin probes were found to be equal in gels of different degree of deacetylation, whereas the translational diffusion of lidocaine was strongly affected. They concluded that the free space (pores) available for the rotation of the spin probes was not affected significantly.

4.2.1.2 Investigation of water dynamics by $^1\text{H-NMR}$ Relaxometry

In the past the thermal gelation of chitosan/ β -GP systems was mainly studied by rheometry [200;207;209-211]. In the course of which rheological studies focused either on the determination of the phase transition temperatures or gelation times. Several factors have been identified to influence the gelation process, such as concentration [200;210], molecular weight [64] and DD of chitosan [64;137], concentration of β -GP [137;200;210], type of organic or inorganic acids [136] or the influence of additives like urea [209]. Although rheology methods are widely used to characterize hydrogels, they suffer several limitations. They report only on macroviscosity and are often time consuming, thereby risking dehydration of the gels. Alternatively *Lavertu et al.* used light transmittance measurements to determine precipitation in chitosan/ β -GP solutions as a surrogate for gelation [212]. The vial inversion method (VIM, also called benchtop rheology) represents another widely accepted simple, inexpensive and quick method to study sol gel transitions of thermosensitive polymers [63;136;137]. By inverting the test tube, solution is defined as sol phase if it deforms by flow and nonflowing as a gel phase [137]. Although transition temperatures determined by turbidity measurements or VIM correspond to results of rheological measurement, there are distinct differences in the ascertained gelation times [213]. It is common to all of the presented methods, that they give no information about the state of water in the hydrogels. Methods that analyses the physicochemical properties of water in hydrogels are calorimetry, differential thermal analysis or NMR spectroscopy. Relaxation in $^1\text{H-NMR}$ is highly sensitive to the dynamics of water molecules and mainly controlled by dipole-dipole interactions of neighbouring protons [214]. Due to the dependence between the dynamics of the molecular groups and the temperature, phase transitions can be also observed by $^1\text{H-NMR}$ [215]. The $^1\text{H-NMR}$ transverse relaxation time T_2 , as a marker

for proton mobility (see 3.2.2, page 31), inversely correlates to the dynamic viscosity (η) as shown for example for Newtonian fluids [5], carbohydrate solutions, fruit juices, beer and wine [216]. Further studies demonstrated that T_2 - η correlation can be applied to suspensions [217], sucrose ester nanodispersions [218] and hydrogels of bolaamphiphiles [215], dextran [214], gellan [219] and chitosan-cyclodextrin [219].

Proton relaxation times (T_2) of water in chitosan/ β -GP solutions were measured at 20 MHz in the temperature range of 5 to 75 °C to get an insight into the dynamics of the water molecules resulting from their environment. The obtained curves of the transverse magnetization decays were fitted with the program WinDXP, which uses Laplace inversion to calculate T_2 distributions [215].

Figure 41 displays the full-range T_2 distributions for a chitosan/ β -GP system (chitosan 2.5 % (w/v); β -GP 16 % (w/v)) before and after gelation with distilled water as reference. The water sample showed one major peak at about 2.7 s representing the majority of the water protons of the unperturbed water. The additional small peaks at lower relaxation times have been related in previous investigations to water protons at the glass surface of the sample vials [215]. *Bastrop et al.* proved that under the present experimental conditions the major T_2 peak was not attributed to surface phenomena.

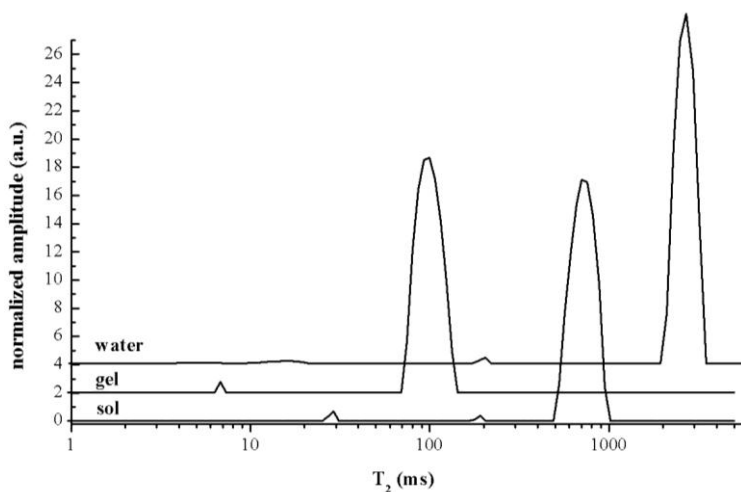


Figure 41 Normalized T_2 distributions for chitosan/ β -GP sol and gel compared to that of distilled water (chitosan 2.5 % (w/v) and β -GP 16 % (w/v))

Instead it reflected the dynamical properties of the main fraction of the water molecules in the sample. For the chitosan/ β -GP solution the major T_2 peak, that represented the majority of the water of protons, was slightly broadened and shifted to lower values of T_2 , reflecting a more viscous environment. Gelation of the systems resulted in a more viscous environment expressed by a further shift of the major T_2 peak by the power of

ten to about 100 ms. The formation of the gel network affected the relaxation behaviour of water protons. The protons of the water molecules in the gel network were motionally restricted and therefore showed lower T_2 values [219]. The distinct differences between the sol and gel state in the macroviscosity confirmed by rheology were even reflected by differences in the relaxation behaviour of water protons.

In general the dynamics of water molecules in hydrogels are affected by their interaction with the matrix network. Thereby several factors are important, such as the hydrophobicity of the matrix, flexibility and charge density of the polymer chains and the degree of cross-linking defining the network pore size [219]. At least two average states of water can be distinguished, which relax with different time constants. The domain of “free” or unperturbed water is related to water molecules that do not interact with solid particles or dissolved molecules located in the meshes of the gel [214;219]. The second domain, called “bound” or perturbed water, comprise water molecules which are tightly bound to the matrix or water molecules in the hydration shell [216]. If the two domains are not coupled and differ in their time constant by orders of magnitudes, a bimodal decay in the magnetization can be observed [219]. Generally these fractions of water exchange with each other leading to shorter T_2 values in comparison to pure water [217]. The chitosan/ β -GP systems possess high water content. Despite the existence of different water fractions (free water, water in hydration shell or matrix bound water), only mono-exponential relaxation process was observed. This can be explained due to the fast exchange between free and bound water [214]. Concurring relaxation behaviour has been reported for chemically cross-linked chitosan gels [220]. In those, the amount of unperturbed water was so high that it hid the signals of the chitosan protons and water protons tightly bound to the polymer or located in solvation shells around the chitosan chains. Chitosan/ β -GP solutions were prepared with D_2O to study the relaxation behaviour of the protons of the chitosan molecules (Figure 42). During sample preparation protons of the chitosan molecules partly exchanged with D_2O , producing small amounts HDO and H_2O . Figure 42 shows that besides the major T_2 peak, that represents HDO and H_2O molecules, a small peak around 30 ms was detectable that could be associated with chitosan. The gelation process did not influence the mobility of the chitosan protons in the dimension as observed for water protons. T_2 peaks below 10 ms can be related to HDO molecules interacting with the glass surface.

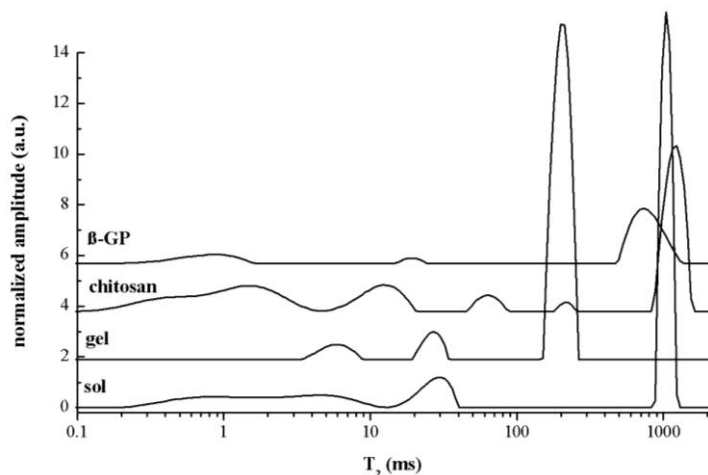


Figure 42 Normalized T_2 distributions for chitosan/ β -GP sol and gel compared to that of chitosan and β -GP obtained in D_2O (chitosan 2.5 % (w/v) and β -GP 16 % (w/v))

Because of the high amount of water in the chitosan/ β -GP systems and the main attribution of water molecule protons to T_2 , mono-exponential analysis of the magnetization decay curves was performed to calculate an average transverse relaxation time (T_{2m}) of the whole system. To monitor the phase transition process, the temperature dependence of T_{2m} was studied for several chitosan/ β -GP solutions with varying β -GP content. In the low-temperature range T_{2m} increased linearly with increasing temperature in all solutions independent on the β -GP content (Figure 43).

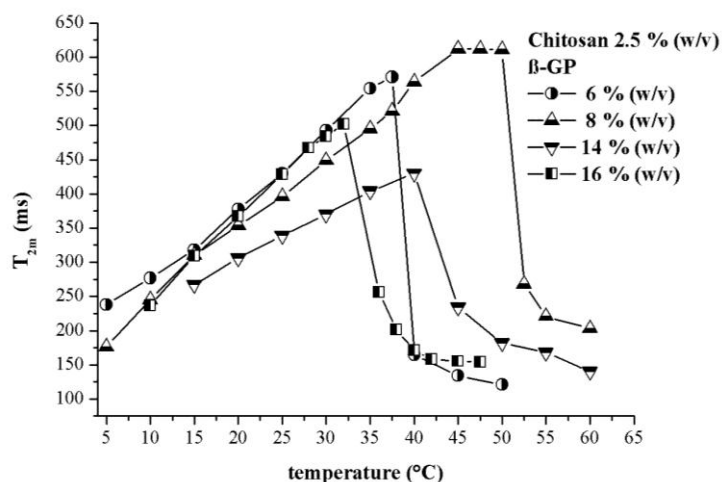


Figure 43 Temperature dependence of T_{2m} water relaxation times in chitosan (2.5 % (w/v))/ β -GP solutions with varying β -GP content

Similar behaviour have been recently observed for distilled water [215]. The predominant relaxation mechanism is based on intra- and intermolecular dipole-dipole interactions [214]. The phase transition temperature was marked by a sharp decline in T_{2m} (Figure 43). The decrease of the relaxation time with increasing temperature is typical if the proton exchange process is dominated via chemical exchange between the protons of the matrix, especially from the hydroxylic groups, and water. Proton

exchange processes overlap with the dipole-dipole interactions [214]. The activation energy of the proton exchange process is responsible for the inversion of the temperature dependence of T_2 and explains the endothermic gelation of chitosan/ β -GP solutions.

Chenite et al. described a broad range of molecular interactions between the cationic polyelectrolyte chitosan and the divalent anionic base glycerol phosphate to contribute to the gelation mechanism of chitosan/ β -GP solutions [200]. The authors specified mainly electrostatic repulsion between alike charged chitosan-chains, electrostatic attraction between the opposite charged chitosan and β -GP and attractive hydrophobic and hydrogen bonding between the polymer chains. At low temperatures water molecules enclosed the alike charged polymer chains [209]. The addition of β -GP prevented the chitosan solution to precipitate at $\text{pH} > 6.2$ by potential attraction of the β -GP phosphate groups to remaining charged amine moieties of chitosan. Thereby the glycerol moieties separated the chitosan chains sterically [200]. Upon heating the vibrational and rotational energy of the water molecules increased and thus reduced the weak hydrogen bonding interactions that oriented dipolar water molecules around the polymer chains [209]. The higher molecular mobility and decreased number of hydrogen bonds was reflected by a lower systems viscosity which is expressed by higher values of T_{2m} (Figure 43). Above the sol-to-gel transition temperature a physical gel network was formed. The water molecules which enclosed the polymer chains were removed promoted by the increased structuring of free water by the glycerol moiety of β -GP. The dehydrated polymer chains aggregated via interchain hydrophobic interactions. *Cho et al.* reported an increased ionic strength of the chitosan/ β -GP solutions as a function of temperature [209;210]. They suggested that enhanced screening of electrostatic repulsion and increased hydrophobic effect along with the decreased chitosan solubility to be the main driving force for chitosan/ β -GP gelation at elevated temperatures [209;210]. Indeed hydrophobic interactions between polysaccharide chains can be favoured in the presence of water structuring molecules, such as polyols [221]. *Cho et al.* further observed, that increasing the temperature decreased the ratio of $-\text{NH}_3^+$ in chitosan and $-\text{OPO}(\text{O})_2$ in β -GP [211]. The reduction of ionic interactions with increasing temperature and the fact that β -GP is freely diffusible after gelation excludes purely ionic cross-linking to be responsible for

gelation of aqueous chitosan solutions [200;211]. *Filion et al.* observed that heated chitosan/ β -GP solutions got partly neutralized by proton transfer from chitosan amine groups to β -GP phosphate groups [212;222]. The proton transfer led to diminution of chain charge density and chitosan attraction to β -GP and further allowed attractive interchain forces to form physical cross-lined gels. Temperature induced precipitation of chitosan also occurred using disodium phosphate or 2-(4-morpholino)ethanesulfonic acid (MES) instead of β -GP. *Filion et al.* concluded that the key feature of the used buffering agents was the ability to absorb heat-stimulated released chitosan protons for facilitating chitosan neutralization [212]. In addition the formation of hydrogen bonds between chitosan macromolecular chains have been reported by *Zeng et al.* [223]. To sum it up heat-induced gelation of chitosan/ β -GP systems is mainly attributed to secondary hydrophobic and hydrogen bonding interactions between the polysaccharide chains.

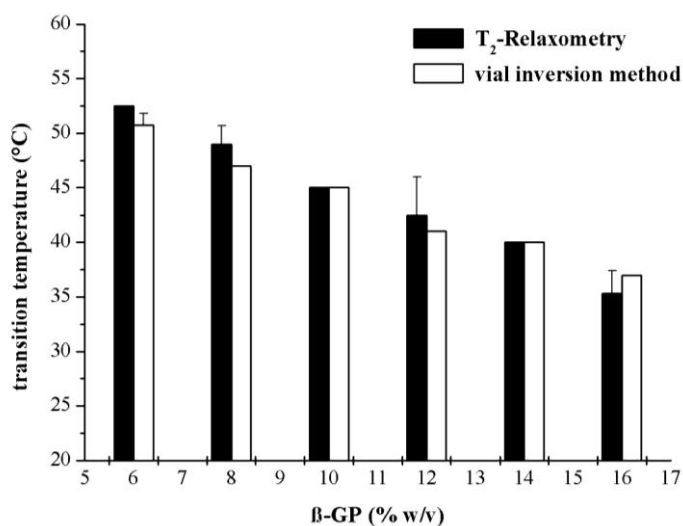


Figure 44 Phase transition temperature of chitosan(2.5 % (w/v))/ β -GP solution in dependence of β -GP content

With ascending β -GP contents, the sol-to-gel transition point shifted to lower temperatures (Figure 43 and Figure 44) from about 55 °C (6 % β -GP) to about 37 °C (16 % β -GP). This effect has been reported in literature before [200;210]. *Cho et al.* assumed that with increasing β -GP concentration and increasing pH the chitosan protonation decreased [210]. Therefore higher β -GP concentrations promoted polymer contacts via hydrophobic and hydrogen bonding interactions and accelerated gelation. The authors confirmed an enhanced screening of electrostatic repulsion between glucosamine groups, measurable by an increase of the ionic strength of the solutions at higher β -GP contents. *Lavertu et al.* proposed an alternative hypothesis: higher amounts

of β -GP were more effectively to accept heat-stimulated released chitosan protons, such that chitosan gelled at lower temperatures [212].

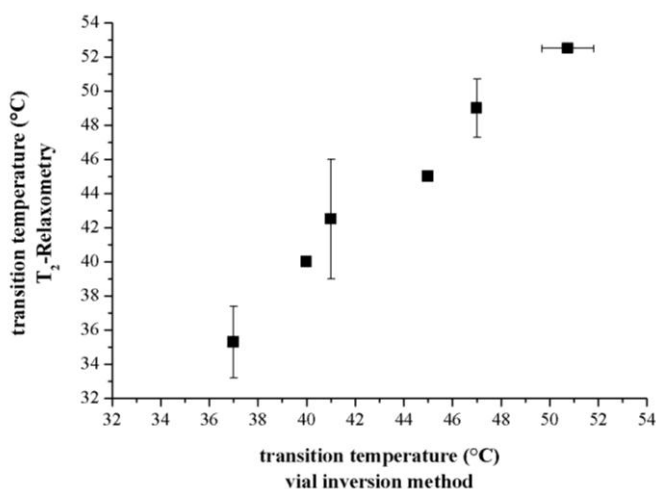


Figure 45 Correlation of phase transition temperature of chitosan/ β -GP solutions determined by different techniques (chitosan 2.5 % (w/v) and β -GP 6 % (w/v) - 16 % (w/v))

The phase transitions temperatures determined from T_{2m} graphs were consistent with that obtained by classical vial inversion method (Figure 45). The good correlation, is expressed by a linear correlation of the values ($R = 0.99$). This suggests that $^1\text{H-NMR}$ relaxometry is capable of detection temperature induced sol-to-gel transitions in chitosan/ β -GP solutions. Because of the opposite temperature dependence of the relaxation mechanism the matrix-solvent proton transfer could be distinguished from dipolar interactions of the solvent.

In addition to LCST determination, $^1\text{H-NMR}$ relaxometry have been used to determine gelation time at the accordant LCST for different β -GP concentrations (Figure 46). During gelation T_{2m} decreased mono-exponentially indicating the formation of the gel network. The initial gelation is characterized by a rapid decrease of T_{2m} within the first 30 minutes (Figure 46) and optically visible as an increase in turbidity (Figure 37). The initial results were in good agreement with previous reports where gelation times were determined by rheology [224;225] or vial inversion method [137]. The further gel formation slowed diffusion and mobility of the polymer chains. The system viscosity stabilized within one to two hours. Previous time-dependent rheological measurements have shown that complete gel formation took from one to nine hours, dependent on the chitosan/ β -GP composition and acids used [136;225]. Several factors have been reported to shorten the gelation time e.g. increasing both chitosan and β -GP concentration or temperature [137;210]. At isothermal conditions the gelation time

could be reduced by increasing the β -GP content [137]. In contrast at transition temperature the gelation kinetics were nearly independent of the β -GP content [210].

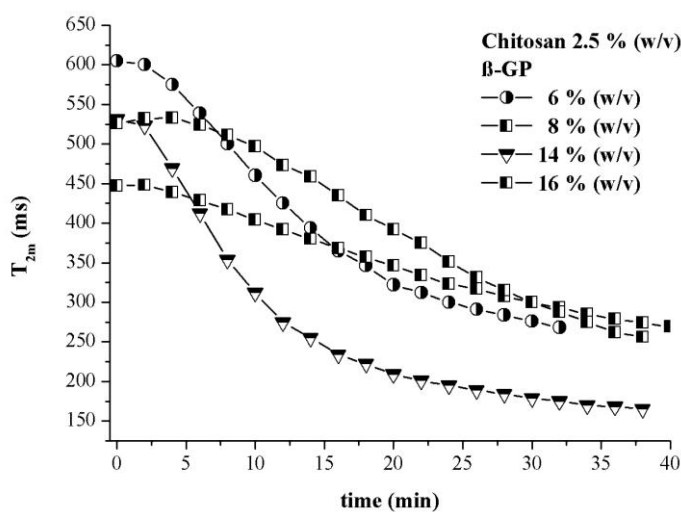


Figure 46 Time dependence of T_{2m} water relaxation times at phase transition temperature (based on mono-exponential analysis) of chitosan(2.5% (w/v))/ β -GP solutions with varying β -GP content

Storage stability is a major concern in the development of licensable and merchantable products. So far studies concerning the storage stability of chitosan/ β -GP solutions or about the selection adequate storage methods are quite rare. *Chenite et al.* stated that their chitosan/ β -GP solutions were storage stable at 4 °C for at least three months [200]. In contrast *Schuetz et al.* showed, that gelation was also induced by time at room temperature as well as during refrigeration [221]. Also *Cho et al.* detected spontaneous gelation at 5 °C when chitosan concentration was increased above 0.02 M.

Upon storage at 4 °C to 6 °C the chitosan/ β -GP solutions showed a remarkable increase in the system viscosity expressed by a decrease in T_{2m} (Figure 47). Thereby spontaneous gelation was favoured in systems with higher β -GP content and yielded to a loss of injectability. *Montembault et al.* proposed that above a critical concentration chitosan solutions initially contain precursors of the gelation, constituted of chitosan-chain self-aggregates in the nanometric size [226]. So high molecular weight chitosan, at high concentration could gel without any external trigger. Slightly higher pH of higher β -GP concentrated chitosan solutions seem to facilitate chitosan precipitation. *Ruel-Gariépy et al.* reported, that chitosan/ β -GP solutions also gelled at low temperatures, depending on the DD [65]. They found that chitosan/GP solutions with a DD of 95 % of chitosan gelled after 8-10 hours at 4 °C. They were able to slow down the gelation rate by adding chitosan with a lower DD. The authors concluded that sol-to-gel transition started with the addition of β -GP and does not require a certain temperature.

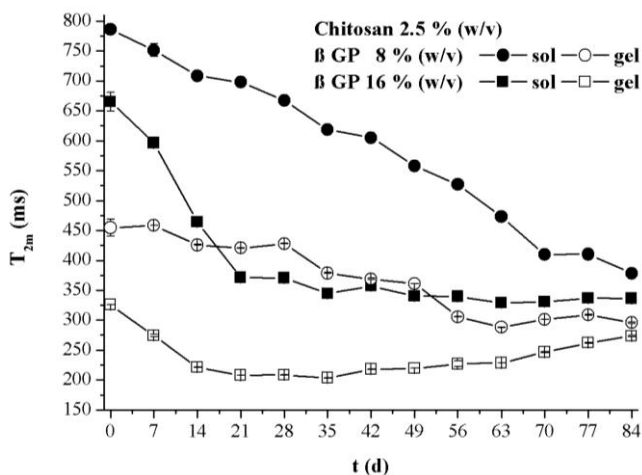


Figure 47 Storage time dependence of T_{2m} water relaxation times of chitosan (2.5 % (w/v))/ β -GP solutions with varying β -GP content

Also for the gels used in this study a post curing effect was observed under refrigeration (Figure 47). Though after 8 weeks of storage at 4 °C to 6 °C T_{2m} increased in chitosan (2.5 % (w/v))/ β -GP (16 % (w/v)) gels. This effect could be attributed to syneresis of the system. The hydrogel shrank and expelled water. Figure 48 shows the T_2 distribution curves of the gel after different storage times. With increasing storage time the major T_2 peak is considerably broadened and shifted to higher T_2 values. After three months an additional peak was detectable that could be related to unperturbed water (Figure 48).

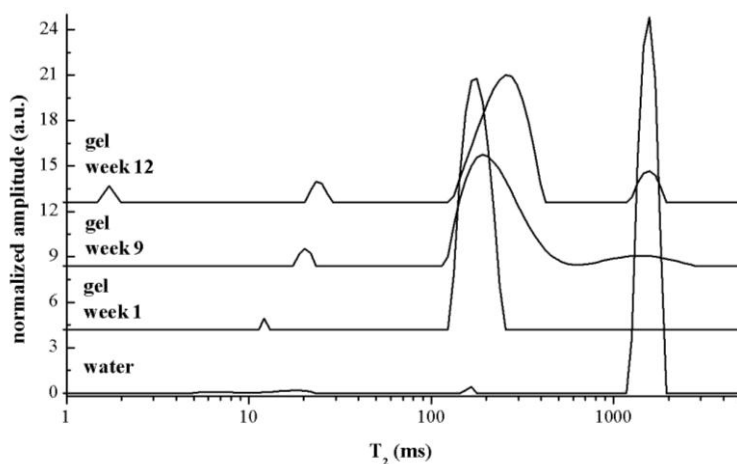


Figure 48 Normalized T_2 distributions for chitosan/ β -GP gel after different storage times compared to that of distilled water (chitosan 2.5 % (w/v) and β -GP 16 % (w/v))

4.2.1.3 Determination of microclimate pH

The microclimate pH of chitosan gels depending on the β -GP content was investigated by EPR spectroscopy. The incorporated spin probe AT has a pKa value of 6.1 and permits the measurement of pH values around pH 6.1 \pm 2 pH units. As with pH sensitive dyes, the accuracy is highest at the pKa and decreases with increasing differences between pH and pKa values. The $2a_N$ values of the nitroxide AT in β -GP

solutions were around 3.26 mT. These values indicated the fully deprotonated state of the probe. The conclusion from the EPR measurement was that the pH of the β -GP solution is 7.9 or higher. No exact pH can be measured due to the large difference between the pKa of AT (6.1) and the alkaline pH. The EPR results were in agreement with the pH determination by a glass electrode, which resulted in pH values between 9.1 and 9.2. Mixing of the acidic chitosan (pH values around 1.8) and alkaline β -GP solution resulted in pH_m values between 6.62 and 6.78 (Figure 49). Slight increase in the pH values with increasing quantities of β -GP have been described for other combinations of chitosan/ β -GP solutions before [207;224].

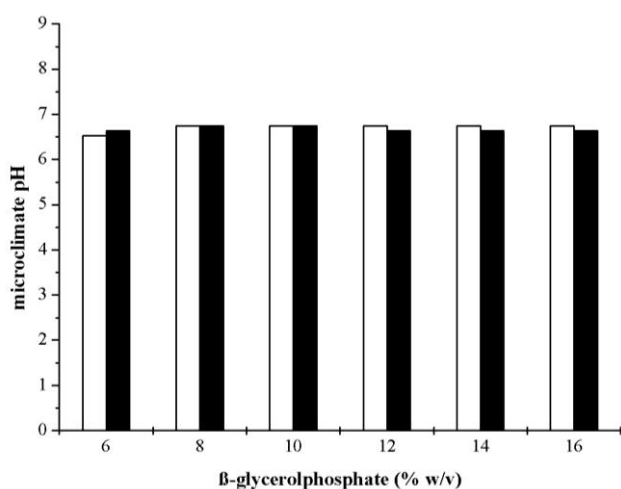


Figure 49 Influence of the β -GP content on the pH of the chitosan/ β -GP solutions and gels (white bars – sol, black bars – gel)

Two findings emerge from the experiments. Firstly, it is evident, that despite the ratio of the protonated chitosan to the alkaline β -GP changed by a factor of 2.66 between the 6 % (w/v) and 16 % (w/v) β -GP solutions, there was no significant impact of the chitosan/ β -GP ratio on the internal pH. Secondly, the pH_m values measured by EPR before and after thermogelling of the samples show, that the gelation formation process does not change the microacidity inside the sample. The pH remains all the time within a very narrow range. The chitosan and β -GP solutions and gels act as a buffering system. *Cho et al.* also observed a nearly temperature-indepenent pH in acetate containing chitosan/ β -GP and related it to the buffering capacity of the system [209]. Figure 50 shows, that upon incubation with neutral phosphate buffer the pH_m of chitosan/ β -GP gels increased.

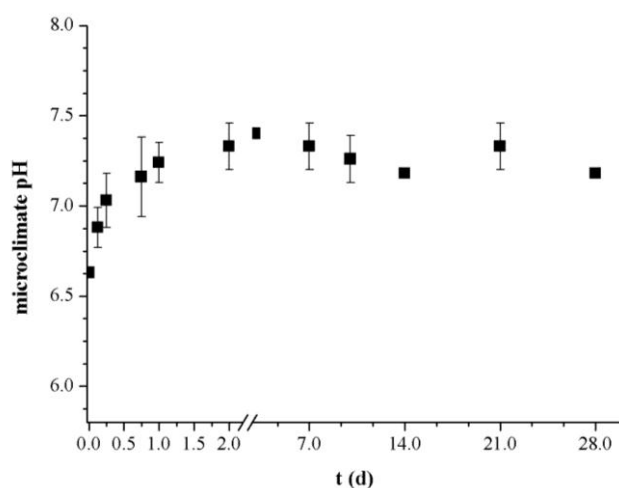


Figure 50 Changes in the average microclimate pH in chitosan gels (chitosan 2.5 % (w/v) and β -GP 16 % (w/v)) during incubation with phosphate buffer pH 7.4 (determined by EPR in vitro)

Proton exchange inside the gel yield to an adaptation of the pH_m up to the pH of the surrounding medium. Most of the β -GP diffused out of the gel leading to an overall neutral charge of the system [65]. The electro-neutrality of the gel combined with the large stability of the pH within a physiological range makes the system very attractive for protein delivery.

4.2.1.4 Feasibility study for sustained insulin delivery

In a further step, the impact of the chitosan/ β -GP gel on the protein status and release rate was explored. Insulin was chosen as a model protein and spin-labelled according to established procedures [95]. The EPR spectra of spin-labelled insulin are shown in Figure 51. The spectral shape indicated a high mobility in buffer, which was reflected in rotation correlation times of less than 0.2 ns (Table 5). However, lower insulin concentrations showed the lowest rotation correlation times and therefore the highest mobility. In contrast the hyperfine splitting parameter was independent from the insulin concentration, indicating no differences in polarity of the microenvironment for the spin-labelled insulin.

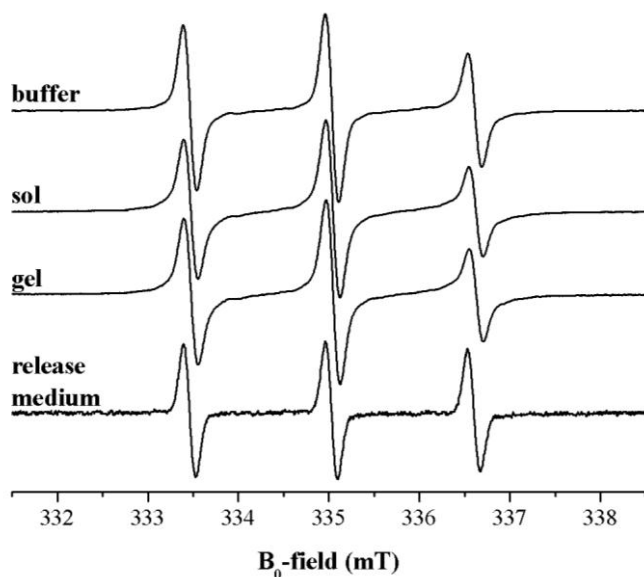


Figure 51 In vitro X-band EPR spectra of spin-labelled insulin in different environments: phosphate buffer, chitosan/ β -GP solution, chitosan/ β -GP gel (all conc.: 2 mg/ml), and released spin-labelled insulin in phosphate buffer (conc. ca. 0.005 mg/ml) (chitosan 2.5 % (w/v)/ β -GP 16 % (w/v))

The EPR spectra of spin-labelled insulin in the chitosan/ β -GP sol and gel showed also high mobility (Figure 51). Quantitative analysis of the EPR spectra yielded to the fact, that the gelation process had no impact on the molecular mobility of insulin. The EPR spectra of sol and gel states were superimposable. This finding indicated that insulin, although larger compared to the nitroxide AT was not hindered in its mobility by the formation of the gel network. However, it was found that the β -GP concentration affected the molecular mobility. Higher concentrations showed a slower tumbling rate and a higher rotational correlation time. This results agreed with the general knowledge about insulin, which tends to aggregate at higher concentrations [227]. The rotation correlation of spin-labelled insulin was (although still very fast) more than doubled in 8 % (w/v) β -GP systems compared to 16 % (w/v) β -GP preparations. The formulation with the higher β -GP content, higher gel strength and a higher macroviscosity had, in contrast to the expectations, a lower microviscosity inside the gel network. The EPR spectra of the released insulin overlapped with their spectral shape in the buffer with low insulin concentrations (Table 5). This led to the supposition that the spin-labelled insulin is released without denaturation (Figure 51).

Table 5 EPR parameters of spin-labelled insulin in chitosan/ β -GP sol and gels. High rotation correlation times indicate a slow tumbling rate and low mobility. High hyperfine splitting values indicate a polar environment. (standard deviations are below 5 percent)

Sample	τ_c (ns)	a_N (mT)
Insulin solution (conc. mg/ml)		
2	0.16	1.60
0.5	0.14	1.59
0.21	0.10	1.59
0.009	0.03	1.59
Chitosan 2.5 % (w/v)/ β -GP 8 % (w/v)		
sol	0.29	1.60
gel	0.28	1.60
Chitosan 2.5 % (w/v)/ β -GP 16 % (w/v)		
sol	0.13	1.60
gel	0.11	1.60
Released insulin in buffer	0.03	1.60

In order to investigate the impact of the β -GP content on the insulin release rate, chitosan/ β -GP gels with high (16 % (w/v)) and low (8 % (w/v)) β -GP concentrations were selected. A controlled release was achieved despite the high mobility of insulin within the gel (Figure 52). The insulin release rate did not differ between the formulations at early time points (up to 50 % release within 48 h). However, in the subsequent period a faster release from the gel with high β -GP content was observed. The faster release rate corresponded with the higher mobility of insulin in the 16 % (w/v) β -GP system (Table 2). It is evident, that the release was not linear, but more typical for diffusion controlled systems. Furthermore, the release is incomplete, about 15 % of insulin remain in the gel in case of the 8 % (w/v) β -GP and 10 % for the 16 % (w/v) β -GP formulation. Negatively charged moiety of the protein may displace β -GP and bind to the chitosan network via ionic interaction with the ammonium groups.

These results are supported by experiments from *Kofuji et al.*, who described the release of bioactive insulin from chitosan glycine gel beads [228]. They did also observe incomplete insulin release. However, their systems showed faster release rates of few hours, with 50 % release in 60 min.

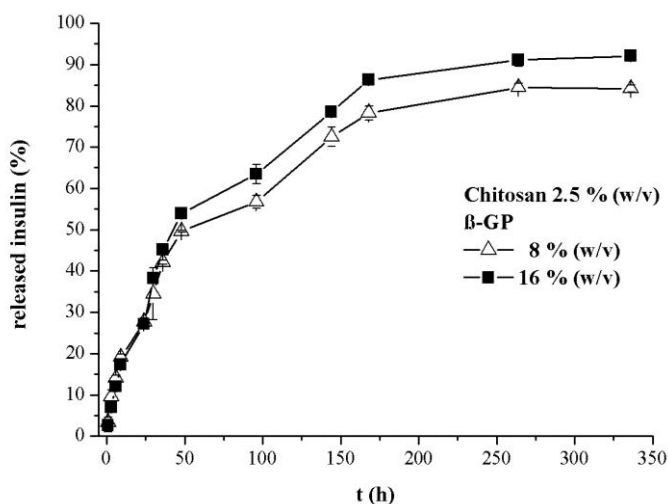


Figure 52 In vitro release kinetics of spin-labelled insulin from chitosan/ β -GP gels with different β -GP contents

Incomplete release of a albumin from chitosan matrices has also been described by *Ruel-Gariépy et al.* [65]. The initial drug loading considerably affected the release. At concentrations of less than 0.2 % the release rate was not affected by the electrostatic charge of the API. But at 3 % albumin loading part of the albumin was physically linked to the polymeric network allowing only partial release and reached a plateau after tree days. The addition of lysozyme speeded up the release rate by degrading the chitosan matrix [65]. Ionic interactions between oppositely charged groups have also been reported for positively charged peptides, proteins and anionic gels [229].

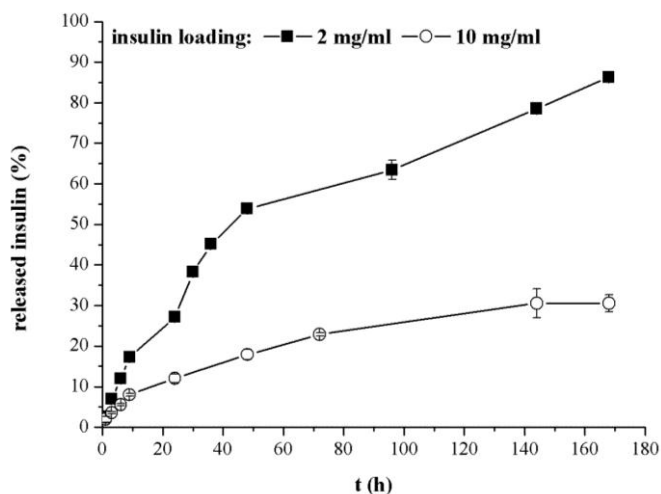


Figure 53 In vitro release kinetics of spin-labelled insulin from chitosan/ β -GP gels with different initial insulin loading (chitosan 2.5 % (w/v)/ β -GP 16 % (w/v))

Besides the composition of the chitosan/ β -GP gels, the release of insulin was affected by the initial drug loading (Figure 53). A fivefold increase in the initial insulin concentration decreased both the initial and total release rate. The 10 mg/ml insulin loaded gels possessed a minor initial burst effect (Figure 53) in comparison with the

2 mg/ml insulin loaded ones ($12.0 \% \pm 1.1 \%$ versus $27.1 \% \pm 1.2 \%$). The release of insulin from 10 mg/ml loaded gels reached a plateau after 7 days and a cumulative release of $30.5 \% \pm 2.1 \%$. By contrast with 2 mg/ml loaded gels a release period of 14 days and total release of $92.1 \% \pm 1.1 \%$ was achieved. Similar effects of the initial drug loading on the *in vitro* release profiles of paclitaxel from chitosan/ β -GP systems have been reported by *Ruel-Gariépy et al.* [66]. A tenfold increase in the initial paclitaxel loading reduced by half the initial burst as well as the cumulative release after one month.

One possible explanation for the delayed release from the gels with higher insulin load provides the higher feasibility for ionic interactions between insulin and chitosan. As observed for 2 mg/ml insulin loaded gels, also the EPR spectra of the insulin released from the 10 mg/ml insulin loaded gels are congruent with EPR spectra of low concentrated insulin in phosphate buffer (Figure 54), suggesting no conformational changes.

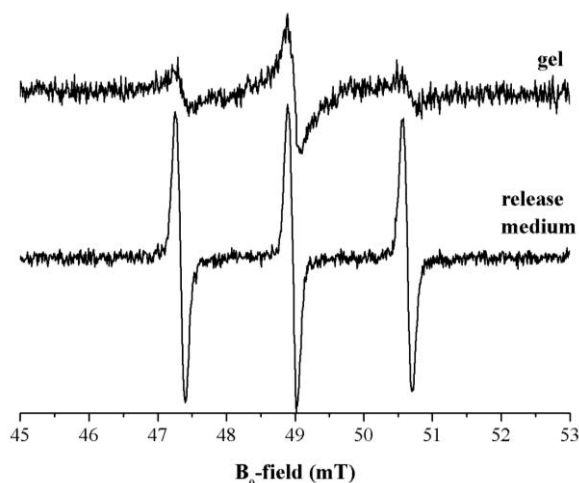


Figure 54 *In vitro* L-band EPR spectra of spin-labelled insulin in chitosan/ β -GP gel and release media after 7 days of incubation (chitosan 2.5 % (w/v)/ β -GP 16 % (w/v), insulin 10 mg/ml)

On the other hand the spectral shape of the spin-labelled insulin entrapped inside the chitosan gels at the end of the release period showed line broadening (Figure 54). The changes in the spectra pattern were expressed by a distinct increase in τ_c from $0.509 \text{ ns} \pm 0.03 \text{ ns}$ prior to $2.02 \text{ ns} \pm 0.02 \text{ ns}$ at the end of the release experiment. The spectral changes of the entrapped insulin can be related to conformational changes of the insulin or adsorption effects. *Boonsongrit et al.* investigated the drug-chitosan interactions of insulin in chitosan microparticles by IR spectroscopy and isothermal titration calorimetry [230]. Their results revealed that only a small amount of insulin

interact with the amine groups of chitosan. The entrapment of insulin was more linked to adsorption of insulin on the microparticle surface. Further they observed conformational changes of insulin caused by electrostatic interactions and hydrogen bonds between amino acid groups and charged chitosan molecule moieties or hydrophobic interaction with nonpolar moieties [230].

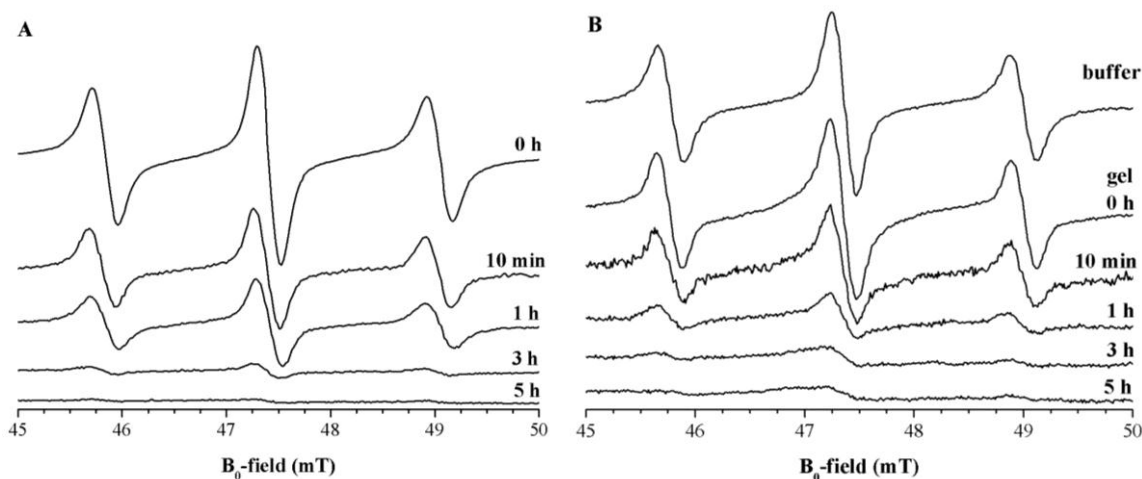


Figure 55 *In vivo* L-Band EPR spectra of spin-labelled insulin (10 mg/ml) in (A) phosphate buffer pH 7.4 and in (B) chitosan 2.5 % (w/v)/ β -GP 16 % (w/v) solution after subcutaneous injection in mice (with buffer as reference)

In connection with the *in vitro* experiments the release of spin-labelled insulin was investigated by EPR *in vivo*. Only insulin loading of 10 mg/ml yielded to a sufficient signal to noise ratio (Figure 55). Spin-labelled insulin was both dissolved in phosphate buffer pH 7.4 or chitosan/ β -GP solution and injected in the femoral of mice. The elimination of the injected insulin formulations from the injection site was followed continuously by EPR spectroscopy (Figure 55). The animal study was performed without the application of narcotics. Because narcotics may affect the kinetics of the model drug substance by influencing the central nervous systems and associated regulation metabolism [218].

Spin-labelled insulin administered in buffer solution rapidly diffused from injection site with first order kinetic (Figure 56). Within 10 minutes the amount of insulin at the injection site decreased to $63.5 \% \pm 8.8 \%$ and reached $33.4 \% \pm 10.6 \%$ after two hours. After 6 hours the signal was hardly distinguishable from the background noise (Figure 55). Within the first 120 minutes the release from the chitosan/ β -GP solutions showed a

similar pattern to the buffer solution. But after two hours the elimination of insulin was sustained and still $15.95\% \pm 4.8\%$ were detectable after 24 hours.

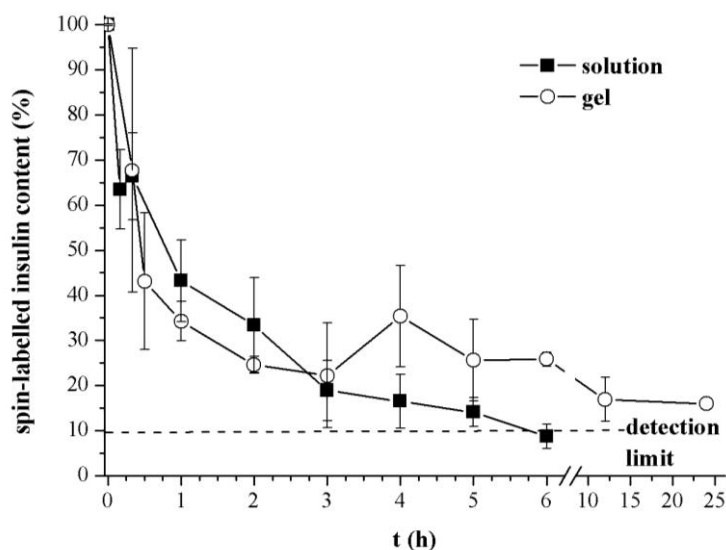


Figure 56 In vivo elimination of spin-labelled insulin (10 mg/ml) from injection site (chitosan 2.5 % (w/v)/ β -GP 16 % (w/v))

Several factors attributed to the quite different insulin release from chitosan/ β -GP gels *in vitro* and *in vivo*. First of all, the *in vitro* release experiments were carried out from pre-gelled gels with one site restricted access to the release media. Second, under *in vivo* conditions the gels still had to form. Further the tissue compressive forces and the poor mechanical strength of the gelling solutions limited the spreading of the implants. This yielded to flat architectures and shorter diffusions path compared to *in vitro*. Therefore for chitosan/ β -GP solutions the *in vivo* insulin elimination from injection site corresponded to solutions in buffer and was not sustained until the gelation of the implant was completed (Figure 56).

4.2.2 Characterization of thermosensitive chitosan-based emulsions

Several approaches have been attempted to achieve controlled release with chitosan/ β -GP gels. Because of the high water content of the hydrogels and the large pore size (1-20 μm) [213], hydrophilic compounds of low molecular weight generally diffused out the gels during the first hours of release [231]. Their release could be sustained by incorporating drug containing liposomes into the thermosensitive hydrogel [231;232]. In contrary macromolecules showed release periods of several hours to days [67]. Using the fat binding [233] and emulsifying [234] properties of

chitosan, olive oil was added to chitosan/ β -GP solutions to make the thermosensitive hydrogel systems accessible for lipophilic drugs.

4.2.2.1 Impact of formulation parameters on the water dynamics and macro- and microviscosity

The addition of olive oil to the chitosan/ β -GP solutions did not alter the overall thermosensitive gelling behaviour of the systems. The obtained emulsions were injectable and turned into solid gels upon heating. With increasing oil content the initial viscosity of the emulsions increased. The effect of the oil content on the storage and loss moduli, also called elastic and viscous moduli, is shown in Figure 57.

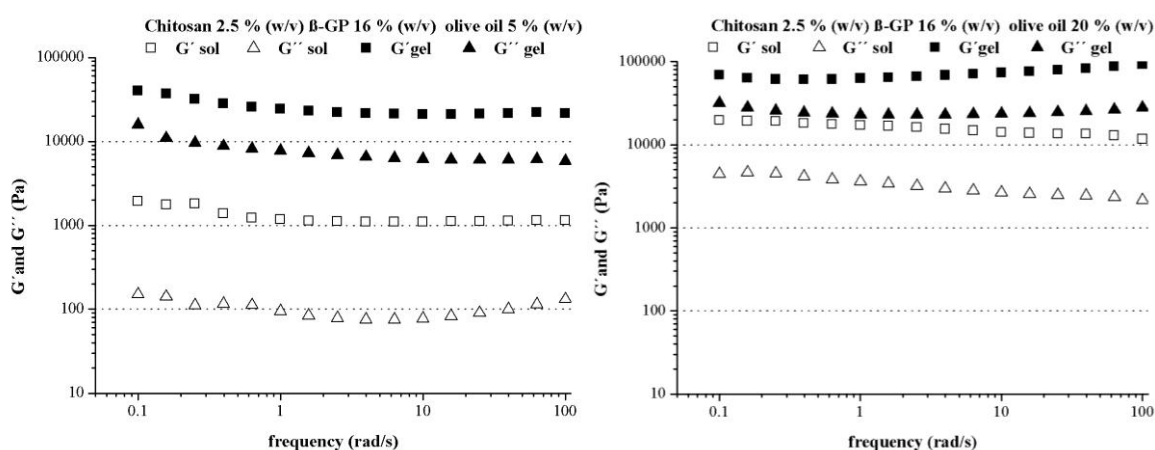


Figure 57 Frequency dependence of storage (G') and loss (G'') moduli of chitosan/ β -GP/olive oil emulsions with different oil content before and after thermally-induced gelation

By emulsifying 5 % (w/v) olive oil into the chitosan/ β -GP system, both moduli increased, with a marked enhancement for the elastic modulus by two orders of magnitude. Compared to the oil free chitosan/ β -GP solutions (Figure 38, page 76), the emulsion G' showed a nearly frequency independent demeanour. The 5 percent emulsion showed a fluid-like behaviour with a high degree of elasticity the 20 percent emulsion can be classified as a viscoelastic gel (Figure 57). After incubation at 50 °C for at least 60 min, both G' and G'' further increased due to the formation of the gel network. Strong gels were formed with $G' > G''$ and elastic moduli in the range of several kPa. The increase in the viscosity of the thermo-gelled emulsion can be related to the strong potential of chitosan to hydrophobic interactions. As explained in section 4.2.1.2 (page 79) hydrophobic interactions play a major role in the gel formation process. Hydrophobic interactions are expected to occur between chitosan and the oil.

They reduce the energy barrier which is required for gelation and thus promote association of the chitosan chains.

The increased viscosity in the thermally-induced gelling emulsion directly affected the dynamics of the water molecules in the sol state. Figure 58 shows the T_2 distribution for chitosan/ β -GP/olive oil emulsions with different oil contents before and after thermal treatment. Pure olive oil and distilled water are displayed as references. Compared to the oil free chitosan/ β -GP solutions (Figure 41, page 80), the major T_2 peak, which represents the protons of the water molecules, is broadened and shifted to lower values with increasing oil contents. Gelation of the emulsion led to a further restriction of proton mobility.

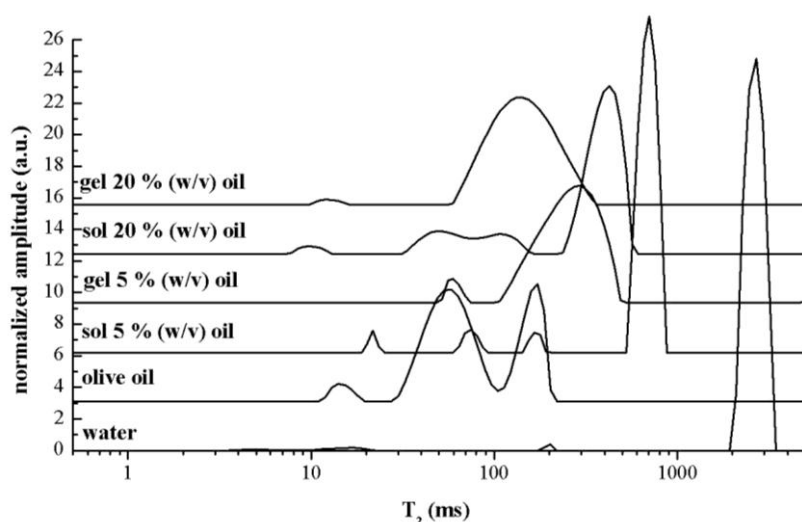


Figure 58 Normalized T_2 distributions for chitosan-based emulsions before (sol) and after (gel) thermal treatment compared to distilled water and olive oil (chitosan 2.5 % (w/v), β -GP 16 % (w/v) and olive oil 5/20 % (w/v))

Olive oil possessed a bimodal T_2 peak distribution with peaks at approximately 60 ms and 170 ms (Figure 58). As mentioned in section 4.2.1.2 (page 79), the additional small T_2 peaks at lower relaxation times are caused by protons interacting with the glass surface of the sample vials. In the chitosan-based emulsions the olive oil T_2 peaks could be easily distinguished from the water T_2 peak. As expected, their amplitude increased with higher percentage of oil in the emulsions. Gelation of the emulsion did not restrict the mobility of the oil protons as observed for the water protons. In the 20 percent emulsion the T_2 peak of water protons overlapped with the T_2 peaks of the oil.

Like for the chitosan/ β -GP solutions, the temperature dependence of T_{2m} was determined to monitor the phase transition processes (see section 4.2.1.2). The addition of olive oil to chitosan/ β -GP solutions and associated enhanced hydrophobic interactions lead to a decrease in the gelling temperature from about 37 °C to about 30 °C (Figure 59). Similar effects have been reported for thermosensitive chitosan/ β -GP solutions containing liposomes [67;232]. The drop in T_{2m} marking the phase transition temperature flattened with increasing oil content. Since the higher percentage of oil in the emulsions increased the viscosity of the systems, which was expressed by lower T_{2m} values.

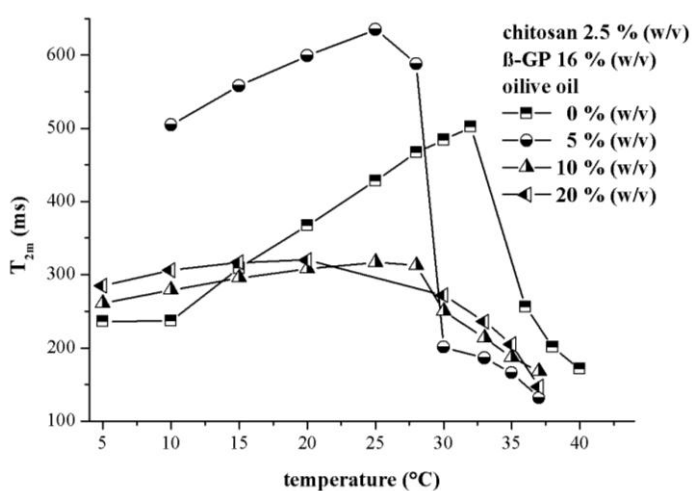


Figure 59 Temperature dependence of T_{2m} water relaxation times of chitosan-based emulsions with varying oil content (chitosan (2.5 % w/v)/ β -GP(16 w/v))

The addition of oil to the chitosan/ β -GP solution also decreased the gelation time at the phase transition temperature (Figure 60).

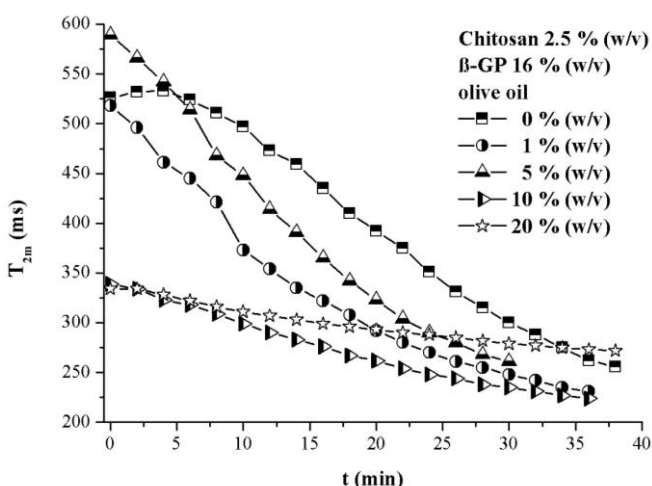


Figure 60 Time dependence of T_{2m} water relaxation times at phase transition temperature of chitosan-based emulsions with varying oil content (chitosan (2.5 % w/v) and β -GP(16 w/v))

Both effects, the decrease in gelling temperature and gelling time can be directly related to hydrophobic interaction between chitosan and olive oil that promote chitosan chain entanglement and formation of the gel network.

4.2.2.2 Feasibility study for sustained drug delivery

EPR spectroscopy was used to determine the viscosity at the molecular level and to test the feasibility of the thermally-induced gelling emulsion for sustained drug delivery. By using nitroxyl radicals of the ^{14}N and ^{15}N isotopes the simultaneous investigation of the release pattern of molecules with different lipophilicity or location is possible. Since the EPR spectra differ from each other due to the different nuclear spins. This approach has been previously used to investigate the encapsulation efficacy and *in vivo* fate of PLGA based nanocapsules [235] and sucrose ester nanodispersions [218]. Therefore, the hydrophilic spin probe (^{15}N -PCM, logP -0.63 [236]) and a lipophilic spin-probe (^{14}N -HD-PMI, logP ≈ 9 [235]) were incorporated into *in situ* gelling chitosan-based emulsions as models for low molecular weight drugs (Figure 61).

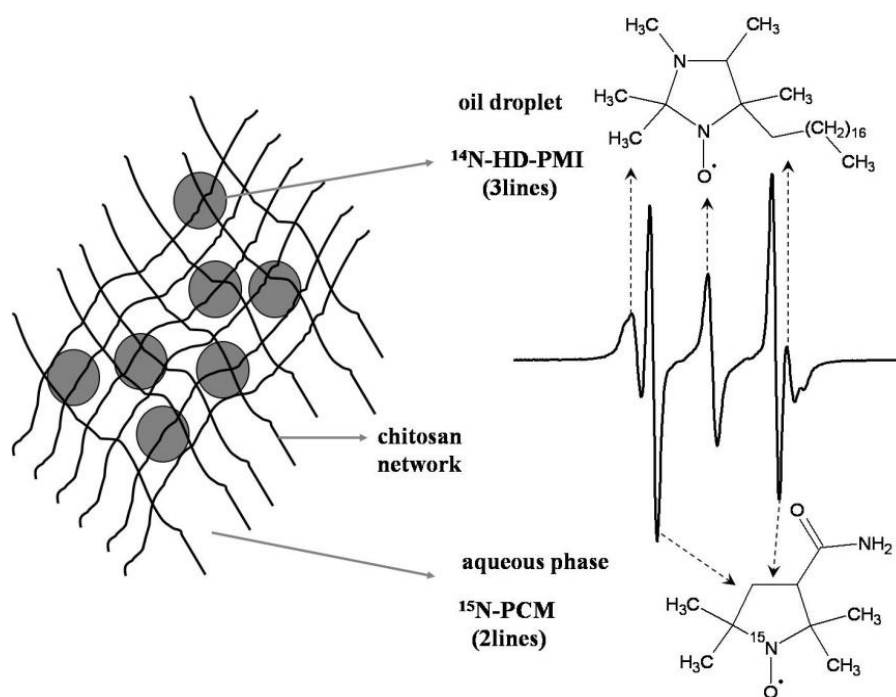


Figure 61 The principle of the simultaneous assessment of multiple sites of an oil/water chitosan-based *in situ* gelling emulsion by EPR. The lipophilic ^{14}N -nitroxide (HD-PMI) is localised in the oily droplets, the ^{15}N -nitroxide (PCM) in the outer aqueous phase. Spectral contribution of the ^{14}N -nitroxide (HD-PMI) and ^{15}N -nitroxide (PCM) to the recorded EPR spectrum of the chitosan-based emulsion: The ^{14}N -nitrogen has a nuclear spin of 1, resulting in a three line spectrum. The nuclear spin of $1/2$ of the ^{15}N -nitrogen results in a hyperfine splitting of 2 lines. The outer line of the ^{14}N -hyperfine splitting is superimposed by the 2 line of the ^{15}N -nitrogen.

^{15}N -PCM, the “reporter” molecule for the aqueous phase, gave a typical 2-line spectrum. The spectral shape and the hyperfine splitting indicated that it was entirely located in the aqueous environment of the gel (Figure 61). ^{14}N -HD-PMI, the “reporter”

molecule for the oil phase, showed a 3-line spectrum. Its spectral parameters revealed that ^{14}N -HD-PMI was only dissolved in the small oil droplets distributed within the chitosan-backbone of the gel (Figure 61).

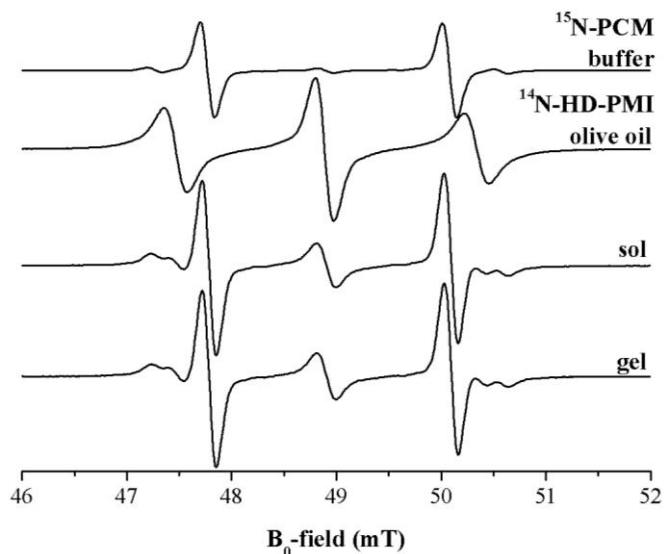


Figure 62 In vitro L-Band EPR spectra of ^{15}N -PCM and ^{14}N -HD-PMI loaded chitosan-based in situ gelling emulsion before (sol) and after (gel) thermal treatment in comparison to ^{15}N -PCM dissolved in phosphate buffer and ^{14}N -HD-PMI dissolved in olive (chitosan 2.5 % (w/v), β -GP 16 % (w/v) and olive oil 20 % (w/v))

Figure 62 displays the EPR spectra of ^{15}N -PCM and ^{14}N -HD-PMI dissolved in the chitosan-based in situ gelling emulsions before and after thermal treatment for at least 60 minutes at 50 °C. Both spin probes showed highly symmetric spectra with narrow lines indicating a high mobility inside the emulsion. Despite the formation of high viscous gels, the spin probes were located in a low viscous microenvironment, congruent to the spectra of the emulsion and the corresponding references in phosphate buffer or olive oil respectively. Viscosity enhancement by either oil incorporation or thermal treatment did not influence the local mobility of the low molecular weight nitroxide molecules. The results indicated that in either case the free space for the nitroxide rotation in the oil droplets and network pores of the in situ gelling emulsions was not affected. Similar effects were already discussed in section 4.2.1.1 (page 76). The spectral shape of both spin probes did not change over the whole time of release (Figure 63). The amplitudes originating from ^{15}N -PCM rapidly decreased due to fast diffusion of small hydrophilic molecule out of the gels (Figure 63). The release of the water soluble ^{15}N -PCM was completed after 6 hours *in vitro* and after 3 hours *in vivo* (Figure 64). The exponential decay of the signal intensity described a linear like elimination by diffusion as it has been already reported by *Ullrich* for nanoemulsions [218]. *Ullrich* found out that the aqueous phase of the nanoemulsions was completely

exchanged by body fluids within less than 90 minutes [218]. Compared with this result the thermo-gelled chitosan-based emulsions provided a more sustained release.

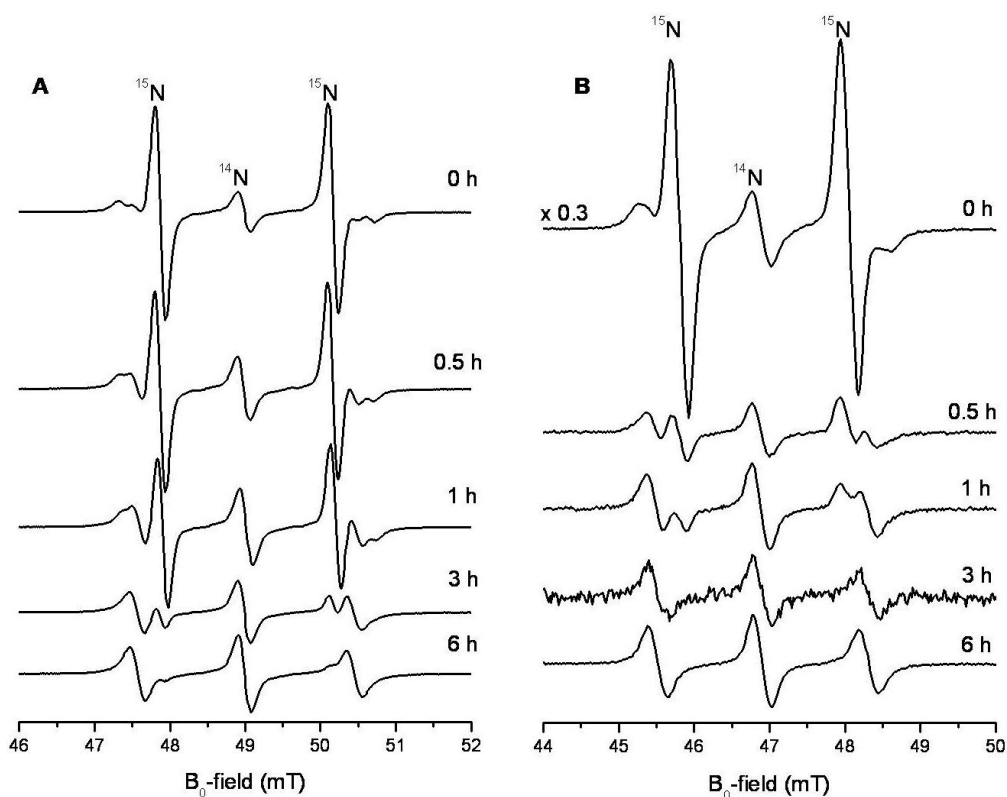


Figure 63 *In vitro* (A) and *in vivo* (B) EPR spectra of ^{14}N -HD-PMI and ^{15}N -PCM in chitosan-based *in situ* gelling emulsions (chitosan 2.5 % (w/v), β -GP 16 % (w/v) and olive oil 20 % (w/v))

The faster *in vivo* elimination of the spin probe may be caused by several factors, such as slower gelation or different surface to volume ratios depending on the subcutaneous cavity. Further the rapid reduction of the radical at the implant surface by antioxidants in the body fluids, which are missing in the *in vitro* buffer system, might have contributed to the signal loss. Additionally a surface coil type resonator was used for the *in vivo* measurements. With this type of resonator small changes in the positioning of the animal will result in considerable loss of signal amplitude and changes of the signal baseline [130;218], that makes quantification of *in vivo* EPR signals a challenging task. Similar to ^{15}N -PCM the signal amplitudes of the lipophilic ^{14}N -HD-PMI decreased within the first hour of incubation and then remained almost unchanged for one week, *in vitro* and *in vivo* (Figure 63). Ullrich reported similar release behaviour of ^{14}N -HD-PMI from nanoemulsions [218]. He further stated that the lipophilic spin probe portioned in the environmental subcutaneous fat tissue, where it was subsequently slowly released.

The initial decrease in signal intensities in the thermo-gelled emulsions can be attributed to the gelation process itself.

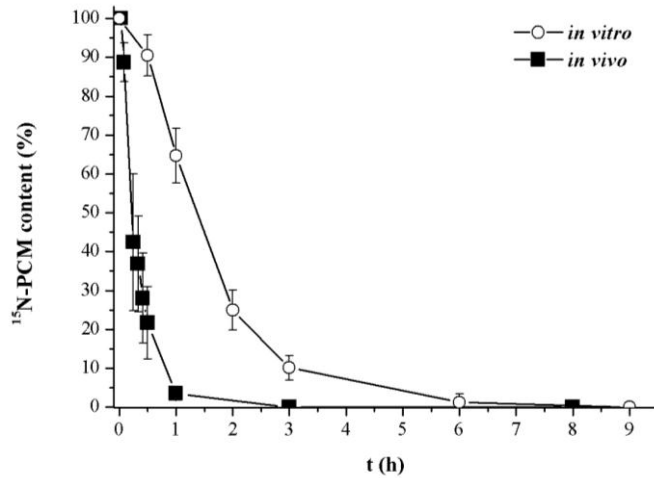


Figure 64 In vitro and in vivo elimination of ¹⁵N-PCM from chitosan-based in situ gelling emulsion (chitosan 2.5 % (w/v), β -GP 16 % (w/v) and olive oil 20 % (w/v))

As for ¹⁵N-PCM the higher decay in the *in vivo* signal amplitude can be attributed to the radical reduction by body fluids, different implant architectures and the experimental setup with the surface coil resonator. Furthermore the reference value for the signal intensity at the time point zero for the *in vivo* experiment was determined in plastic vials. The animal itself produced additional signal intensity loss by a factor of three, due to the higher water content and therewith higher microwave adsorption. First EPR spectra could be obtained two minutes after injection. When using this value as reference value, ¹⁴N-HD-PMI contents inside the implants 24 hours after injection *in vivo* (82.2 ± 27 %) were comparable to *in vitro* (72.3 ± 14.5 %).

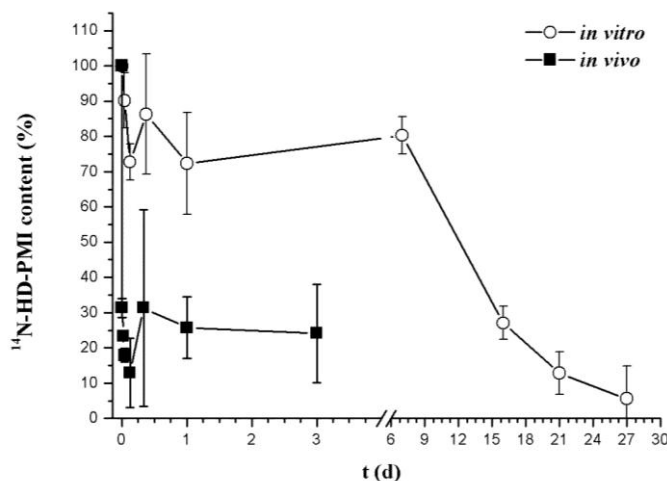


Figure 65 In vitro and in vivo elimination of ¹⁴N-HD-PMI from chitosan-based in situ gelling emulsion (chitosan 2.5 % (w/v), β -GP 16 % (w/v) and olive oil 20 % (w/v))

After a steady state of about one week the content of ¹⁴N-HD-PMI steadily decreased within the next three weeks *in vitro* (Figure 65). The release process was dominated by

surface erosion, as it has been previously reported for chitosan/ β -GP gels with a similar composition [137] Unfortunately no further *in vivo* data were available after three days due to the technical collapse of the *in vivo* spectrometer with spoilt surface coil resonator.

4.2.3 Conclusions and outlook

Mixtures of chitosan and β -GP have been investigated with respect to their ability to temperature induced gel formation. These systems combined low viscosity at room temperature with thermo-gelling properties. Oscillating rheology was used to characterize the macroviscosities of the sol and gel systems. Gel formation was associated with a dramatic increase of the storage modulus G' . In addition to rheology, $^1\text{H-NMR}$ Relaxometry was applied to study non-invasively the gelation process and the water mobility inside the gels. The dynamics of the water molecules were restricted in the gel state due to their interactions with the chitosan network. So the phase transition process could be monitored by measuring the temperature dependence of the average transverse relaxation time of the whole systems. The obtained phase transition temperatures were interdependent to the β -GP content and correlated well with values obtained by the vial inversion method. Stability investigation on the refrigerated chitosan/ β -GP solution showed a time-dependent gelation within three months. Whereas after two months syneresis occurred in the gel systems. By comparing the obtained results with the literature, secondary hydrophobic and hydrogen bonding interactions between the chitosan chains were postulated to be the main driving force for gelation. Additionally to $^1\text{H-NMR}$, EPR was applied for a better understanding of the chitosan/ β -GP system performance by monitoring microviscosity and pH_m inside the gels. For this reasons a pH sensitive low molecular weight nitroxide as well as spin-labelled insulin were incorporated into the gelling solutions. It was found, that both substances are highly mobile despite the formation of a strong gel, indicating the existence of a low viscous microenvironment. Furthermore, EPR based pH measurements indicate, that the internal pH is slightly below 7 within a narrow range, which fits to the physiological pH. Neither the gelation process nor the chitosan/ β -GP ratios affected the pH to a significant amount. The EPR studies with spin-labelled insulin showed, that insulin is not immobilized locally within the gel. The incorporation into the gel had no impact on

insulin stability. Controlled release over several days was achieved *in vitro* from the pre-gelled formulations. *In vivo* the chitosan/ β -GP systems sustained the release of spin-labelled insulin compared to a spin-labelled insulin solution. But the release was quite faster than *in vitro* because of the long time of in situ gelation of about 30 minutes. In conclusion, the chitosan β -GP thermo-gelling system may act an attractive delivery system for peptides and proteins.

To expand the use of chitosan-based hydrogel to the delivery of hydrophobic drugs, olive oil was emulsified in the systems. The obtained o/w emulsions maintained their thermosetting behaviour and the composition were optimized to get injectable formulations with a high oil content and sol-to-gel transition at body temperature. Pilot investigations showed that the system was able to sustain the release of a small model drug compounds. Compared to a previous study [218], the in situ gelling emulsions were more effective in retarding the model drug release than nanoemulsions. But the systems still need further optimization, especially with respect to intrinsic viscosity and gelling rate.

For a more practical application chitosan-based thermally-induced gelling systems should be optimized to faster gelation times. The gelation rate can be modified by varying the composition of chitosan/ β -GP systems. Faster gelation can be achieved by using chitosan with a high DD [65], increasing the chitosan or β -GP content [224]. However increasing the content of chitosan and above all the content of β -GP will increase the osmolarity of the systems [224;225]. Especially β -GP concentrations above 10 % (w/v) produce a hypertonic environment [224] that may lead to local irritations after injection. With time the osmolarity of the gel will be reduced by water exchange and diffusion of β -GP out of the gel [225]. The other side of the picture is that acceleration of the sol-to-gel transition negatively effects the storage stability of the systems [65]. *Schuetz et al.* suggested freezing as a conceivable storage [221]. The authors further proposed replacing β -GP by threhalose or manitol and subsequent freeze-drying. The reconstituted solutions from the lyophilizate still possessed their thermosetting properties and were injectable. The strength of the thermally-induced chitosan-based gelling systems lie besides their potential in drug delivery to act as a vehicle for other drug delivery systems or cells, especially for tumour treatment or tissue engineering purposes. Recent applications include the local delivery of liposomes

[231], microparticles [237] and the use *in vivo* scaffold for rat bone marrow mesenchymal stem cells [238] or as a vehicle to immobilize chondrocytes for cartilage repair [239]. But the major obstacle of all chitosan-based drug delivery systems is that it chitosan not approved by the FDA for drug delivery purposes or as a generally regarded as safe (GRAS) material [240]. Chitosan is not a uniform chemical substance. Instead the natural polysaccharide describes a steadily increasing group chemical entities with differing Mw, DD and chemical modifications that all posses different distribution, degradation and toxilogical profiles [240]. Several companies supply chitosan in various grades of purity, Mw and DD. The quality and characteristics of chitosan strongly depends on the manufacturing process. Therefore thorough analytical description of chitosan is necessary to achieve a product of constant quality. The sole specification of DD is not sufficient as this parameter strongly depend on the analytical method employed [241]. So *Augsten et al.* reported a high batch-to-batch variability of chitosan of the same DD from the same supplier [94]. Availability of high and constant quality chitosan types is an urgent need for further development.

5 Summary and further perspectives

5.1 English version

Injectable in situ forming implants have received considerable attention in the past years. They represent an alternative to common parental depot formulations such as implants or microspheres. ISFI have several advantages compared to pre-shaped implants and microparticles, as they are simple to fabricate and avoid invasive techniques such as surgery or the use of needles with large diameters for its implantation. The knowledge about the detailed mechanism of in vivo implant formation was very limited, despite the intense research recent years, which yielded to two commercial products. Therefore it was the aim of this thesis was to characterize non-invasively the mechanism of in situ forming depot formation.

This is the first report that used EPR spectroscopy, $^1\text{H-NMR}$ Relaxometry and Bt-MRI for ISFI characterization. The selection of these non-destructive analytical methods allowed for the first time serial measurement of the same sample over a long time span.

The present work can be divided into two parts. The first part covers the characterization of in situ forming implants based on phase separation by solvent exchange. EPR was successfully applied to monitor the major steps of the implant formation process from PLGA/NMP solutions. For the first time it was possible to quantify simultaneously polymer precipitation and the solvent exchange *in vitro* and *in vivo*. The kinetics of the NMP-water exchange as well as PLGA precipitation showed good *in vitro/in vivo* correlation. The method could be further expanded to another solvent (PEG 400) and to novel AB diblock copolymers of PLGA and PEG. Implants prepared with PEG 400 as the solvent possessed a faster polymer precipitation and complete solvent exchange, compared to NMP. One of the major challenges for in situ forming implants based on phase separation by solvent exchange is to protect on the one side the biological individual and on the other side the incorporated API. With respect to API protection, PEG-PLGA diblock copolymers had advantages to PLGA, especially with reference to proteins or other acid pH sensitive drugs. Due to their more hydrophilic character these polymers facilitated the rapid influx of water and fast solvent exchange and prevented the accumulation of acidic degradation products inside the implants.

To get more information about the *in vivo* fate of the implants and their localisation and the response of the biological system on them, Bt-MRI was used as complementary method to EPR. The present work is the first MRI study which monitors the formation and disintegration of in situ forming implants. It was conducted with a newly developed *in vivo* benchtop MRImager prototype without the use of contrast agents. The PEG 400 based systems yield a good MRI signal and contrast to the biological tissue, so that beside the implant formation process the implant erosion could be followed. The results confirmed the previous EPR measurements. Because of the hygroscopic character of PEG 400 a transient edema formation in the implant neighbourhood was observed. Furthermore the encapsulation of the implant as a response of the biological system to all investigated polymers was detected, followed by disintegration within two months.

The second part of this thesis describes the characterization of thermally-induced chitosan-based gelling systems. The main focus was set on the non-destructive and real-time examination of the phase transition of chitosan/ β -GP hydrogels and newly developed chitosan-based o/w emulsions. The dynamics of the water molecules and their relaxation behaviour were strongly influenced by the gelation process. The influence of the formulation parameters on the thermally-induced gelling systems was investigated by ^1H -NMR Relaxometry. The obtained results were confirmed by oscillating rheology and the vial inversion method. Further EPR spectroscopy was applied to get a deeper insight into the microstructure of the chitosan/ β -GP systems. By EPR the microviscosity and pH_m inside the gels was examined depending on the β -GP concentration. Following experiments investigated the loading and release of spin-labelled insulin. All chitosan/ β -GP solutions showed a physiological pH ranging from 6.6-6.8 that did not change during gelation, irrespective of the proportion of β -GP. The dynamics of spin-labelled insulin and its microviscosity inside the gels and during release were monitored by EPR spectroscopy. The results indicated that the insulin was incorporated into the aqueous environment of the gel and was released in its native form. The *in vitro* drug release from the gels was governed by diffusion of the drug from the gel matrix. A sustained release of insulin was observed over a period of two weeks. In contrast to pure insulin solutions, sustained *in vivo* release of spin-labelled insulin from the gel was achieved. However a large burst effect was observed before the

gelation was completed. Further novel o/w emulsions were developed to expand the use of thermally-induced chitosan-based hydrogel systems to lipophilic drugs. The emulsification of oil into the chitosan/ β -GP systems did not alter the general thermosetting behaviour but had a deep impact on the systems viscosity. The release of small model drug molecules with different lipophilicity was observed by EPR spectroscopy. The small hydrophilic molecules were released from the gel matrix within three to six hours. Whereas the small lipophilic molecules entrapped in oil droplets were released over 30 days with a gelation dependent initial burst. Although these first results were promising these thermogelling emulsions need further optimization.

The presented analytical methods EPR spectroscopy, $^1\text{H-NMR}$ Relaxometry and Bt-MRI have shown their high potential for the non-invasive and continuous characterization of different type of in situ forming implants. EPR offered unique information about the micropolarity, microviscosity and microclimate pH inside the implants. $^1\text{H-NMR}$ Relaxometry detected online phase transition processes in thermoresponsive hydrogels. And Bt-MRI gave new insights in the *in vivo* fate of in situ forming implants as well as parenteral formulations. The obtained results with the prototype of the benchtop apparatus proofed that Bt-MRI is a new alternative for common superconducting MRI machines for *in vivo* MRI on small mammals. All presented techniques extend the spectra of analytical methods for in situ forming implants characterization. This work proved that they can be used as valuable tools for further development and optimization, especially for pre-clinical formulation research.

In summary both investigated in situ forming implant types possessed some positive and negatives. The results show, that need and the toxicity of the organic solvent is the biggest formulation challenge for in situ forming implants based on solvent exchange. Future research is necessary to reduce the portion of the solvent. Approaches for solving this issue provide the use of modified polymers or multiparticulate systems. Further research should focus on more compatible solvents with respect to the patient and the polymer and API as well. The commercial availability of constant quality of the natural product chitosan is one of the major issues for thermally-induced chitosan-based gelling systems. As intended for parenteral application, the development of adequate sterilization methods and the guarantee of storage stability represent further research fields for both implant types.

5.2 German version

Aufgrund einer Vielzahl von vor allem neu entwickelten Arzneistoffen, die nicht peroral verabreicht werden können, hat sich in den vergangenen zwei Dekaden die Forschung auf dem Gebiet parenteraler Depotarzneiformen intensiviert. Als alternative Depotform zu Implantaten und Mikropartikel wurden in den 1990ern *in situ* bildende Implantate entwickelt. *In situ* bildende Implantate weisen eine Vielzahl von Vorteilen gegenüber konventionellen bioabbaubaren Implantaten auf. An erster Stelle steht die erhöhte Patientenakzeptanz. Da die Applikation mittels Injektion unter Verwendung kleiner Injektionsnadeln erfolgt, können chirurgische Eingriffe zur Platzierung und Entfernung des Implantats vermieden werden. Des Weiteren kann bei der kostengünstigen Herstellung auf erhöhte Prozesstemperaturen verzichtet werden. Aufgrund der geringen Komplexität sind die Fertigungstechniken gut vom Labor in die Großproduktion übertragbar. Trotz der intensiven Forschung der letzten Jahre und der Existenz zweier Marktprodukte war bisher wenig über die detaillierten Mechanismen der Implantat-Bildung speziell *in vivo* bekannt. Das Ziel der vorliegenden Arbeit lag in der nicht-invasiven Charakterisierung der *in situ* Implantatsbildungsmechanismen.

Erstmals wurden dafür die analytischen Verfahren EPR-Spektroskopie, ¹H-NMR-Relaxometrie und Benchtop-Magnetresonanztomographie (Bt-MRT) verwendet. Diese analytischen Verfahren wurden ausgewählt, da sie eine nicht-destruktive und kontinuierliche pharmazeutische Analyse der Implantate über einen längeren Zeitraum ermöglichten.

Die vorliegende Arbeit kann in zwei Teile untergliedert werden. Der erste Teil der Dissertation beinhaltet die Charakterisierung von sich *in situ* bildenden Implantaten geformt durch das Prinzip der Polymer-Ausfällung mittels Lösungsmittel-Austausch. Mit Hilfe der EPR Spektroskopie konnte der Prozess der Implantat-Bildung aus PLGA/NMP-Lösungen verfolgt werden. Dabei gelang erstmals *in vitro* und *in vivo* die simultane Quantifizierung der Polymer-Präzipitation als auch des Lösungsmittel-Austausches. Dabei zeigten beide Kinetiken eine gute *in vitro* – *in vivo* Korrelation. In einem weiteren Schritt konnte dieses Analyseverfahren auf ein anderes Lösungsmittel (PEG 400) und auf neuartige AB Diblockcopolymere aus PEG und PLGA übertragen werden. Verglichen mit NMP zeigte PEG 400 eine schnellere Polymer-Ausfällung und einen schnelleren vollständigen Lösungsmittel-Austausch. Die größte Herausforderung

in der Entwicklung von sich *in situ* bildender Arzneiformen nach dem Prinzip der Polymer-Ausfällung durch Lösungsmittel-Austausch stellt zum einem der Schutz des biologischen Individuums und zum anderen der des inkorporierten Arzneistoffes dar. In Hinblick auf den Schutz des Arzneistoffes, insbesondere von Proteinen oder anderer säurelabiler Substanzen, waren PEG-PLGA Copolymere PLGA überlegen. Aufgrund ihres hydrophileren Charakters erleichterten diese Polymere die Diffusion von Wasser in und von Lösungsmitteln aus dem Implantat. Des Weiteren verhinderten sie dadurch die Akkumulation saurer Abbauprodukte im Inneren der Implantate.

Als komplementäres Verfahren zu EPR wurde Bt-MRT angewendet um mehr über das *in vivo* Schicksal der Implantate, ihre Lokalisation und die Reaktion des biologischen Systems auf die Implantate zu erfahren. Zum ersten Mal konnte die Bildung und der Abbau von sich *in situ* bildenden Implantaten mittels MRT ohne die Zugabe von kontrastverstärkenden Mitteln verfolgt werden. Dabei kam der Prototyp eines neu entwickelten *in vivo* Bt-MRT Gerät zum Einsatz. Die auf PEG 400 basierenden Systeme lieferten ein gutes MRT Signal und ausreichend Kontrast zu dem umgebenden biologischen Gewebe, so dass sowohl die Formung als auch der Abbau der Implantate verfolgt werden konnten. Die so gewonnenen Ergebnisse zeigten eine gute Übereinstimmung mit denen durch EPR Messungen erzielten Daten. Nach der Injektion kam es aufgrund der wasseranziehenden Eigenschaften von PEG 400 zu einer zeitweisen Ödembildung. Während des Abbauprozesses innerhalb von 2 Monaten konnte des Weiteren eine Einkapselung aller Polymere durch Bindegewebe beobachtet werden.

Der zweite Teil der Arbeit beschreibt die Charakterisierung von thermisch-induzierten gelierenden Systemen auf Chitosan-Basis. Hauptaugenmerk lag dabei auf der nicht-destruktiven Bestimmung des Phasenüberganges von *in situ* gelierenden Chitosan/ β -GP Hydrogelen und neu entwickelten O/W Emulsionen auf Chitosan-Basis. Da die Dynamik der Wassermoleküle und ihr Relaxationsverhalten stark durch den Geliervorgang beeinflusst wurden, konnte mit Hilfe der ^1H -NMR Relaxometrie der Einfluss von Formulierungsparametern auf das thermische Gelierverhalten der Systeme untersucht werden. Die so erhalten Ergebnisse wurde durch die klassischen Analyseverfahren Oszillierende Rheologie und der Vial Inversion Methode bestätigt. Als weiterer Schwerpunkt wurde die Mikrostruktur der Chitosan/ β -GP Systeme genauer

untersucht. Mit Hilfe der EPR Spektroskopie erfolgte die Untersuchung der Mikroviskosität und des pH-Wertes der Gele in Abhängigkeit des β -GP Gehaltes, sowie der Freisetzung von spinmarkierten Insulin. Alle Chitosan/ β -GP Lösungen hatten einen physiologischen pH-Wert im Bereich von 6,6-6,8 unabhängig von ihrem β -GP-Gehalt und unbeeinflusst durch den Geliervorgang. ESR Untersuchungen der Mikroviskosität von spinmarkierten Insulin während des Freisetzungsprozesses zeigten, dass das Insulin in einer wässrigen Umgebung eingebettet war und unverändert freigesetzt wurde. Die *in vitro* Freisetzung erfolgte hauptsächlich über Diffusion verzögert über einen Zeitraum von zwei Wochen. *In vivo* erfolgte im Vergleich zu einer reinen Insulin-Lösung die Freisetzung von Insulin aus den Gelen verzögert. Jedoch konnte ein starker Burst-Effekt vor Abschluss der Gelierung beobachtet werden. In einem weiteren Schritt wurden O/W Emulsionen entwickelt, um die Anwendbarkeit von thermisch-induzierten gelierenden Hydrogelsystemen auf Chitosan-Basis auf lipophile Arzneistoffe auszudehnen. Das Emulgieren von Öl in die Chitosan/ β -GP Systeme veränderte nicht ihr generelles thermosensitives Verhalten, hatte aber einen großen Einfluss auf die Systemviskosität. Mit der EPR Spektroskopie konnte die Freisetzung von kleinen Modell-arzneistoffmolekülen mit unterschiedlicher Lipophilie verfolgt werden. Die kleinen hydrophilen Modellstoffe wurden innerhalb von drei bis sechs Stunden aus der Gelmatrix freigesetzt. Wohingegen die kleinen lipophilen Modellstoffe, welche primär in den Öltröpfen eingeschlossen waren, über einen Zeitraum von 30 Tagen freigesetzt wurden. Erneut wurde initial ein durch den Geliervorgang bedingter Burst-Effekt beobachtet. Obwohl die ersten Ergebnisse sehr zuversichtlich stimmen, besteht für die thermisch gelierenden Emulsionen weiterer Optimierungsbedarf.

In der vorliegenden Arbeit konnte gezeigt werden, dass die vorgestellten analytischen Verfahren EPR-Spektroskopie, $^1\text{H-NMR-Relaxometrie}$ und Bt-MRT ein hohes Potential bei der nicht-invasiven, kontinuierlichen Charakterisierung verschiedener Typen von sich *in situ* bildenden Implantaten besitzen. Mittels EPR konnten dabei einzigartige Informationen über die Mikropolarität, Mikroviskosität und der pH-Werte im Inneren der Implantate gewonnen werden. Des Weiteren wurden Phasenübergänge von thermosensitiven Hydrogelen wurden mittels $^1\text{H-NMR-Relaxometrie}$ detektiert. Bt-MRT erlaubte neue Einblicke in das *in vivo* Schicksal von sich *in situ* bildenden Implantaten und parenteraler Formulierungen. Die dabei mit einem Prototyp Bt-MRT

Gerät gewonnenen Ergebnisse zeigen, dass Bt-MRT eine neue Alternative zu herkömmlichen superleitenden MRT Maschinen für die *in vivo* Tomographie von kleinen Säugetieren darstellt. Mit Hilfe der vorgestellten Methoden konnten erstmals die komplexen Prozesse der Implantat-Bildung, Wirkstofffreigabe und des Implantat-Abbaus nicht-invasiv kontinuierlich analytisch erfasst und quantifiziert werden. Es konnte ferner gezeigt werden, dass die vorgestellten Techniken das Spektrum analytischer Verfahren zur Charakterisierung von sich *in situ* bildenden Implantaten bedeutend erweitern. Sie stellen damit zukünftig ein wertvolles Werkzeug zur weiteren Entwicklung und Optimierung von *in situ* bildenden Depot-Formulierungen speziell in der Präklinischen Entwicklung dar.

Zusammenfassend lässt sich sagen, dass beide untersuchten sich *in situ* bildenden Implantatarten sowohl Vor- als auch Nachteile besitzen. Die größte Herausforderung in der Formulierung von sich *in situ* bildenden Implantaten basierend auf Lösungsmittel-Austausch besteht in der Notwendigkeit und der Toxizität der organischen Lösungsmittel. Zukünftige Forschungsschwerpunkte liegen daher in der Reduzierung des Lösungsmittelanteiles in den Formulierungen. Ein weiterer Schwerpunkt bildet die Suche nach für den Patienten, als auch für den Arzneistoff und die Polymere kompatibleren Lösungsmitteln. Andere Lösungsansätze bieten der Gebrauch von modifizierten Polymeren oder multipartikulärer Systeme. Die kommerzielle Verfügbarkeit des Naturproduktes Chitosan in gleichbleibender Qualität stellt dagegen eine der größten Herausforderungen in der Entwicklung von thermisch-induzierten gelierenden Systemen auf Chitosan-Basis dar. Da beide Implantatarten hauptsächlich für den parenteralen Gebrauch entwickelt wurden, liegen weitere Forschungsschwerpunkte in der Entwicklung von adäquaten Sterilisationsverfahren und der Sicherstellung der Lagerstabilität der Produkte.

6 Appendix

6.1.1 References

- [1] R. Mank, G. Rafler, B. Nerlich, Parenterale Depotarzneiformen auf der Basis von biologisch abbaubaren Polymeren, *Pharmazie* 46 (1991), 9-17.
- [2] S. Tamilvanan, Oil-in-water lipid emulsions: implications for parenteral and ocular delivering systems, *Progress in Lipid Research* 43 (2004), 489-533.
- [3] A. Sharma, U.S. Sharma, Liposomes in drug delivery: progress and limitations, *International Journal of Pharmaceutics* 154 (1997), 123-140.
- [4] A.N. Lukyanov, V.P. Torchilin, Micelles from lipid derivatives of water-soluble polymers as delivery systems for poorly soluble drugs, *Advanced Drug Delivery Reviews* 56 (2004), 1273-1289.
- [5] S. Thatte, K. Datar, R.M. Ottenbrite, Perspectives on: Polymeric drugs and drug delivery systems, *Journal of Bioactive and Compatible Polymers* 20 (2005), 585-601.
- [6] S. Freiberg, X.X. Zhu, Polymer microspheres for controlled drug release, *International Journal of Pharmaceutics* 282 (2004), 1-18.
- [7] P. Couvreur, C. Vauthier, Nanotechnology: intelligent design to treat complex disease, *Pharmaceutical Research* 23 (2006), 1-34.
- [8] E. Ruel-Gariepy, J.C. Leroux, In situ-forming hydrogels - review of temperature-sensitive systems, *European Journal of Pharmaceutics and Biopharmaceutics* 58 (2004), 409-426.
- [9] A. Hatefi, B. Amsden, Biodegradable injectable in situ forming drug delivery systems, *Journal of Controlled Release* 80 (2002), 9-28.
- [10] C.B. Packhaeuser, J. Schnieders, C.G. Oster, T. Kissel, In situ forming parenteral drug delivery systems: an overview, *European Journal of Pharmaceutics and Biopharmaceutics* 58 (2004), 445-455.
- [11] A. Gutowska, B. Jeong, M. Jasionowski, Injectable gels for tissue engineering, *The Anatomical Record* 263 (2001), 342-349.
- [12] M.K. Joo, M.H. Park, B.G. Choi, B. Jeong, Reverse thermogelling biodegradable polymer aqueous solutions, *Journal of Materials Chemistry* 19 (2009), 5891-5905.
- [13] A.K. Burkoth, K.S. Anseth, A review of photocrosslinked polyanhydrides: in situ forming degradable networks, *Biomaterials* 21 (2000), 2395-2404.

- [14] S.Y. Lee, G. Tae, Formulation and in vitro characterization of an in situ gelable, photo-polymerizable pluronic hydrogel suitable for injection, *Journal of Controlled Release* 119 (2007), 313-319.
- [15] J. Berger, M. Reist, J.M. Mayer, O. Felt, N.A. Peppas, R. Gurny, Structure and interactions in covalently and ionically crosslinked chitosan hydrogels for biomedical applications, *European Journal of Pharmaceutics and Biopharmaceutics* 57 (2004), 19-34.
- [16] F.L. Mi, S.S. Shyu, T.B. Wong, S.F. Jang, S.T. Lee, K.T. Lu, Chitosan-polyelectrolyte complexation for the preparation of gel beads and controlled release of anticancer drug. II. Effect of pH-dependent ionic crosslinking or interpolymer complex using triphosphate or polyphosphate as reagent, *Journal of Applied Polymer Science* 74 (1999), 1093-1107.
- [17] K.S. Anseth, S.M. Newman, C.N. Bowman, Polymeric dental composites: properties and reaction behavior of multimethacrylate dental restorations, *Biopolymers* 122 (1995), 177-217.
- [18] J.A. Burdick, L.M. Philpott, K.S. Anseth, Synthesis and characterization of tetrafunctional lactic acid oligomers: a potential in situ forming degradable orthopaedic biomaterial, *Journal of Polymer Science Part A: Polymer Chemistry* 39 (2001), 683-692.
- [19] J.A. Burdick, R.F. Padera, J.V. Huang, K.S. Anseth, An investigation of the cytotoxicity and histocompatibility of in situ forming lactic acid based orthopedic biomaterials, *Journal of Biomedical Materials Research* 63 (2002), 484-491.
- [20] A.S. Sawhney, C.P. Pathak, J.J. Van Rensburg, R.C. Dunn, J.A. Hubbell, Optimization of photopolymerized bioerodible hydrogel properties for adhesion prevention, *Journal of Biomedical Materials Research* 28 (1994), 831-838.
- [21] M.D. Lyman, D. Melanson, A.S. Sawhney, Characterization of the formation of interfacially photopolymerized thin hydrogels in contact with arterial tissue, *Biomaterials* 17 (1996), 359-364.
- [22] B. Balakrishnan, A. Jayakrishnan, Self-cross-linking biopolymers as injectable in situ forming biodegradable scaffolds, *Biomaterials* 26 (2005), 3941-3951.
- [23] T. Vermonden, N.E. Fedorovich, D. Van Gemen, J. Alblas, C.F. van Nostrum, W.J.A. Dhert, W.E. Hennink, Photopolymerized thermosensitive hydrogels: synthesis, degradation, and cytocompatibility, *Biomacromolecules* 9 (2008), 919-926.
- [24] J.B. Leach, C.E. Schmidt, Characterization of protein release from photocrosslinkable hyaluronic acid-polyethylene glycol hydrogel tissue engineering scaffolds, *Biomaterials* 26 (2005), 125-135.

- [25] K. Ono, Y. Saito, H. Yura, K. Ishikawa, Photocrosslinkable chitosans a biological adhesive, *Journal of Biomedical Materials Research Part A* 49 (2000), 289-295.
- [26] M. Ishihara, K. Obara, S. Nakamura, M. Fujita, K. Masuoka, B. Kanatani, H. Takase, Y. Hattori, M. Morimoto, T. Ishihara, T. Maehara, M. Kikuchi, Chitosan hydrogel as a drug delivery carrier to control angiogenesis, *Journal of Artificial Organs* 9 (2006), 8-16.
- [27] X.Z. Shu, K.J. Zhu, W. Song, Novel pH-sensitive citrate cross-linked chitosan film for drug controlled release, *International Journal of Pharmaceutics* 212 (2001), 19-28.
- [28] M. Hamdine, M.C. Heuzey, A. Begin, Viscoelastic properties of phosphoric and oxalic acid-based chitosan hydrogels, *Rheologica Acta* 45 (2006), 659-675.
- [29] J. Berger, M. Reist, O. Felt, R. Gurny, Structure and interactions in chitosan hydrogels formed by complexation or aggregation for biomedical applications, *European Journal of Pharmaceutics and Biopharmaceutics* 57 (2004), 35-52.
- [30] M.T. Nickerson, J. Patel, D.V. Heyd, D. Rousseau, A.T. Paulson, Kinetic and mechanistic considerations in the gelation of genipin-crosslinked gelation, *International Journal of Biological Macromolecules* 39 (2006), 298-302.
- [31] T.R. Hoare, D.S. Kohane, Hydrogels in drug delivery, *Polymer* 49 (2008), 1993-2007.
- [32] A. Bernkop-Schurch, M. Hornof, T. Zoidl, Thiolated polymers-thiomers: synthesis and in vitro evaluation of chitosan-2-iminothiolane conjugates, *International Journal of Pharmaceutics* 260 (2003), 229-237.
- [33] A.H. Krauland, V.M. Leitner, A. Bernkop-Schurch, Improvement of the in situ gelling properties of deacytulated gellan gum by the immobilization of thiol groups, *Journal of Pharmaceutical Science* 92 (2003), 1234-1241.
- [34] A. Bernkop-Schurch, A.H. Krauland, V.M. Leitner, Thiomers: potential excipients for non-invasive peptide delivery systems, *European Journal of Pharmaceutics and Biopharmaceutics* 58 (2004), 253-263.
- [35] K. Kafedjiiski, R.K.R. Jetti, F. Föger, H. Hoyer, M. Werle, M. Hoffer, A. Bernkop-Schurch, Synthesis and in vitro evaluation of thiolated hyaluronic acid for mucoadhesive drug delivery, *International Journal of Pharmaceutics* 343 (2007), 48-58.
- [36] B. Qui, S. Stefanos, J. Ma, A. Laloo, B.A. Perry, M.J. Leibowitz, P.J. Sinko, S. Stein, A hydrogel prepared by in situ cross-linking of a thio-containing poly(ethylene glycol)-based copolymer: a new biomaterial for protein drug delivery, *Biomaterials* 24 (2002), 11-18.

- [37] B. Balakrishnan, M. Mohanty, P.R. Umashankar, A. Jayakrishnan, Evaluation of an in situ forming hydrogel wound dressing based on oxidized alginate and gelatin, *Biomaterials* 26 (2005), 6335-6342.
- [38] A. Vintiloui, J.C. Leroux, Organogels and their use in drug delivery - A review, *Journal of Controlled Release* 125 (2008), 179-192.
- [39] A. Vintiloui, M. Lafleur, G. Bastiat, J.C. Leroux, In situ-forming oleogel implant for rivastigmine delivery, *Pharmaceutical Research* 25 (2008), 845-852.
- [40] F. Plourde, A. Motulsky, A.C. Couffin-Hoarau, D. Hoarau, H. Ong, J.C. Leroux, First report on the efficacy of L-alanine-based in situ-forming implants for the long-term parenteral delivery of drugs, *Journal of Controlled Release* 108 (2005), 433-441.
- [41] Z.H. Gao, A.J. Shukla, J.R. Johnson, W.R. Crowley, Controlled release of contraceptive steroids from biodegradable and injectable gel formulation - in vivo evaluation, *Pharmaceutical Research* 12 (1995), 864-868.
- [42] M.N.V.R. Kumar, R.A.A. Muzzarelli, C. Muzzarelli, H. Sashiwa, A.J. Domb, Chitosan chemistry and pharmaceutical perspectives, *Chemical Reviews* 104 (2004), 6017-6084.
- [43] R. Joshi, D.H. Robinson, K.J. Himmelstein, In vitro properties of an in situ forming gel for the parenteral delivery of macromolecular drugs, *Pharmaceutical Development and Technology* 4 (1999), 515-522.
- [44] P.E. Alonso, L.A. Perula, L.F. Rioja, Pain-temperature relation in the application of local anaesthesia, *British Journal of Plastic Surgery* 46 (1993), 76-78.
- [45] J. Heller, J. Barr, S.Y. Ng, H.R. Shen, K. Schwach-Abdellaoui, S. Einmahl, A. Rothen-Weinhold, R. Gurny, Poly(ortho esters) - their development and some recent applications, *European Journal of Pharmaceutics and Biopharmaceutics* 50 (2000), 121-137.
- [46] S. Einmahl, K. Schwach-Abdellaoui, J. Heller, R. Gurny, Poly(ortho esters): Recent developments for biomedical applications, *Chimia* 55 (2001), 218-222.
- [47] S. Einmahl, S. Capancioni, K. Schwach-Abdellaoui, M. Moeller, F. Behar-Cohen, R. Gurny, Therapeutic applications of viscous and injectable poly(ortho esters), *Advanced Drug Delivery Reviews* 53 (2001), 45-73.
- [48] R. S. Bezwada and S. C. Arnold, "Liquid absorbable copolymers for parenteral applications," 5653992, Aug.5, 1997.
- [49] Y. Liu, W.L. Lu, J.C. Wang, X. Zhang, H. Zhang, X.Q. Wang, T.Y. Zhou, Q. Zhang, Controlled delivery of recombinant hirudin based on thermo-sensitive Pluronic(R) F127 hydrogel for subcutaneous administration: in vitro and in vivo characterization, *Journal of Controlled Release* 117 (2007), 387-395.

- [50] A. Sosnik, D. Cohn, J.S. San Roman, G.A. Abraham, Crosslinkable PEO-PPO-PEO-based reverse thermo-responsive gels as potentially injectable materials, *Journal of Biomaterials Science-Polymer Edition* 14 (2003), 227-239.
- [51] A. Sosnik, D. Cohn, Reverse thermo-responsive poly(ethylene oxide) and poly(propylene oxide) multiblock copolymers, *Biomaterials* 26 (2005), 349-357.
- [52] F. Tirnaksiz, J.R. Robinson, Rheological, mucoadhesive and release properties of Pluronic F-127 gel and Pluronic F-127/polycarbophil mixed gel systems, *Pharmazie* 60 (2005), 518-523.
- [53] D.C. Coughlan, O.I. Corrigan, Drug-polymer interactions and their effect on thermoresponsive poly(N-isopropylacrylamide) drug delivery systems, *International Journal of Pharmaceutics* 313 (2006), 163-174.
- [54] B. Jeong, S.W. Kim, Y.H. Bae, Thermosensitive sol-gel reversible hydrogels, *Advanced Drug Delivery Reviews* 54 (2002), 37-51.
- [55] B. Jeong, A. Gutowska, Lessons from nature: stimuli-responsive polymers and their biomedical applications, *TRENDS in Biotechnology* 20 (2002), 305-311.
- [56] H. Hyun, Y.H. Kim, I.B. Song, J.W. Lee, M.S. Kim, G. Khang, K. Park, H.B. Lee, In vitro and in vivo release of albumin using a biodegradable MPEG-PCL diblock copolymer as an in situ gel-forming carrier, *Biomacromolecules* 8 (2007), 1093-1100.
- [57] G.M. Zentner, R. Rathi, J.C. Shih, J.C. McRea, M.H. Seo, H. Oh, B.G. Rhee, J. Mestecky, Z. Moldoveana, M. Morgan, S. Weiman, Biodegradable block copolymers for delivery of proteins and water insoluble drugs, *Journal of Controlled Release* 72 (2001), 203-215.
- [58] Y.M. Chung, K.L. Simmons, A. Gutowska, B. Jeong, Sol-gel transition temperature of PLGA-g-PEG aqueous solutions, *Biomacromolecules* 3 (2002), 511-516.
- [59] B. Jeong, L.Q. Wang, A. Gutowska, Biodegradable thermoreversible gelling PLGA-g-PEG copolymers, *Chemical Communications* (2001), 1516-1517.
- [60] K. Mäder, B. Gallez, K.J. Liu, H.M. Swartz, Non-invasive in vivo characterization of release processes in biodegradable polymers by low-frequency electron paramagnetic resonance spectroscopy, *Biomaterials* 17 (1996), 457-461.
- [61] A.G. Ding, A. Shenderova, S.P. Schwendeman, Prediction of microclimate pH in poly(lactic-co-glycolic acid) films, *Journal of the American Chemical Society* 128 (2006), 5384-5390.
- [62] K. Kobayashi, C. Huang, T.P. Lodge, Thermoreversible gelation of aqueous methylcellulose solutions, *Macromolecules* 32 (1999), 7070-7077.

- [63] D. Gupta, C.H. Tator, M.S. Shoichet, Fast-gelling injectable blend of hyaluronan and methylcellulose for intrathecal, localized delivery to the injured spinal cord, *Biomaterials* 27 (2006), 2370-2379.
- [64] A. Chenite, C. Chaput, D. Wang, C. Combes, M.D. Buschmann, C.D. Hoemann, J.C. Leroux, B.L. Atkinson, F. Binette, A. Selmani, Novel injectable neutral solutions of chitosan form biodegradable gels in situ, *Biomaterials* 21 (2000), 2155-2161.
- [65] E. Ruel-Gariepy, A. Chenite, C. Chaput, S. Guirguis, J.C. Leroux, Characterization of thermosensitive chitosan gels for the sustained delivery of drugs, *International Journal of Pharmaceutics* 203 (2000), 89-98.
- [66] E. Ruel-Gariepy, M. Shive, A. Bichara, M. Berrada, D. Le Garrec, A. Chenite, J.C. Leroux, A thermosensitive chitosan-based hydrogel for the local delivery of paclitaxel, *European Journal of Pharmaceutics and Biopharmaceutics* 57 (2004), 53-63.
- [67] E. Ruel-Gariepy, G. Leclair, P. Hildgen, A. Gupta, J.C. Leroux, Thermosensitive chitosan-based hydrogel containing liposomes for the delivery of hydrophilic molecules, *Journal of Controlled Release* 82 (2002), 373-383.
- [68] M. Iliescu, C.D. Hoemann, M.S. Shive, A. Chenite, M.D. Buschmann, Ultrastructure of hybrid chitosan-glycerolphosphate blood clots by environmental scanning electron microscopy, *Microscopy Research and Technique* 71 (2008), 236-247.
- [69] LeDuc, C. and Benarrosh, J., *BioSyntech 2007 Annual Report*, Biosyntech, Laval (Canada) (20-7-2007).
- [70] D. Steinberg, M. Friedman, Dental drug delivery devices: local and sustained release applications, *Critical Reviews in Therapeutic Drug Carrier Systems* 16 (1999), 425-459.
- [71] O. Sator, M.K. Dineen, R. Perez-Marreno, F.M. Chu, G.J. Carron, R.C. Tyler, An eight-month clinical study of LA-2575 30,0 mg: A new 4-month, subcutaneous delivery system for leuprolide acetate in the treatment of prostate cancer, *Urology* 62 (2003), 319-323.
- [72] R. L. Dunn, A. J. Tipton, G. L. Southard, and J. A. Rogers, "Biodegradable polymer composition," US Patent 5599552, 1997.
- [73] G. Chandrashekar, N. Udupa, Biodegradable injectable implant system for long term drug delivery using poly (lactic-co-glycolic) acid copolymers, *Journal of Pharmaceutical Pharmacology* 48 (1996), 669-674.
- [74] Y. Tang, J. Singh, Controlled delivery of aspirin: Effect of aspirin on polymer degradation and in vitro release from PLGA based phase sensitive systems, *International Journal of Pharmaceutics* 357 (2008), 119-125.

- [75] H.B. Ravivarapu, K.L. Moyer, R.L. Dunn, Sustained activity and release of leuprolide acetate from an in situ forming polymeric implant, *AAPS Pharmaceutical Science Technology* 1 (2000), article 1.
- [76] W.J. Lambert, K.D. Peck, Development of an in situ forming biodegradable poly-lactide-co-glycolide system for the controlled release of proteins, *Journal of Controlled Release* 33 (1995), 189-195.
- [77] K.J. Brodbeck, S. Pushpala, A.J. Mchugh, Sustained release of human growth hormone from PLGA solution depots, *Pharmaceutical Research* 16 (1999), 1825-1829.
- [78] R. Eliaz, J. Kost, Characterization of a polymeric PLGA-injectable implant delivery system for the controlled release of proteins, *Journal of Biomedical Materials Research* 50 (2000), 388-396.
- [79] M. Dittgen, S. Fricke, H. Gerecke, I. P. Möller, and C. Völkel, "Injection Implant," Germany Patent WO/1998/030245, 1998.
- [80] A. McHugh, The role of polymer membrane formation in sustained release drug delivery systems, *Journal of Controlled Release* 109 (2005), 211-221.
- [81] W.Y. Dong, M. Körber, V. Lopez Esguerra, R. Bodmeier, Stability of poly(D,L-lactide-co-glycolide) and leuprolide acetate in-situ forming drug delivery systems, *Journal of Controlled Release* 115 (2006), 158-167.
- [82] X. Luan, R. Bodmeier, Influence of the poly(lactide-co-glycolide) type on the leuprolide release from in situ forming microparticle systems, *Journal of Controlled Release* 110 (2006), 266-272.
- [83] P.D. Graham, K.J. Brodbeck, A.J. Mchugh, Phase inversion dynamics of PLGA solutions related to drug delivery, *Journal of Controlled Release* 58 (1999), 233-245.
- [84] K.J. Brodbeck, J.R. DesNoyer, A.J. Mchugh, Phase inversion dynamics of PLGA solutions related to drug delivery - Part II. The role of solution thermodynamics and bath-side mass transfer, *Journal of Controlled Release* 62 (1999), 333-344.
- [85] N.H. Shah, A.S. Railkar, F.C. Chen, R. Tarantino, S. Kumar, M. Murjani, D. Palmer, M.H. Infeld, A.W. Malick, A biodegradable injectable implant for delivering micro and macromolecules using poly(lactid-co-glycolic) acid (PLGA) copolymers, *Journal of Controlled Release* 27 (1993), 139-147.
- [86] F. Kang, J. Singh, In vitro release of insulin and biocompatibility of in situ forming gel systems, *International Journal of Pharmaceutics* 304 (2005), 83-90.
- [87] Y. Lu, Y. Yu, X. Tang, Sucrose acetate isobutyrate as an in situ forming system for sustained risperidone release, *Journal of Pharmaceutical Sciences* 96 (2007), 3252-3262.

- [88] F. Okumu, L. Dao, P. Fielder, N. Dybdal, D. Brooks, S. Sane, J. Cleland, Sustained delivery of human growth hormone from a novel gel system: SABER™, *Biomaterials* 23 (2002), 4353-4358.
- [89] M.A. Royals, S.M. Fujita, G.L. Yewey, J. Rodriguez, P.C. Schultheiss, R.L. Dunn, Biocompatibility of a biodegradable in situ forming implant system in rhesus monkeys, *Journal of Biomedical Materials Research* 45 (1999), 231-239.
- [90] H. Kranz, G.A. Brazeau, J. Napaporn, R.L. Martin, W. Millard, R. Bodmeier, Myotoxicity studies of injectable biodegradable in-situ forming drug delivery systems, *International Journal of Pharmaceutics* 212 (2001), 11-18.
- [91] W. Rungseevijitprapa, G.A. Brazeau, J.W. Simkins, R. Bodmeier, Myotoxicity studies of O/W-in situ forming microparticle systems, *European Journal of Pharmaceutics and Biopharmaceutics* 69 (2008), 126-133.
- [92] H. Kranz, R. Bodmeier, A novel in situ forming drug delivery system for controlled parenteral drug delivery, *International Journal of Pharmaceutics* 332 (2007), 107-114.
- [93] M. Voigt, "Biodegradable non-aqueous in situ forming microparticle drug delivery systems." FU Berlin, 2011.
- [94] C. Augsten, K. Mader, Characterizing molar mass distributions and molecule structures of different chitosans using asymmetrical flow field-flow fractionation combined with multi-angle light scattering, *International Journal of Pharmaceutics* 351 (2008), 23-30.
- [95] A. Besheer, K.M. Wood, N.A. Peppas, K. Mäder, Loading and mobility of spin-labeled insulin in physiologically responsive complexation hydrogels intended for oral administration, *Journal of Controlled Release* 111 (2006), 73-80.
- [96] E. Zavoiskii, Paramagnetic absorption of a solution in parallel fields, *Journal of Physics* 8 (1944), 377-380.
- [97] M. Carini, G. Aldini, M. Orioli, R.M. Facino, Electron Paramagnetic Resonance (EPR) spectroscopy: A versatile and powerful tool in pharmaceutical and biomedical analysis, *Current Pharmaceutical Analysis* 2 (2006), 141-159.
- [98] J. A. Weil J. R. Bolton, *Electron Paramagnetic Resonance - Elementary theory and practical applications*, Second edition, John Wiley & Sons, Hoboken, New Jersey, (2007).
- [99] N. M. Atherton, *Principles of Electron Spin Resonance*, Ellis Horwood PTR, Prentice Hall, New York, (1993).
- [100] W. Gordy, *Theory and Applications of Electron Spin Resonance*, Wiley & Sons, New York, (1980).

- [101] D.J. Lurie, K. Mäder, Monitoring drug delivery processes by EPR and related techniques - principles and applications, *Advanced Drug Delivery Reviews* 57 (2005), 1171-1190.
- [102] S. Lüsse, K. Arnold, Water binding of polysaccharides - NMR and ESR studies, *Macromolecules* 31 (1998), 6891-6897.
- [103] K. Mäder, B. Bittner, Y.X. Li, W. Wohlauf, T. Kissel, Monitoring microviscosity and microacidity of the albumin microenvironment inside degrading microparticles from poly(lactide-co-glycolide) (PLG) or ABA-triblock polymers containing hydrophobic poly(lactide-co-glycolide) A blocks and hydrophilic poly(ethyleneoxide) B blocks, *Pharmaceutical Research* 15 (1998), 787-793.
- [104] R.G. Evans, A.J. Wain, C. Hardcare, R.G. Compton, An electrochemical and ESR spectroscopic study on the molecular dynamics of TEMPO in room temperature ionic liquid solvents, *ChemPhysChem* 6 (2005), 1035-1039.
- [105] D.E. Budil, S. Lee, S. Saxena, J.H. Freed, Nonlinear-least-squares analysis of slow-motion EPR spectra in one and two dimensions using a modified Levenberg-Marquardt algorithm, *Journal of Magnetic Resonance, Series A* 120 (1996), 155-189.
- [106] K. Mäder, Characterization of Nanoscaled Drug Delivery Systems by Electron Spin Resonance (ESR), *Nanosystem Characterization Tools in the Life Science*, Wiley-VCH, Weinheim, (2006), 241-258.
- [107] V.V. Khrantsov, Biological imaging and spectroscopy of pH, *Current Organic Chemistry* 9 (2005), 909-923.
- [108] V.V. Khrantsov, I.A. Grigor'ev, M.A. Foster, D.J. Lurie, I. Nicholson, Biological applications of spin pH probes, *Cellular and Molecular Biology* 46 (2000), 1361-1374.
- [109] D.I. Potapenko, M.A. Foster, D.J. Lurie, I.A. Kirilyuk, J.M.S. Hutchison, I.A. Grigor'ev, E.G. Bagryanskaya, V.V. Khrantsov, Real-time monitoring of drug-induced changes in the stomach acidity of living rats using improved pH-sensitive nitroxides and low-field EPR techniques, *Journal of Magnetic Resonance* 182 (2006), 1-11.
- [110] I.A. Kirilyuk, A.A. Bobko, V.V. Khrantsov, I.A. Grigor'ev, Nitroxides with two pK values - Useful spin probes for pH monitoring within a broad range, *Organic & Biomolecular Chemistry* 3 (2005), 1269-1274.
- [111] N. Khan, B.B. William, H. Hou, H. Li, H.M. Swartz, Repetitive tissue pO₂ measurements by Electron Paramagnetic Resonance Oximetry: Current status and future potential for experimental and clinical studies, *Antioxidants & Redox Signaling* 9 (2007), 1169-1182.

- [112] S. Kempe, H. Metz, K. Mäder, Application of Electron Paramagnetic Resonance (EPR) spectroscopy and imaging in drug delivery research - Chances and challenges, *European Journal of Pharmaceutics and Biopharmaceutics* 74 (2010), 55-66.
- [113] K.I. Momot, P.W. Kuchel, Pulsed field gradient nuclear magnetic resonance as a tool for studying drug delivery systems, *Concepts in Magnetic Resonance Part A* 19A (2003), 51-64.
- [114] J.C. Richardson, R.W. Bowtell, K. Mäder, C.D. Melia, Pharmaceutical applications of magnetic resonance imaging (MRI), *Advanced Drug Delivery Reviews* 57 (2005), 1191-1209.
- [115] R. Winter F. Noll, *Kernmagnetische Resonanz (NMR), Methoden der Biophysikalischen Chemie*, B. G. Teubner, Stuttgart, (1998), 7, 383-461.
- [116] M. Rudin, N. Beckmann, R. Porzasz, T. Reese, D. Bochelen, A. Sauter, In vivo magnetic resonance methods in pharmaceutical research: current status and perspectives, *NMR in Biomedicine* 12 (1999), 69-97.
- [117] H. Metz, K. Mäder, Benchtop-NMR and MRI-A new analytical tool in drug delivery research, *International Journal of Pharmaceutics* 364 (2008), 170-175.
- [118] I. Katzhendler, K. Mäder, M. Friedman, Correlation between drug release kinetics from proteinaceous matrix and matrix structure: EPR and NMR study, *Journal of Pharmaceutical Sciences* 89 (2000), 365-381.
- [119] K.P. Nott, Magnetic resonance imaging of tablet dissolution, *European Journal of Pharmaceutics and Biopharmaceutics* 74 (2010), 78-83.
- [120] R. Hinrichs, S. Bulca, U. Kulozik, Water mobility during renneting and acid coagulation of casein solutions: a differentiated low-resolution nuclear magnetic resonance analysis, *International Journal of Dairy Technology* 60 (2007), 37-43.
- [121] P. Cornillon, L.C. Salim, Characterization of water mobility and distribution in low- and intermediate-moisture food systems, *Magnetic Resonance Imaging* 18 (2000), 335-341.
- [122] M. Ballari, F. Bonetto, E. Anardo, NMR relaxometry analysis of lubricant oils degradation, *Journal of Physics D: Applied Physics* 38 (2005), 3746-3750.
- [123] G.E. Schaumann, E. Hobbey, J. Hurraß, W. Rotard, H-NMR relaxometry to monitor wetting and swelling kinetics in high-organic matter soils, *Plant and Soil* 275 (2005), 1-20.
- [124] P. T. Callaghan, *Principles of Nuclear Magnetic Resonance Microscopy*, Clarendon, Oxford, (1991).
- [125] R. Kimmich, *NMR Tomography, Diffusometry, Relaxometry*, Springer, Berlin, Heidelberg, (1997).

- [126] H. Metz, K. Mäder, Benchtop-NMR and MRI - A new analytical tool in drug delivery research, *International Journal of Pharmaceutics* (2008)
- [127] S. Strubing, H. Metz, K. Mader, Characterization of poly(vinyl acetate) based floating matrix tablets, *Journal of Controlled Release* 126 (2008), 149-155.
- [128] S. Strubing, T. Abboud, R.V. Contri, H. Metz, K. Mader, New insights on poly(vinyl acetate)-based coated floating tablets: Characterisation of hydration and CO₂ generation by benchtop MRI and its relation to drug release and floating strength, *European Journal of Pharmaceutics and Biopharmaceutics* 69 (2008), 708-717.
- [129] V. Malaterre, H. Metz, J. Ogorka, R. Gurny, N. Loggia, K. Mäder, Benchtop-magnetic resonance imaging (BT-MRI) characterization of push-pull osmotic controlled release systems, *Journal of Controlled Release* 133 (2009), 31-36.
- [130] K. Mäder, G. Bacic, A. Domb, O. Elmalak, R. Langer, H.M. Swartz, Noninvasive in vivo monitoring of drug release and polymer erosion from biodegradable polymers by EPR spectroscopy and NMR imaging, *Journal of Pharmaceutical Sciences* 86 (1997), 126-134.
- [131] K. Mäder, Y. Cremmilleux, A.J. Domb, J.F. Dunn, H.M. Swartz, In vitro in vivo comparison of drug release and polymer erosion from biodegradable P(FAD-SA) polyanhydrides - A noninvasive approach by the combined use of electron paramagnetic resonance spectroscopy and nuclear magnetic resonance imaging, *Pharmaceutical Research* 14 (1997), 820-826.
- [132] B. Madhu, I. Elmroth, A. Lundgren, B. Abrahamsson, B. Soussi, A novel evaluation of subcutaneous formulations by in vivo magnetic resonance imaging (MRI), *Pharmaceutical Research* 45 (2002), 207-212.
- [133] A. Steingötter, D. Weishaupt, P. Kunz, K. Mader, H. Lengsfeld, M. Thumshirn, P. Boesiger, M. Fried, W. Schwizer, Magnetic resonance imaging for the in vivo evaluation of gastric-retentive tablets., *Pharmaceutical Research* 20 (2003), 2001-2007.
- [134] H. Nitzsche, A. Noack, A. Lochmann, C. Oliveira, A. Besheer, H. Metz, A. Bernstein, G. Hause, T. Groth, K. Mader, Scaffold properties and interaction with cells investigated by magnetic resonance methods, *Tissue Engineering Part A* 14 (2008), 345.
- [135] A. Besheer, "Nanomedicine based on hydroxyethyl starch - from synthesis to in vivo evaluation." Martin Luther University Halle-Wittenberg, 2008.
- [136] Q.S. Zhao, X.J. Cheng, Q.X. Ji, C.Z. Kang, X.G. Chen, Effect of organic and inorganic acids on chitosan/glycerolphosphate thermosensitive hydrogel, *Journal of Sol-Gel Science and Technology* 50 (2009), 111-118.

- [137] F. Ganji, M.J. Abdekhodaie, A. Ramazani, Gelation time and degradation rate of chitosan-based injectable hydrogel, *Journal of Sol-Gel Science and Technology* 42 (2007), 47-53.
- [138] R. Astaneh, M. Erfan, H. Moghimi, H. Mobedi, Changes in morphology of in situ forming PLGA implant prepared by different polymer molecular weight and its effect on release behaviour, *Journal of Pharmaceutical Sciences* 98 (2009), 135-145.
- [139] E. Pamula, E. Menaszek, In vitro and in vivo degradation of poly(l-lactide-co-glycolide) films and scaffolds, *Journal of Materials Science-Materials in Medicine* 19 (2008), 2063-2070.
- [140] L.W. Wang, S. Venkatraman, L. Kleiner, Drug release from injectable depots: two different in vitro mechanisms, *Journal of Controlled Release* 99 (2004), 207-216.
- [141] L. Solorio, B.M. Babib, R.B. Patel, J. Mach, N. Azar, A.A. Exner, Noninvasive characterization of in situ forming implants using diagnostic ultrasound, *Journal of Controlled Release* 143 (2010), 183-190.
- [142] S. Li, Hydrolytic Degradation Characteristics of Aliphatic polyesters derived from Lactic and Glycolic Acids, *Journal of Biomedical Materials Research* 48 (1999), 342-352.
- [143] A. Rube, S. Klein, K. Mader, Monitoring of in vitro fat digestion by electron paramagnetic resonance spectroscopy, *Pharmaceutical Research* 23 (2006), 2024-2029.
- [144] A. Rube, K. Mader, Electron spin resonance study on the dynamics of polymeric nanocapsules, *Journal of Biomedical Nanotechnology* 1 (2005), 208-213.
- [145] H. Kranz, E. Yilmaz, G.A. Brazeau, R. Bodmeier, In vitro and in vivo drug release from a novel in situ forming drug delivery system, *Pharmaceutical Research* 25 (2008), 1347-1354.
- [146] D. Klose, F. Siepmann, K. Elkharraz, J. Siepmann, PLGA-based drug delivery systems: Importance of the type of drug and device geometry, *International Journal of Pharmaceutics* 354 (2011), 95-103.
- [147] N. Faisant, J. Akiki, F. Siepmann, J.P. Benoit, J. Siepmann, Effects of the type of release medium on drug release from PLGA-based microparticles: Experiment and theory, *International Journal of Pharmaceutics* 314 (2006), 189-197.
- [148] D. Klose, C. Delplace, J. Siepmann, Unintended potential of perfect sink conditions on PLGA degradation in microparticles, *International Journal of Pharmaceutics* 404 (2011), 75-82.

- [149] V. Nagy, Quantitative EPR: Some of the most difficult problems, *Applied Magnetic Resonance* 6 (1994), 259-285.
- [150] K. Schoenhammer, H. Petersen, F. Guethlein, A. Goepferich, Poly(ethyleneglycol)500 dimethylether as novel solvent for injectable in situ forming depots, *Pharmaceutical Research* 26 (2009), 2568-2577.
- [151] R. Bakhshi, H. E.Mobedi, H. Mobedi, A. Jamshidi, M. Khakpour, The effect of additives on naltrexone hydrochloride release and solvent removal rate from an injectable in situ forming PLGA implant, *Polymers for advanced Technologies* 17 (2006), 354-359.
- [152] R. Langer, N.A. Peppas, *Advanced in Biomaterials, drug delivery, and bionanotechnology*, *AIChE Journal* 49 (2003), 2990-3006.
- [153] M.L. Houchin, K. Heppert, E.M. Topp, Deamidation, acrylation and proteolysis of a model peptide in PLGA films, *Journal of Controlled Release* 112 (2006), 111-119.
- [154] M.L. Houchin, E.M. Topp, Chemical degradation of peptides and proteins in PLGA: a review of reactions and mechanisms, *Journal of Pharmaceutical Sciences* 97 (2008), 2395-2404.
- [155] L. Li, S.P. Schwendeman, Mapping neutral microclimate pH in PLGA microspheres, *Journal of Controlled Release* 101 (2005), 163-173.
- [156] T. Kissel, Y. Li, F. Unger, ABA-Triblock copolymers from biodegradable polyester A-blocks and hydrophilic poly(ethylene oxide) B-blocks as a candidate for in situ forming hydrogel delivery systems for proteins, *Advanced Drug Delivery Reviews* 54 (2002), 99-134.
- [157] K.M. Huh, Y.W. Cho, K. Park, PLGA-PEG Block Copolymers for Drug Formulations, *Drug Delivery Technology* 3 (2003), 1-9.
- [158] A.S. Hoffman, Hydrogels for biomedical applications, *Advanced Drug Delivery Reviews* 43 (2002), 3-12.
- [159] C. Witt, K. Mäder, T. Kissel, The degradation, swelling and erosion properties of biodegradable implants prepared by extrusion or compression moulding of poly(lactide-co-glycolide) and ABA triblock copolymers, *Biomaterials* 21 (2000), 931-938.
- [160] G.N. Teww, N. Sanabria-DeLong, S.K. Agrawal, New properties from PLA-PEO-PLA hydrogels, *Soft Matter* 1 (2005), 253-258.
- [161] J. Cheng, B.A. Teply, I. Sherifi, J. Sung, G. Luther, F.X. Gu, E. Levy-Nissenbaum, A.F. Radovic-Moreno, R. Langer, O.C. Farokhzad, Formulation of functionalized PLGA-PEG nanoparticles for in vivo targeted drug delivery, *Biomaterials* 28 (2007), 869-876.

- [162] A. Lochmann, H. Nitzsche, S. von Einem, E. Schwarz, K. Mäder, The influence of covalently linked and free polyethylene glycol on the structural and release properties of rhBMP-2 loaded microspheres, *Journal of Controlled Release* 147 (2010), 92-100.
- [163] R. Astaneh, H.R. Moghimi, M. Erfan, H. Mobedi, Formulation of an injectable implant for peptide delivery and mechanistic study of the effect of polymer molecular weight on its release behaviour, *DARU* 14 (2006), 65-70.
- [164] R. L. Dunn and A. J. Tipton, "Polymeric composition useful as controlled release implants," US Patent 5702716, 1997.
- [165] J.P. Moreau, P.J. Vachon, M.C. Huneau, Elevated glycemia and local inflammation after injecting N-methyl-2-pyrrolidone (NMP) into the marginal ear vein of rabbits, *Journal of American Association for Laboratory Animal Science* 40 (2001), 38-40.
- [166] J.P. Payan, D. Beydon, J.P. Fabry, I. Boudry, B. Cossec, E. Ferrari, Toxicokinetics and metabolism of N-[14C]methylpyrrolidone in male sprague-dawley rats. A saturable NMP elimination process, *Drug Metabolism and Disposition* 30 (2002), 1418-1424.
- [167] K. Schoenhammer, H. Petersen, F. Guethlein, A. Goepferich, Injectable in situ forming depot systems: PEG-DAE as novel solvent for improved PLGA storage stability, *International Journal of Pharmaceutics* 371 (2009), 33-39.
- [168] R.G. Strickley, Solubilizing excipients in oral and injectable formulations, *Pharmaceutical Research* 21 (2004), 201-230.
- [169] H. Kranz, R. Bodmeier, Structure formation and characterization of injectable drug loaded biodegradable devices: in situ implants versus in situ microparticles, *European Journal of Pharmaceutical Sciences* 34 (2008), 164-172.
- [170] C.A. Fyfe, A.I. Blazek-Welsh, Quantitative NMR imaging study on the mechanism of drug release from swelling hydroxypropylmethylcellulose tablets, *Journal of Controlled Release* 68 (2000), 313-333.
- [171] S. Strübing, T. Abboud, R.V. Contri, H. Metz, K. Mäder, New insights on polyvinylacetate based coated floating tablets: characterization of hydration and CO₂ generation by benchtop MRI and its relation to drug release and floating strength, *European Journal of Pharmaceutics and Biopharmaceutics* 69 (2009), 708-717.
- [172] D.A.I. Ashiru, R. Patel, A.W. Basit, Polyethylene glycol 400 enhances the bioavailability of a BCS class III drug (Ranitidine) in male subjects but not females, *Pharmaceutical Research* 25 (2008), 2327-2333.
- [173] P.J. Lee, R. Langer, V.P. Shastri, Role of n-methyl pyrrolidone in the enhancement of aqueous phase transdermal transport, *Journal of Pharmaceutical Sciences* 94 (2005), 912-917.

- [174] H.B. Ravivarapu, K.L. Moyer, R.L. Dunn, Sustained suppression of pituitary-gonadal axis with an injectable, in situ forming implant of leuprolide acetate, *Journal of Pharmaceutical Sciences* 89 (2000), 732-741.
- [175] A. Tschakaloff, H.W. Losken, R. von Oepen, W. Michaeli, O. Mortitz, M.P. Mooney, A. Losken, Degradation kinetics of biodegradable D,L-poly(lactic acid) biodegradable implants depending on the site of implantation, *International Journal of Oral & Maxillofacial Surgery* 23 (1994), 443-445.
- [176] J.M. Anderson, In vivo biocompatibility of implantable delivery systems and biomaterials, *Journal of Pharmaceutics and Biopharmaceutics* 40 (1994), 1-8.
- [177] P.E. LeRenard, O. Jordan, A. Faes, A. Petri-Fink, H. Hofmann, D. Rufenacht, F. Bosman, F. Buchegger, E. Doelker, The in vitro performance of magnetic particle-loaded injectable, in situ gelling, carriers for the delivery of local hyperthermia, *Biomaterials* 31 (2010), 691-705.
- [178] K. Schoenhammer, J. Biosclair, H. Schuetz, H. Petersen, A. Goepferich, Biocompatibility of an injectable in situ forming depo for peptide delivery, *Journal of Pharmaceutical Sciences* 99 (2010), 4390-4399.
- [179] R.B. Patel, L. Solorio, H. Wu, T. Krupka, A.A. Exner, Effect of injection site on in situ implant formation and drug release in vivo, *Journal of Controlled Release* 147 (2010), 350-358.
- [180] A. Shenderova, A.G. Ding, S.P. Schwendeman, Potentiometric method for determination of microclimate pH in poly(lactic-co-glycolic acid) films, *Macromolecules* 37 (2004), 10052-10058.
- [181] A. Rothen-Weinhold, N. Oudry, K. Schwach-Abdellaoui, S. Frutiger-Hughes, D. Jeannerat, U. Burger, K. Besseghir, R. Gurny, Formation of peptide impurities in polyester matrices during implant manufacturing, *European Journal of Pharmaceutics and Biopharmaceutics* 49 (2000), 253-257.
- [182] G. Zhu, S.R. Mallery, S.P. Schwendeman, Stabilization of proteins encapsulated in injectable poly(lactide-co-glycolide), *Nature Biotechnology* 18 (2000), 52-57.
- [183] A. Lucke, J. Kiermaier, A. Göpferich, Peptide Acylation by Poly(α -Hydroxy Esters), *Pharmaceutical Research* 19 (2002), 175-181.
- [184] P.A. Burke, Determination of internal pH in PLGA microspheres using ^{31}P NMR spectroscopy, *Proceedings of the International Symposium of Controlled Release Bioactive Materials* 23 (1996), 133-134.
- [185] A. Brunner, K. Mäder, A. Göpferich, pH and osmotic pressure inside biodegradable microspheres during erosion, *Pharmaceutical Research* 16 (1999), 847-853.

- [186] A.G. Ding, S.P. Schwendeman, Acidic microclimate pH distribution in PLGA microspheres monitored by confocal laser scanning microscopy, *Pharmaceutical Research* 25 (2008), 2041-2052.
- [187] K. Mäder, S. Nitschke, R. Stösser, H.H. Borchert, A. Domb, Non-destructive and localized assessment of acidic microenvironments inside biodegradable polyanhydrides by spectral spatial electron paramagnetic resonance imaging, *Polymer* 38 (1997), 4785-4794.
- [188] S. Siepe, W. Herrmann, H.H. Borchert, B. Lueckel, A. Kramer, A. Ries, R. Gurny, Microenvironmental pH and microviscosity inside pH-controlled matrix tablets: An EPR imaging study, *Journal of Controlled Release* 112 (2006), 72-78.
- [189] T. Trimaille, R. Gurny, M. Möller, Poly(hexyl-substituted lactides): novel injectable hydrophobic drug delivery systems, *Journal of Biomedical Materials Research Part A* 80A (2007), 55-65.
- [190] L. Klouda, A.G. Mikos, Thermoresponsive hydrogels in biomedical applications, *European Journal of Pharmaceutics and Biopharmaceutics* 68 (2008), 34-45.
- [191] E.A. Ho, V. Vassileva, C. Allen, M. Piquette-Miller, In vitro and in vivo characterization of a novel biocompatible polymer-lipid implant system for the sustained delivery of paclitaxel, *Journal of Controlled Release* 104 (2005), 181-191.
- [192] A. Kikuchi, T. Okano, Pulsatile drug release control using hydrogels, *Advanced Drug Delivery Reviews* 54 (2002), 53-77.
- [193] H. Dai, Q. Chen, H.L. Qin, Y. Guan, D.Y. Shen, Y.Q. Hua, Y.L. Tang, J. Xu, A temperature-responsive copolymer hydrogel in controlled drug delivery, *Macromolecules* 39 (2006), 6584-6589.
- [194] P. Gerentes, L. Vachoud, J. Doury, A. Domard, Study of a chitin-based gel as injectable material in periodontal surgery, *Biomaterials* 23 (2002), 1295-1302.
- [195] A. Chenite, C. Chaput, D. Wang, C. Combes, M.D. Buschmann, C.D. Hoemann, J.C. Leroux, B.L. Atkinson, F. Binette, A. Selmani, Novel injectable neutral solutions of chitosan form biodegradable gels in situ, *Biomaterials* 21 (2000), 2155-2161.
- [196] P. Roughley, C. Hoemann, E. Desrosiers, F. Mwale, J. Antoniou, M. Alini, The potential of chitosan-based gels containing intervertebral disc cells for nucleus pulposus supplementation, *Biomaterials* 27 (2006), 388-396.
- [197] J. Li, Z. Xu, Physical characterization of a chitosan-based hydrogel delivery system, *Journal of Pharmaceutical Science* 91 (2007), 1669-1677.

- [198] E. Ruel-Gariepy, J.C. Leroux, Chitosan: A natural polycation with multiple applications, *Polysaccharides for Drug Delivery and Pharmaceutical Applications* 934 (2006), 243-259.
- [199] J. Berger, A. Reist, A. Chenite, O. Felt-Baeyens, J.M. Mayer, R. Gurny, Pseudo-thermosetting chitosan hydrogels for biomedical application, *International Journal of Pharmaceutics* 288 (2005), 197-206.
- [200] A. Chenite, M. Buschmann, D. Wang, C. Chaput, N. Kandani, Rheological characterisation of thermogelling chitosan/glycerol-phosphate solutions, *Carbohydrate Polymers* 46 (2001), 39-47.
- [201] V. Dodane, V.D. Vilivalam, Pharmaceutical applications of chitosan, *PSTT* 1 (1998), 246-252.
- [202] R.A.A. Muzzarelli, Human enzymatic activities related to the therapeutic administration of chitin derivatives, *Cellular and Molecular Life Sciences* 53 (1997), 131-140.
- [203] A. Bernkop-Schurch, Chitosan and its derivatives: potential excipients for peroral peptide delivery systems, *International Journal of Pharmaceutics* 194 (2000), 1-13.
- [204] C. Alemdaroglu, Z. Degim, N. Celebi, F. Zor, S. Öztürk, D. Erdogan, An investigation on burn wound healing in rats with chitosan gel formulation containing epidermal growth factor, *Burns* 32 (2006), 319-327.
- [205] C.C. Lin, A.T. Metters, Hydrogels in controlled release formulations: network design and mathematical modeling, *Advanced Drug Delivery Reviews* 58 (2006), 1379-1408.
- [206] E.A. El-hefian, A.H. Yahaya, Rheological study of chitosan and its blends: An overview, *Maejo International Journal in Science Technology* 4 (2010), 210-220.
- [207] D. Wang, "Characterization of thermoreversible pH-sensitive physical gels of chitosan." Université de Montréal, 1999.
- [208] J. Kristl, J. Smid-Korbar, E. Struc, M. Shara, H. Rupprecht, Hydrocolloids and gels of chitosan as drug carriers, *International Journal of Pharmaceutics* 99 (1993), 13-19.
- [209] J. Cho, M.C. Heuzey, A. Begin, P.J. Carreau, Effect of urea on solution behavior and heat-induced gelation of chitosan- β -glycerophosphate, *Carbohydrate Polymers* 63 (2006), 507-518.
- [210] J. Cho, M.C. Heuzey, A. Begin, P.J. Carreau, Chitosan and glycerolphosphate concentration dependence on solution behaviour and gel point using small amplitude oscillatory rheometry, *Food Hydrocolloids* 20 (2006), 936-945.

- [211] J. Cho, M.C. Heuzey, A. Begin, P.J. Carreau, Physical gelation of chitosan in the presence of β -glycerophosphate: the effect of temperature, *Biomacromolecules* 6 (2005), 3267-3275.
- [212] M. Lavertu, D. Fillion, M. Buschmann, Heat-induced transfer of protons from chitosan to glycerol phosphate produces chitosan precipitation and gelation, *Biomacromolecules* 9 (2008), 640-650.
- [213] K.E. Crompton, R.J. Prankerd, D.M. Paganin, T.F. Scott, M.K. Horne, D.I. Finkelstein, K.A. Gross, J.S. Forsythe, Morphology and gelation of thermosensitive chitosan hydrogels, *Biophysical Chemistry* 117 (2005), 47-53.
- [214] T. Watanabe, N. Murase, M. Staemmler, K. Gersonde, Multiexponential proton relaxation processes of compartmentalized water in gels, *Magnetic Resonance in Medicine* 27 (1992), 118-134.
- [215] M. Bastrop, A. Meister, H. Metz, S. Drescher, B. Dobner, K. Mäder, A. Blume, Water Dynamics in Bolaamphiphile Hydrogels Investigated by ^1H NMR Relaxometry and Diffusometry, *Journal of Physical Chemistry B* 115 (2011), 14-22.
- [216] J. Götz, J. Schneider, P. Först, H. Weisser, A comparative nuclear magnetic resonance and rheological study on mash and spent grain suspension, worts, and carbohydrate solutions, *Journal of the American Society of Brewing Chemist* 61 (2003), 37-47.
- [217] H. Ono, H. Yamada, S. Matsuda, K. Okajima, T. Kawamoto, H. Iijima, ^1H -NMR relaxation of water molecules in the aqueous microcrystalline cellulose suspension systems and their viscosity, *Cellulose* 5 (1998), 231-247.
- [218] S. Ullrich, "Amphiphilic sucrose esters as new ingredients for lipid based drug delivery systems." Martin Luther University Halle-Wittenberg, 2008.
- [219] G. Paradossi, F. Cavalieri, V. Crescenzi, ^1H -NMR relaxation study of a chitosan-cyclodextrin network, *Carbohydrate Research* 300 (1997), 77-84.
- [220] D. Capitani, V. Crescenzi, A.A. DeAngelis, A.L. Segre, Water in hydrogels. An NMR study of water/polymer interactions in weakly cross-linked chitosan networks, *Macromolecules* 34 (2001), 4136-4144.
- [221] Y.B. Schuetz, R. Gurny, O. Jordan, A novel thermoresponsive hydrogel based on chitosan, *European Journal of Pharmaceutics and Biopharmaceutics* 68 (2008), 19-25.
- [222] D. Fillion, M. Lavertu, M. Buschmann, Ionization and solubility of chitosan solutions related to thermosensitive chitosan/glycerol-phosphate systems, *Biomacromolecules* 8 (2007), 3224-3234.

- [223] R. Zeng, Z.C. Feng, R. Smith, Z.Z. Shao, X. Chen, Y.H. Yang, Exploring study of chitosan/glycerophosphate thermosensitive hydrogel with variable-temperature NMR, *Acta Chimica Sinica* 65 (2007), 2459-2465.
- [224] R. Ahmadi, J.D. deBruijn, Biocompatibility and gelation of chitosan-glycerolphosphate hydrogels, *Journal of Biomedical Materials Research Part A* 86 (2008), 824-832.
- [225] K.E. Crompton, J.D. Goud, R.V. Bellamkonda, T.R. Gengenbach, D.I. Finkelstein, M.K. Horne, J.S. Forsythe, Polylysine-functionalised thermoresponsive chitosan hydrogel for neutral tissue engineering, *Biomaterials* 28 (2007), 441-449.
- [226] A. Montembault, C. Viton, A. Domard, Rheometric study of the gelation of chitosan in aqueous solution without cross-linking agent, *Biomacromolecules* 6 (2005), 653-662.
- [227] J.E. Nettleton, P. Tito, M. Sunde, M. Bouchard, C.M. Dobson, C.V. Robinson, Characterization of the oligomeric states of insulin in self-assembly and amyloid fibril formation by mass spectroscopy, *Biophysical Journal* 79 (2000), 1053-1065.
- [228] K. Kofuji, H. Akamine, H. Oshirabe, Y. Maeda, Y. Murata, S. Kawashima, Retention and release behavior of insulin in chitosan gel beads, *Journal of Biomaterials Science-Polymer Edition* 14 (2003), 1243-1253.
- [229] H. Bysell, M. Malmsten, Visualizing the interaction between poly-L-lysine and poly(acrylic acid) microgels using microscopy techniques: effect of electrostatics and peptide size, *Langmuir* 22 (2006), 5476-5484.
- [230] Y. Boonsongrit, B.W. Mueller, A. Mitrevej, Characterization of drug-chitosan interaction by ¹H-NMR, FTIR and isothermal titration calorimetry, *European Journal of Pharmaceutics and Biopharmaceutics* 69 (2008), 388-395.
- [231] R. Mulik, V. KulKarni, R.S.R. Murthy, Chitosan-based thermosensitive hydrogel containing liposomes for sustained delivery of cytarabine, *Drug Development and Industrial Pharmacy* 35 (2009), 49-56.
- [232] K.M. Hosny, Preparation and evaluation of thermosensitive liposomal hydrogel for enhanced transcorneal permeation of ofloxacin, *AAPS PharmsciTech* 10 (2009), 1336-1337.
- [233] H.K. No, K.S. Lee, S.P. Meyers, Correlation between physicochemical characteristics and binding capacities of chitosan products, *Journal of Food Science* 65 (2000), 1134-1137.
- [234] M. Jumaa, F.H. Furkert, B.W. Müller, A new lipid emulsion formulation with high antimicrobial efficacy using chitosan, *European Journal of Pharmaceutics and Biopharmaceutics* 53 (2002), 115-123.

- [235] A. Rube, "Development and physico-chemical characterization of nanocapsules." Martin-Luther-University Halle-Wittenberg, 2006.
- [236] F. Hyodo, The Innovation Center for Medical Redox Navigation, Kyushu University - a good place for interdisciplinary and international research, (2011).
- [237] A. Lochmann, H. Nitzsche, A. Schädlich, S. von Einem, E. Schwarz, K. Mäder, Applicability testing of in situ forming implants with incorporated microspheres: In vivo monitoring of Calcification, *Regenerative Medicine* 4 (2009), 5218-5219.
- [238] M.H. Cho, K.S. Kim, H.H. Ahn, M.S. Kim, S.H. Kim, G. Khang, B. Lee, H.B. Lee, Chitosan gel as an in situ-forming scaffold for rat bone marrow mesenchymal stem cells in vivo, *Tissue Engineering Part A* 14 (2008), 1099-1108.
- [239] C. Hoemann, J. Sun, A. Légaré, M.D. McKee, M. Buschmann, Tissue engineering of cartilage using an injectable and adhesive chitosan-based cell-delivery vehicle, *OsteoArthritis and Cartilage* 13 (2005), 318-329.
- [240] T. Kean, M. Thanou, Biodegradation, biodistribution and toxicity of chitosan, *Advanced Drug Delivery Reviews* 62 (2010), 3-11.
- [241] T.A. Khan, K.K. Peh, H.S. Ch'ng, Reporting degree of deacetylation values of chitosan: the influence of analytical methods, *Journal of Pharmaceutical Sciences* 5 (2002), 205-212.

6.2 Acknowledgement

First of all, I would like to express my deep gratitude to my supervisor, Prof. Karsten Mäder for the introduction in the interesting field of EPR that covers my all my PhD work, for his continuous support, advice and inspiration, not only during this thesis work but also in life.

I would also like to thanks H. Metz for the useful discussions and instructions with respect to ESR simulation, $^1\text{H-NMR-Relaxometry}$ and MRI instrumentation.

I have to express my gratitude to K. Schwarz for her invaluable help with EPR measurement and industrial collaborations.

I also thank M. Henniecke and C. Gottschalk for taking care of the animals.

Thanks to my students J. Kutza, R.V. Contri, A. Hvilson, T. About, P.C.G. Pereira for their help with $^1\text{H-NMR-Relaxometry}$ measurements.

Thank you to all the colleagues at the Institute for Pharmaceutics and Biopharmaceutics, Martin-Luther-University Halle-Wittenberg, for the friendly atmosphere in “our” team.

Special thanks to M. Bastrop and K. Schröter for their help with oscillating rheology, S. Ullrich, and H. Caysa for their support with the animal experiments, A. Schädlich and C. Blümer for technical hardware and software support and my diploma student J. Oidtmann and all members of the group of Prof. Mäder for their friendship.

Further I wish to pay my gratitude to my family for their positive support.

Last but not least I wish to thank Olaf and my little sunshine Elena for appreciating my work, giving me strength and motivation to get things done.

This work is dedicated to my grandfather, who taught me to see behind the curtain.

6.3 List of publications

6.3.1 Reviews

S. Kempe, H. Metz, K. Mäder, Application of Electron Paramagnetic Resonance (EPR) spectroscopy and imaging in drug delivery research – Chances and challenges, *European Journal of Pharmaceutics and Biopharmaceutics*, 74, 55-66 (2010)

6.3.2 Research Papers

S. Kempe, H. Metz, P.C.G. Pereira, K. Mäder, Non-invasive *in vivo* evaluation of *in situ* forming PLGA implants by benchtop magnetic resonance imaging (BT-MRI) and EPR spectroscopy, *European Journal of Pharmaceutics and Biopharmaceutics*, 74, 102-108 (2010)

This paper was awarded by the Phoenix Pharmazie Wissenschaftspreis 2011.

S. Kempe, H. Metz, K. Mäder, Do *in situ* forming PLG/NMP implants behave similar *in vitro* and *in vivo*? A non-invasive and quantitative EPR investigation on the mechanisms of the implant formation process, *Journal of Controlled Release*, 130, 220-225 (2008)

S. Kempe, H. Metz, M. Bastrop, A. Hvilsom, R. Vidor Contri, K. Mäder, Characterization of thermosensitive chitosan-based hydrogels by Rheology and Electron Paramagnetic Resonance Spectroscopy, *European Journal of Pharmaceutics and Biopharmaceutics*, 68, 26-33 (2008)

I. Hinneburg, S. Kempe, H.-H Rüttinger, R.H.H. Neubert, Antioxidant and photoprotective properties of an extract from buckwheat herb (*Fagopyrum esculentum* MOENCH), *Pharmazie* 61, 237-240 (2006)

I. Hinneburg, S. Kempe, H.-H Rüttinger, R.H.H. Neubert, A CE Method for Measuring Phototoxicity in Vitro *Chromatographia* 62, 325-329 (2005)

6.3.3 Oral Presentations

S. Kempe, H. Metz, P.C.G. Pereira, K. Mäder, A novel *in vivo* evaluation of *in situ* forming PLGA implants by benchtop magnetic resonance imaging (BT-MRI), 36th Annual Meeting and Exposition of the Controlled Release Society, Copenhagen (Denmark) 2009

S. Kempe, H. Metz, P.C.G. Pereira, K. Mäder, Noninvasive *in vivo* evaluation of *in situ* forming implants by benchtop magnetic resonance imaging (BT-MRI) and EPR spectroscopy, Controlled Release Society, German Chapter Annual Meeting, Halle (Germany) 2009

S. Kempe, H. Metz, K. Mäder, Non-invasive *in vitro* characterization of chitosan based *in situ* gelling O/W emulsions by 1H-NMR Relaxometry, 6th World Meeting on Pharmaceutics and Biopharmaceutics and Pharmaceutical Technology, Barcelona (Spain) 2008

6.3.4 Abstracts

A Lochmann, H. Nitzsche, S. Kempe, S. von Einem, E. Schwarz, K. Mäder, rhBMP-2 Delivery From Scaffolds, Microparticles And *In Situ*-forming Gels, 6th research festival for life sciences 2007, Dec 14, 2007, Leipzig (Germany), Abstract Book ISBN 3-9810760-2-8

A Lochmann, H. Nitzsche, S. Kempe, S. von Einem, E. Schwarz, K. Mäder, rhBMP-2 Delivery From Scaffolds And *In Situ*-forming Gels, *Regenerative Medicine* 2, 649-650 (2007)

6.3.5 Posters

A. Schädlich, S. Kempe, S. Ullrich, K. Mäder, *In vitro* and *in vivo* pH measurement studies of in situ forming sucrose ester and PLGA implants using EPR spectroscopy and fluorescence imaging, 7th World Meeting on Pharmaceutics and Biopharmaceutics and Pharmaceutical Technology, Malta 2010

S. Kempe, H. Metz, K. Mäder, Influence of the Oil Content on the in situ gelling Behaviour of Chitosan-based O/W emulsions, Euchis, Venice (Italy) 2009

S. Kempe, S. Ullrich, H. Metz, K. Mäder, *In vitro* and *in vivo* investigation of in situ gelling hydrogels by EPR-Spectroscopy, EPR 2007-A Joint Conference of 12th In Vivo EPR Spectroscopy and Imaging and 9th International EPR Spin Trapping/Spin Labeling, Chicago (USA) 2007

S. Kempe, H. Metz, K. Mäder, Optimizing the formulation of oil-loaded thermosensitive Chitosan-based hydrogels by ¹H-NMR Relaxometry, 12th European Conference on Spectroscopy of Biological Molecules (ECSBM – 12), Paris (France) 2007

S. Kempe, H. Metz, A. Hvilson, R. Vidor Contri, K. Mäder, Characterization of thermosensitive chitosan-based hydrogels by Electron Paramagnetic Resonance Spectroscopy, 34th Annual Meeting and Exposition of the Controlled Release Society, Long Beach (USA) 2007

S. Kempe, S. Ullrich, H. Metz, K. Mäder, *In vitro* and *in vivo* investigation of in situ gelling hydrogels by EPR-Spectroscopy, 4th Polish-German Symposium, Halle (Germany) 2007

S. Kempe, K. Mäder, Non-invasive in vivo monitoring of in situ forming implants by EPR spectroscopy, 33rd Annual Meeting and Exposition of the Controlled Release Society, Vienna (Austria) 2006

S. Kempe, K. Mäder, Development and characterization of Polyvinyl-acetate-nanocapsules, PolyPharma 2006 – Polymers in Pharmacy, Halle (Germany) 2006

S. Kempe, K. Mäder, Characterization of in situ forming implants by EPR Spectroscopy, EPR 2005 - A Joint Conference of 11th In Vivo EPR Spectroscopy and

NON-INVASIVE CHARACTERIZATION OF IN SITU FORMING IMPLANTS

D i s s e r t a t i o n

zur Erlangung des akademischen Grades
doctor rerum naturalium (Dr. rer. nat.)

vorgelegt der
Naturwissenschaftlichen Fakultät I
Biowissenschaften
der Martin-Luther-Universität Halle-Wittenberg

von
Frau Apothekerin Sabine Kempe
geb. am: 02.02.1980 in: Frankenberg (Sachsen)

Gutachter /in

1. Prof. Dr. K. Mäder
2. Prof. Dr. J. Siepmann
3. Prof. Dr. J. Kreßler

Halle (Saale), 08.05.2012

S. Kempe, K. Mäder, Monitoring of biodegradable Drug Delivery Systems by Electron Paramagnetic Resonance Imaging, 9th Int. Meeting and Workshop on EPR Studies of viable Systems and Related Techniques, Hanover (USA) 2004

6.4 Curriculum vitae

Sabine Kempe

Born 02.02.1980 in Frankenberg (Sachsen)

Work experience

- Since 06/2011 Research fellow at the Institute of Pharmacy,
Martin-Luther-University Halle-Wittenberg
- 01/2011 Pharmacist at community pharmacy
- 12/2009 – 12/2010 National and European Qualified Person for Pharmacovigilance,
Head of the Drug Safety Unit, Bombastus-Werke AG, Freital
- 10/2009 – 12/2010 Drug Regulatory Affairs and Drug Safety Manager,
Bombastus-Werke AG, Freital
- 04/2004 – 09/2009 Research and teaching assistant at the Institute of Pharmacy,
Martin-Luther-University Halle-Wittenberg
- 01/2004 – 03/2004 Practical training at ECHEM Kompetenzzentrum für Angewandte
Elektrochemie GmbH, Wiener Neustadt, Austria
- 04/2003 – 09/2003 Practical training at Glückauf-Apotheke, Halle-Ammendorf
- 10/2002 – 03/2003 Practical training in the group of Prof. Dr. H.-H. Rüttinger,
Institute of Pharmacy, Martin-Luther-University
Halle-Wittenberg
- 08/2001 – 09/2001 Practical training, Assistant of the Head of Quality Assurance,
Sanofi-Synthelabo AG Garching/München

Education

- Since 04/2004 Ph.D. student in the group of Prof. Dr. K. Mäder, Institute of
Pharmacy, Martin-Luther-University, Halle-Wittenberg
- 10/1998 – 10/2002 Pharmacy studies Martin-Luther-Universität, Halle-Wittenberg
Approbation 12.2003
- 1998 Abitur ,Gellert-Gymnasium, Hainichen (Sachsen)

6.5 Selbständigkeitserklärung

Hiermit erkläre ich, dass ich die vorliegende Dissertationsarbeit selbständig und ohne fremde Hilfe angefertigt, andere als die von mir angegebenen Quellen und Hilfsmittel nicht benutzt und die den Werken wörtlich oder inhaltlich entnommenen Stellen als solche kenntlich gemacht habe.

Die Dissertation wurde bisher keiner anderen Universität oder Hochschule im In- und Ausland vorgelegt.

A handwritten signature in cursive script, reading "Sabie Kenpe".

Halle (Saale), den 08.05.12